Localisation of corneal epithelial progenitors and characterization of cell-cell interactions in the human limbal stem cell niche

A thesis submitted for the degree of Doctor of Philosophy (PhD)

University College London (UCL) 2015

Marc A. Dziasko

Supervised by

Professor Julie T. Daniels, PhD FSB

Mr Stephen J. Tuft MA MChir MD FRCOphth

Division of ORBIT (Ocular Biology and Therapeutics)

UCL Institute of Ophthalmology, 11-43 Bath Street, London, EC1V 9EL

Declaration

I, Marc Alexandre Dziasko confirm that the work presented in this thesis is my own. Where information has been derived from other sources, I confirm that this has been referenced in the thesis.

Name: Marc Alexandre DZIASKO

Signature:

Date: 18/09/2015

Abstract

The cornea, the transparent tissue located at the front of the eye, is a highly specialized tissue that transmits and refracts light onto the retina. Maintenance of the corneal epithelium relies on a population of limbal epithelial stem cells (LESCs) that maintain transparency of the ocular surface that is essential for vision. Despite great advances in our understanding of ocular stem cell biology over the last decade, the exact location of the LESC niche remains unclear.

After observing a high population of basal epithelial cells expressing stem cell markers within the previously identified limbal crypts (LC), the first aim of this study was to demonstrate by *in vitro* clonal analysis that these structures provide a niche for the resident LESCs. High-resolution transmission electron microscopy has been further used to image the basal epithelial layer at the limbus. Cells with morphology consistent with stem cells were present within the basal layer of the limbal crypts but not within the basal layer of non-crypt limbal biopsies. Moreover, LESCs appeared proximal to limbal stromal cell extensions that suggested a possible route for direct cell-to-cell interaction. These observations were further confirmed by serial block-face scanning electron microscopy that revealed, for the first time, direct epithelial-stromal interactions in the LESC niche whereas limbal melanocytes maintained the LESC apically. In order to assess the role of limbal melanocytes (hLM) as niche cells for the maintenance of LESC, a novel co-culture system was developed in which hLM were used as a feeder layer for the expansion of limbal epithelial cells *in vitro*. Interestingly, hLM had the ability to support the clonal growth of LECs that maintained stem cell-like characteristics in 2D and 3D tissue equivalents. Taken

together, these observations suggest an important role for melanocytes as niche cells in the native human limbal crypts.

Acknowledgments

First of all, I would like to thank my supervisor, Prof. Julie T. Daniels for the patient and inspirational guidance, support and continuous encouragement she has provided throughout my PhD. I feel extremely lucky to be a part of such a great research team and I want to acknowledge my colleagues from Cells for Sight for their daily support and availability. I would like to thank my secondary supervisor, Mr Steve Tuft for his regular advices and clinical expertise.

I also want to acknowledge Hannah Armer for teaching me the science of electron microscopy and for her commitment to the project.

Finally, a big thank you goes to my friends and my family for their continuous support and presence despite the distance.

The research was funded by the National Institute for Health (NIHR) Biomedical Research at Moorfields Eye Hospital NHS foundation Trust and UCL Institute of Ophthalmology and a Stem Cell Initiative Award from the Special Trustees of Moorfields Eye Hospital.

List of abbreviations

-ve	negative
+ve	positive
ABS	Adult Bovine Serum
ARK	Aniridic-Related Keratopathy
Bm	Basement membrane
BSEs	Backscattered Electrons
Bv	Blood vessel
C+	Crypt-rich limbal biopsy
C-	Non-crypt limbal biopsy
CECM	Corneal Epithelial Cell Medium
CFE	Colony forming efficiency
CK	Cytokeratin
CLEM	Correlative Light and Electron Microscopy
CSSC	Corneal Stromal Stem Cell
Cx	Connexin
DAPI	4',6-diamidino-2-phenylindole
DMEM	Dulbecco's Modified Eagle Medium
DMSO	Dimethyl Sulfoxide
EGF	Epidermal Growth Factor
EM	Electron Microscopy
ET	Electron Tomography
FACS	Fluorescence-activated cell sorting
FBS	Foetal Bovine Serum
FIB	Focused ion beam
FSP	Focal Stromal Projection
Fz	Frizzled
GSC	Germ Stem Cell
hAM	human Amniotic Membrane

- HE Hematoxylin-Eosin
- hLM human Limbal melanocytes
- HSC Hematopoietic Stem Cell
- ICC Immunocytochemistry
- IHC Immunohistochemistry
- iPS induced Pluripotent Stem cell
- LC Limbal Crypts
- LECs Limbal Epithelial Cells
- LESC Limbal Epithelial Stem Cells
- LM Light Microscopy
- LSCD Limbal Stem Cell Deficiency
- MMC Mitomycin C
- MSC Mesenchymal Stem Cell
- N-cad N-cadherin
- NC Nucleus / cytoplasm
- PBS Phosphate-Buffered Saline
- PFA Paraformaldehyde
- POV Palisade Of Vogt
- RAFT Real Architecture For 3D Tissue
- SBF Serial block-face
- SEM Scanning electron microscopy
- St Stroma
- TAC Transient Amplifying Cell
- TE Tissue Equivalent
- TEM Transmission electron microscopy

Table of contents

List of figures

List of tables

Chapter 1: General Introduction

1.1 Stem cells

1.1.1 General introduction to stem cells

The concept of organ regeneration has been mentioned for the first time by the ancient Greeks in the myth of Prometheus. Prometheus transgressed the law of the ancient gods by introducing fire and knowledge to human beings. As a punishment, Zeus chained the titan to Mount Caucasus where an eagle preyed on his liver, which was regenerated as fast as it was devoured (http://www.ancient.eu/Prometheus/).

Stem cells are undifferentiated cells that are present during throughout the embryonic and adult stages of life. Stem cells present two major characteristics: i) the ability to self-renew, and ii) to differentiate into one or several cell types (also termed potency). Stem cells are found in multicellular organisms and can be classified upon their differentiation potential or their tissue of origin.

1.1.2 Stem cells and Waddington's landscape

Stem cell potency can be illustrated by Waddington's epigenetic landscape (figure 1.1) (Hendry & Little, 2012). In this model, the ball at the top of the mount represents the stem cell with the highest potential. This landscape has a direction: once the ball begins its descent, it cannot roll back up. This direction illustrates the stem cell differentiation. The ball has the ability to descend into a multitude of pathways that reflects the ability of pluri/multipotent stem cells to differentiate into a multitude of lineages. Every single basin where the ball could potentially stop corresponds to a state of potency. The further the ball descends,

the more stem cell potency becomes limited until finally it becomes a terminally differentiated cell at the bottom of the mount.

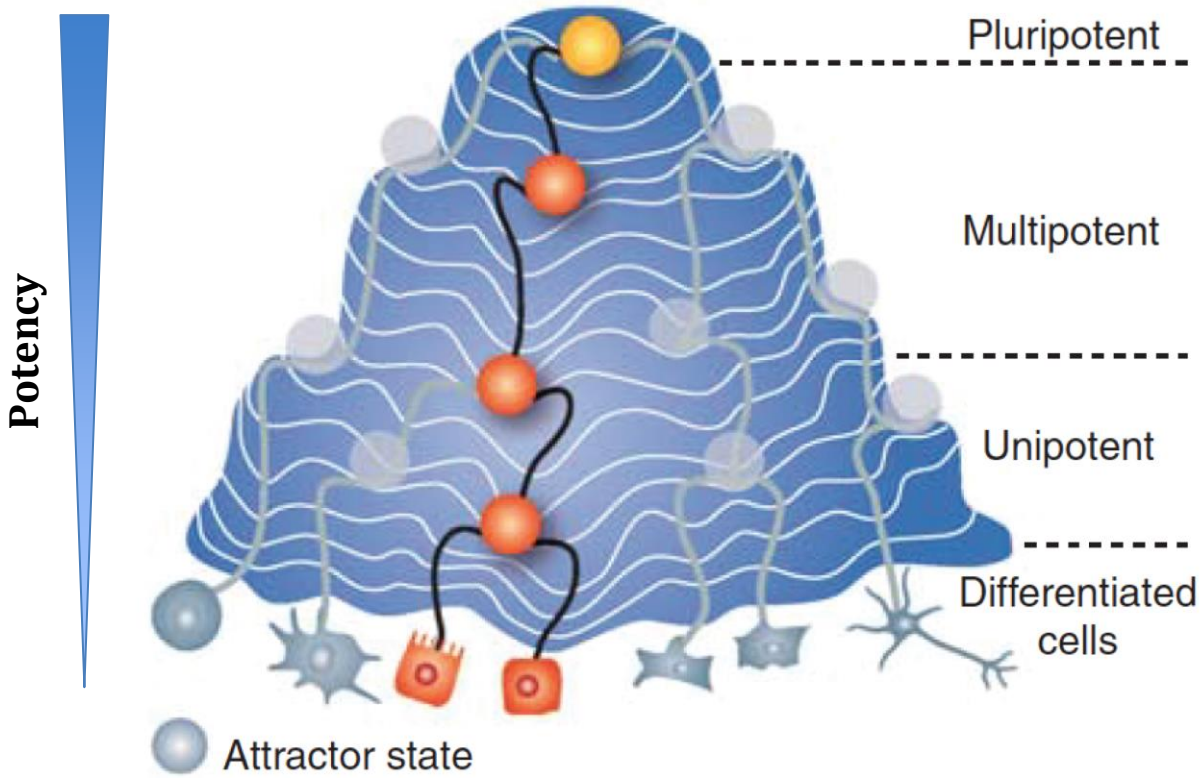

Adapted from Hendry et al. 2012 Kidney international

Figure 1.1 Stem cells in the context of Waddington's landscape

Waddington's epigenetic landscape can be used to illustrate stem cell specification and differentiation. The cell at the top of the mount has the highest potential and can engage into multiple paths or lineages. The landscape is directional and once the cell engages into a path, it cannot roll back up to the top. The cell can stop in various basins, which correspond to the available pathways of differentiation. The cell progressively continues its descent until the bottom of the mount where it becomes highly specialized and terminally differentiated. *Adapted from Hendry et al. 2012 Kidney international*

1.1.3 Totipotent stem cells

Stem cells can be classified according to their potency that corresponds to the range of lineages into which they have the ability to differentiate (figure 1.2). Totipotent stem cells, also called omnipotent stem cells, are the most undifferentiated cells found in the first stage of the development. In human development, the fertilized oocyte or zygote and cells resulting from the two first cell divisions are totipotent. These totipotent cells will further differentiate into both all the extraembryonic and embryonic tissues.

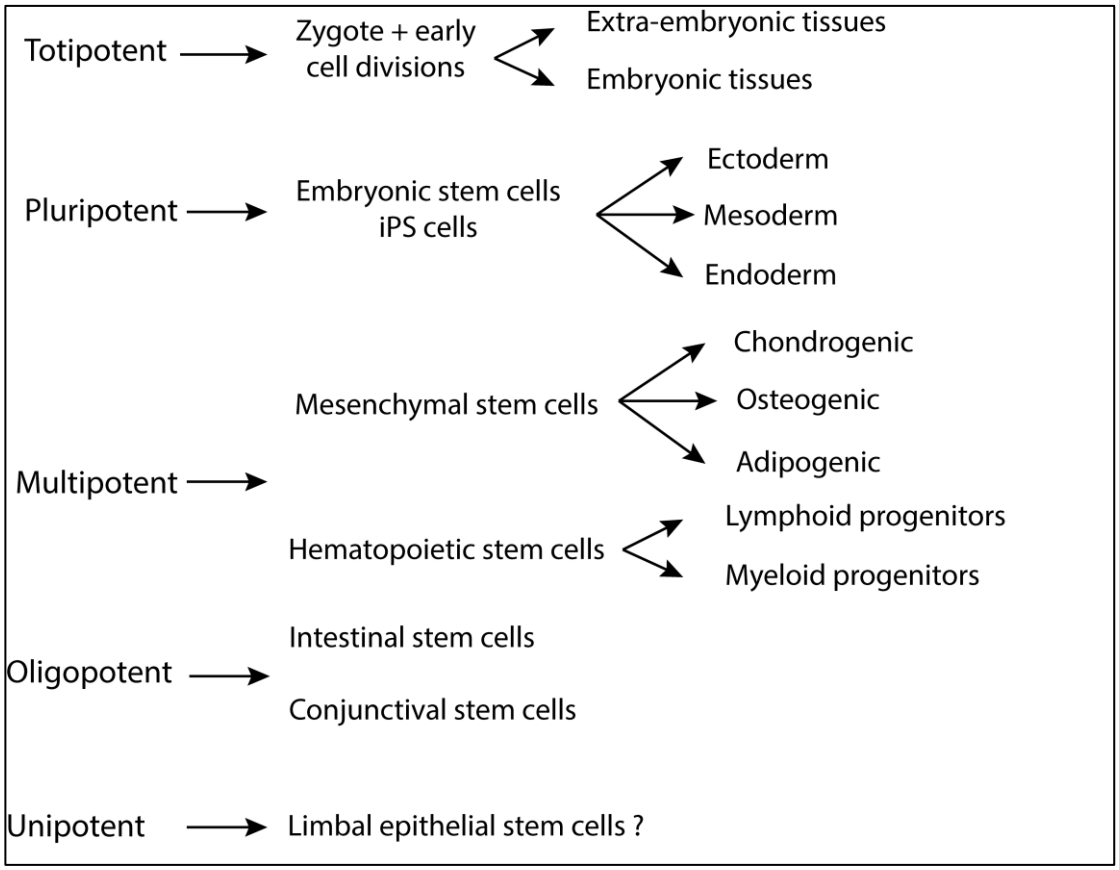

Figure 1.2 Classification of mammalian stem cells according to their potency

Totipotent stem cells have the highest potency and are the origin of both embryonic and extra embryonic tissues. Pluripotent stem cells are either embryonic cells of the blastocyst or artificially induced. These cells have the potential to generate the cells of the 3 germ layers. Multipotent stem cells have the potential to generate multiple cell lineages within an organ. Oligopotent stem cells have a limited ability to generate the different lineages within a specific tissue, such as conjunctival stem cells of the ocular surface that are progenitors for both goblet and conjunctival epithelial cells. Unipotent stem cells still have the potential to self renew but can only differentiate into one type of daughter cell. Recently, it has been shown that LESC of murine ocular surface also had the ability to generate conjunctival goblet cells if put in the appropriate environment. Oligopotency of LESC has been shown in pigs but no data supporting this concept in human has as yet been presented (Majo et al., 2008).

1.1.4 Pluripotent stem cells

The blastocyst is as a structure appearing later in human development (5-6 days after fertilization). The blastocyst is composed by the trophoblast that will form the placenta and the inner cell mass that will form the three primary germ layers (ectoderm, mesoderm, endoderm). Cells composing the inner cell mass are pluripotent and commonly called embryonic stem cells (ESCs). These cells are maintained in an undifferentiated state and are identified by the expression of transcription factors such as NANOG, Sox2 Oct4 and Rex-1 (Hambiliki et al., 2012). Undifferentiated ESCs can be expanded *in vitro* in specific culture conditions involving a feeder layer of mouse irradiated embryonic fibroblasts, or in a culture medium containing the leukemia inhibitory factor cytokine LIF (Evans & Kaufman, 1981; Williams et al., 1988).

1.1.5 Multipotent stem cells

Multipotent stem cells are found in adult tissues and have the ability to differentiate into multiple lineages within a given organ. Mesenchymal stem cells (MSCs) are a typical example. These cells were originally identified in the bone marrow stroma but are also present in a multitude of adult organs such as the heart muscle, the adipose tissue or the corneal stroma (Beltrami et al., 2003; Friedenstein, et al., 1976; Polisetty et al., 2008; Zuk et al., 2002). MSCs adhere to culture plates and they express specific markers such as CD73, CD90 and CD105 (Dominici et al., 2006). Additionally, these cells exhibit the ability to generate colonies in culture and have the potential to differentiate into osteogenic, chondrogenic and adipogenic lineages upon specific culture conditions (Hass, Kasper, Böhm, & Jacobs, 2011). It has recently been shown that mesenchymal stem cells of the limbal stroma have the ability to transdifferentiate into corneal epithelial cells that express E-Cadherin and cytokeratins such as CK3, CK12 and CK15 (Katikireddy et al., 2013). Hematopoietic stem cells are another example of multipotency. These cells, located in the bone marrow, are at the top of the hematopoietic hierarchy and give rise to both lymphoid and myeloid lineages.

1.1.6 Oligopotent stem cells

Oligopotent stem cells still present self-renewal properties but can only follow limited lineages (generally 2) within a specific tissue. Pellegrini et al. 1999, demonstrated the existence of a common oligopotent progenitor for both

conjunctival keratinocytes and goblet cells in the human ocular surface (Pellegrini et al., 1999). Later, Majo et al. 2008 demonstrated the presence of oligopotent keratinocytes that were distributed over the entire porcine ocular surface that were able to generate both corneal and conjunctival colonies (Majo et al., 2008).

1.1.7 Unipotent stem cells

Unipotent stem cells still possess self-renewal properties but can only differentiate into a specific cell type and form a single lineage. LESCs of the human cornea are an example of unipotency.

Classification of human stem cells upon their potency is summarized in figure 1.2.

1.1.8 Induced pluripotent stem cells (iPS)

Induced pluripotent stem cells (iPS) cells are somatic cells that have been reprogrammed into an embryonic state. iPS cells are technically considered to be pluripotent and can generate progeny of the three primary germ layers. This phenomenon occurs when a defined set of embryonic transcription factors are reactivated in the adult cells. Yamanaka et al. 2006, were the first to describe the procedure using mouse fibroblasts. Introduction of the retroviral-mediated transcription factors OCT3/4, Sox2, Myc and Klf4 restored pluripotency of terminally differentiated adult cells (Takahashi & Yamanaka, 2006). Because human iPS cells can be directly derived from a patient's own cells, iPS cells could

potentially be used to generate cells for tissue specific cell therapies, drug screening or for developing human disease models. The reprogramming procedure has been further optimized and applied to other murine (liver and stomach) and human adult cells (Aoi et al., 2008; Okita et al., 2007; Takahashi et al., 2007). The use of retroviral vectors to introduce reprogramming factors, the use of the oncogene Myc and the need to use a selection marker to identify the reprogrammed cells are the main technical challenges that would need to be overcome prior using iPS cells for cellular therapies. Nevertheless, success of iPS based cell therapy has already been reported for the treatment of sickle cell anemia in mice demonstrating the great potential for human iPS based cell therapies in the future (Hanna et al., 2007).

1.2 The ocular surface, ultrastructure and function

The transparent cornea, located at the front of the eyeball, is our window to the world. It is a highly specialized tissue that refracts and transmits light through the lens and onto the retina. The ocular surface comprises the transparent cornea, the opaque conjunctiva and a transition area at the interface called the limbus (Figure 1.3A). All three regions are covered by a multilayered squamous and stratified epithelium that plays a crucial role in the prevention of pathogen entry, fluid loss and resistance to injury. The epithelium of the ocular surface is supported by a connective tissue that conducts nutrients and contains elements of the immune system.

1.2.1 The cornea

a) Corneal epithelium

The cornea is composed of five distinct layers for a central thickness of approximately 0.5mm (Figure 1.3). This includes the non-keratinised and stratified epithelium at the surface, which is a dynamic and physical barrier preventing the entry of pathogens into the eye and protecting the inner tissues. The corneal epithelium is composed of 5 to 7 layers of epithelial cells comprising a single layer of columnar basal cells, intermediate suprabasal cells and superficial squamous cells making a total thickness of 50-52μm. The basal layer consists of a single layer of columnar epithelial cells attached to the underlying basement membrane by hemidesmosomes. These cells are involved in the generation of new suprabasal cells but also in the secretion of matrix molecules important for the maintenance of the underlying epithelial basement membrane and stroma. The suprabasal cells are derived from the inner basal cells and present wing-like extensions, rarely undergo division and migrate to the epithelial surface to terminally differentiate into superficial squamous cells. These superficial squames express extensive microvilli increasing the cell surface area and contain mucins that facilitate the association with the tear film (Pajoohesh-Ganji & Stepp, 2005). The superficial cell layer possesses an important junctional complex consisting of tight junctions binding the cells at their lateral borders preventing the entrance of pathogens and the movement of substances from the tear film into the intercellular space of the epithelium. Corneal epithelial cells have the ability to store glucose as glycogen (Thoft &

Friend, 1977). However, the corneal epithelial metabolism mostly relies on glucose, vitamin and amino acids provided by diffusion from the aqueous humor. As the cornea is avascular oxygen for metabolism comes from the tear film and aqueous humor.

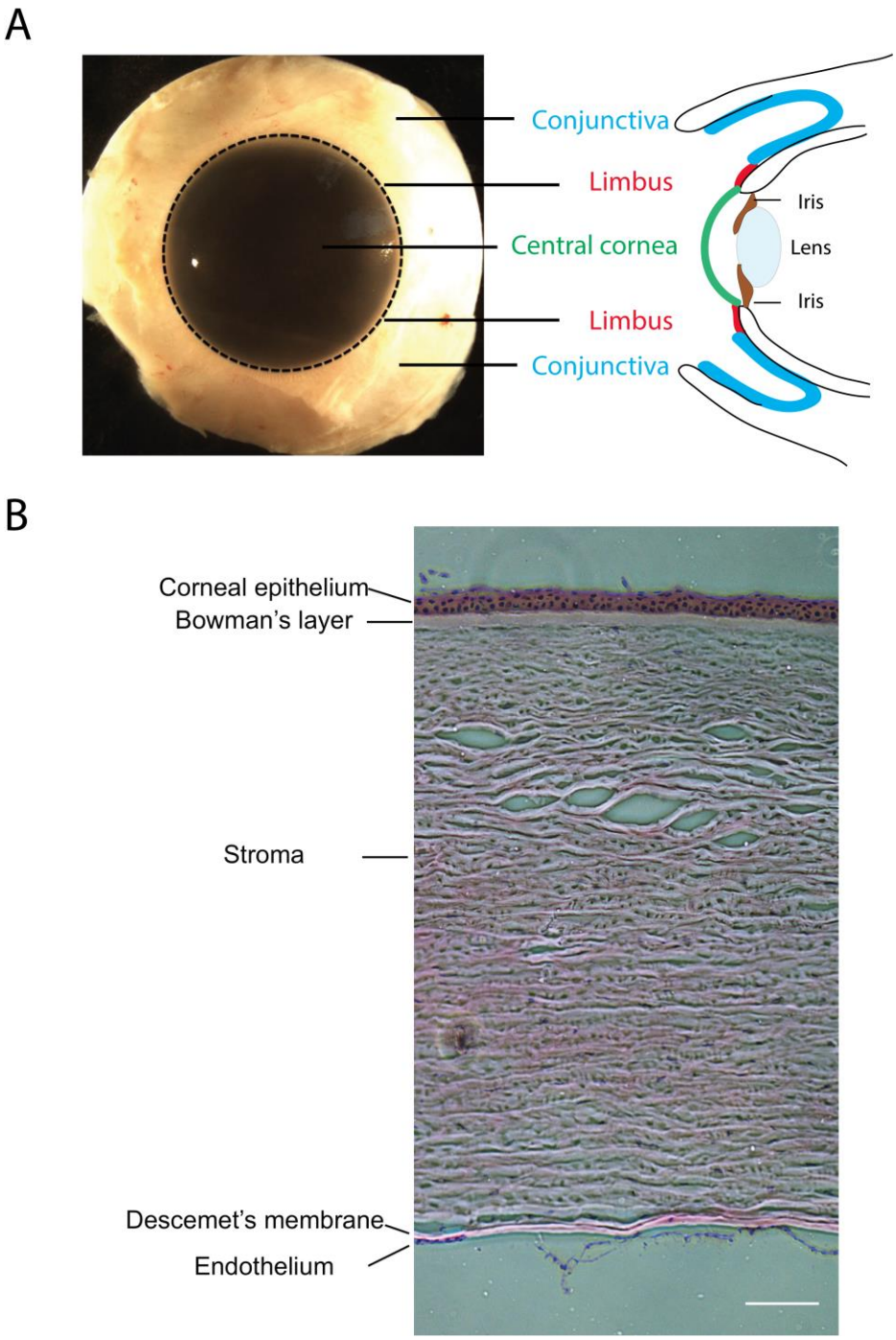

Figure 1.3 Ultrastructure of the human ocular surface

A. Human whole cornea (left) and diagram representing the anterior segment of the human eye (right). Blue: Conjunctiva; Red: Limbus; Green: Central cornea. Dashed circle: limbus.
B. HE histological cross section illustrating the ultrastructure of the central human cornea. Scale bar: 50μm.

b) Corneal stroma

The collagenous and acellular Bowman's layer separates the epithelium from the underlying highly organized stroma, which accounts for 90% of the cornea's total thickness (Figure 1.3B). Rigidity of the anterior stroma is important in maintaining curvature of the tissue, which is essential for accurate refraction of light (Müller et al., 2001). The collagen molecules composing the collagen fibrils of the corneal stroma are mainly composed by heterodimeric chains of collagen I and V. The abundance of collagen V that has the particularity to retain a large N-terminal lobe, regulates, by steric hindrance, the diameter of the collagen fibrils (Birk et al., 1990). Small 25-30nm diameter collagen fibrils associated to keratan, dermatan and chondroitin sulfate proteoglycans form regular lamellae with an orthogonal arrangement that maintain the corneal transparency (Hassell & Birk, 2010). Neural crest-derived fibroblast-like cells called keratocytes, containing numerous lamellapodia and synthetizing the local extracellular matrix, also populate the corneal stroma. Stromal keratocytes comprise approximately 3% to 20% of the corneal stromal volume and produce crystalline proteins that reduce light scattering, an important requirement for corneal transparency (Jester et al., 1999; Young et al., 2014).

c) Corneal endothelium

The corneal endothelium is located on the posterior corneal surface and is separated from the corneal stroma by a basement membrane called Descemet's membrane (Figure 1.3B). The corneal endothelium is 4-6μm thick and composed of a single layer of 20μm wide hexagonal endothelial cells ranging in density from 2300 and 3400 cells/mm^2 in adults and connected by tight junctions (Yee et al. 1985). Endothelial cells are not thought to undergo cell division after birth. For this reason, the number of endothelial cells gradually decreases with age. Endothelial cells have, however, in the absence of disease, the ability to spread and extend their surface allowing the maintenance of a confluent monolayer of cells on the Descemet's membrane after injury. The human corneal endothelium acts as a physical barrier and a pump preserving the corneal stroma in a relatively dehydrated state, which is essential to prevent corneal edema and maintain the corneal transparency (Joyce, 2003). Corneal endothelial cells also pump nutrients from the aqueous humor to the corneal stroma providing nourishment to the corneal keratocytes.

1.2.2 The limbus

Anatomically, the limbus corresponds to the transition area located at the interface between the transparent central cornea and the opaque conjunctiva and sclera. The limbus is a 1mm wide ring of tissue demarcated on the corneal side by the termination of the Bowman's layer. The limbus comprises a non-keratinizing multilayered stratified epithelium and the subjacent highly innervated and vascularized stroma. It has specific characteristics.

a) Limbal epithelium

The limbal epithelium is composed of 7 to 10 layers of epithelial cells and is thus the thickest epithelium of the ocular surface. Cells populating the superficial layer of the limbal epithelium highly express microvilli on their apical surface and tight junctions on the lateral sides. Basal cells of the limbal epithelium appear smaller and less columnar than basal cells of the corneal epithelium. It is generally accepted that a subpopulation of these basal cells corresponds to limbal epithelial stem cells (LESCs) that continuously regenerate the ocular surface. Unlike the central cornea, Langherans cells – the antigen presenting cells of the ocular surface - and melanocytes are also observed within the limbal epithelium.

b) Limbal stroma

The limbal connective tissue underlying the limbal epithelium is more loosely and irregularly arranged than the stroma of the central cornea. The limbal stroma is highly vascularized and contains capillaries, small arterioles, venules and lymphatic vessels reflecting the important metabolism of cells populating this area. A mixed population of limbal stromal cells including mast cells, macrophages, lymphocytes, nerves and fibroblast-like elongated cells also populates the limbal stroma. Some of these stromal cells are believed to interact with basal limbal epithelial cells (LECs) located on the other side of the basement membrane and are therefore considered as a part of the LESC niche.

1.2.3 Structure and functions of the conjunctiva

The conjunctiva is a non-keratinizing squamous epithelium several cell layers thick that forms the mucous membrane lining the inside of the eyelids and

anterior sclera. The main function of this tissue is to support the tear film and to prevent the entrance of microbes into the eye. The conjunctival epithelium lies on a highly vascularized stroma and can be divided in three distinct zones (Pellegrini et al., 1999): The bulbar conjunctiva that extends from the peripheral limbus and covers the sclera of the ocular globe, the forniceal conjunctiva localized in the fornix, the palpebral conjunctiva located between the forniceal and the skin of the eye lid. Pellegrini et al. 1999, demonstrated the ability of a sub-population of forniceal and bulbar conjunctival epithelial cells to generate holoclones *in vitro* by single cell clonal analysis (Pellegrini et al., 1999). Conjunctival stem cells appear to be uniformly distributed within the bulbar and forniceal areas and it has been proposed that conjunctival terminally differentiated keratinocytes and mucin-producing goblet cells are derived from a common transient-amplifying progenitor late in the differentiation process. Goblet cells of the conjunctival epithelium are interspersed between the keratinocytes and are highly concentrated within the medial forniceal and palpebral regions (Vujković et al., 2002). These cells are specialized in the synthesis and release of the gel-forming mucin MUC5AC. Due to high-glycosylation during the maturation process in the Golgi apparatus, mucins are negatively charged and associate with the divalent cation Ca^{2+} in order to be packaged efficiently. Once released, negatively charged mucins move easily over the ocular surface because of repulsion with the glycocalix localised at the surface of epithelial cells.

1.3 Limbal epithelial stem cells

1.3.1 General properties

Historically, several studies have provided evidence of a stem cell niche within the corneal limbus. Cotsarelis et al, 1989 revealed the existence of a subpopulation of basal epithelial cells that were located in the periphery (limbus) of the murine cornea (Cotsarelis, et al., 1989). H^3-thymidine labeling showed these cells had slow cycling properties (quiescence) and could be stimulated upon injury. Cells with such properties could not be detected in the central corneal epithelium. Additionally, Schermer et al, 1986 demonstrated that basic 64kDa keratin (Cytokeratin 3), a marker of advanced corneal epithelial cell differentiation, is expressed in all corneal epithelial layers except the basal layer of the limbus (Schermer et al., 1986). Furthermore, it has been suggested that limbal basal epithelial cells have a much higher proliferative potential in culture than peripheral corneal epithelial cells (Ebato et al., 1988). Pellegrini et al. 1999 evaluated the clonogenic ability of single epithelial cells isolated from different areas of the human ocular surface. They showed that single epithelial cells isolated from superior, inferior, nasal and temporal regions of the limbus were able to generate holoclones *in vitro* confirming the limbus as a niche for human LESCs whereas no holoclone generation could be observed when cells were isolated from the central cornea (Pellegrini et al., 1999).

a) Morphological aspects

Chen et al. 2004 compared the morphology of basal corneal epithelial cells with the basal cells of the limbal epithelium. High-resolution transmission electron

microscopy revealed that cells from the limbal basal epithelium were the smallest and had the highest nucleus/cytoplasm (NC) ratio. Moreover, the smallest cells with the highest N/C ratio were also positive for the expression of stem cell markers such as p63, ABCG2, integrin $\alpha 9$ and $\beta 1$ (Chen et al., 2004). Additionally, Arpitha et al. 2005 investigated the morphological characteristics of epithelial cells isolated from the central cornea, the peripheral cornea and the limbus *in vitro*. They observed that about 5% of the smallest cells were specifically isolated from the limbus and that they had the highest N/C ratio. Moreover, these observations were correlated with elevated expression of p63 confirming the morphological characteristics of limbal epithelial progenitors (Arpitha et al., 2005).

b) Positive and negative stem cell markers

Label-retaining experiments and *in vitro* assessment of LECs proliferative capacity designated the limbus as the site of the LESC niche. Following these observations, there has been an extensive search for a marker for LESC. Although no single reliable LESC marker has been identified, a few proteins seem to be specifically expressed in the limbal basal epithelial layer where LESC are believed to be located. Putative LESC markers can be either positive (expressed by the LESC) or negative (not expressed) (Table 1.1).

	Central cornea		Limbus	
	Basal	Suprabasal	Basal	Suprabasal
	Positive markers			
ABCG2	-	-	+++	+/-
p63	-	-	+++	+/-
Bmi-1	-	-	+	++
Frz7	-	-	+++	+/-
ABCB5	-	-	+++	+/-
N-cadherin	-	-	+	-
Integrin α9	-	-	+++	+/-
Integrin β1	+++	++	+++	+/-
Notch-1	-	-	++	+
	Negative markers			
Connexin 43	+	+++	-	+++
Involucrin	+	+++	-	+++
Integrin α6	++	+	-	++

Table 1.1 Expression of putative positive and negative stem cell markers in human central corneal and limbal epithelium

+++: high expression, ++: moderate expression; +: weak expression; +/-: very weak expression; -: no expression

ABCG2: Hematopoietic stem cells can be identified by flow cytometry as they display low Hoechst staining and have been thus defined as a "side population" (SP) (Goodell et al., 1996). This property has been attributed to the ATP binding cassette subtype G2, which is a multidrug resistance transporter having the ability to effectively efflux Hoechst molecules from dyed cells. Zhou et al. 2001, proposed that expression of ABCG2 is a conserved feature of stem cells from a

wide variety of sources and tissues (Zhou et al., 2001). In the human ocular surface, ABCG2 positive cells are concentrated within the limbal basal epithelial layer (Chen et al., 2004). Later, Budak et al. 2005, observed clusters of ABCG2 positive epithelial cells localized within the limbus and the conjunctiva. ABCG2 positive cells display clonogenic capacities and resistance to phorbol-induced cell differentiation suggesting ABCG2 identifies undifferentiated LECs (Budak, et al., 2005).

p63: p63 belongs to the p53 family of transcription factors. The role of p63 has been defined using a p63 -/- knockout mice model. Whereas p53 plays a role in tumor suppression, p63 -/- mice are characterized by the absence of stratified epithelia (Mills et al., 1999). Pellegrini et al. 2001, demonstrated by single cell clonal analysis that p63 was abundantly expressed by epithelial cells that were also able to generate holoclones *in vitro*. On the other hand, weak expression of p63 was associated with meroclones whereas no expression of p63 was observed in cells generating paraclones (Pellegrini et al., 2001).

N-cadherin: Higa et al, 2009, observed that N-cahderin was expressed in clusters of basal epithelial cells. *In vitro*, N-cad positive (+ve) cells were localized at the edge of the colonies where there was direct contact with 3T3 feeder fibroblasts. Moreover, N-cad +ve limbal epithelial cells were also positive for other stem cell markers such as CK15 and had the greatest proliferative potential in culture (Higa et al., 2009).

Cytokeratins: Cytokeratins compose a complex intracellular network of intermediate filaments in epithelial cells (Watt, 1989). Cytokeratins are divided into two subfamilies, acidic and basic. One member of each family forms the dimeric pair that is necessary for the formation of one filament. Humans possess

a total of 54 keratin genes. Cytokeratin expression patterns are highly tissue specific. Within a tissue, their distribution profile defines the degree of differentiation of the epithelium. In the human ocular surface, cytokeratin (CK) 3 and CK12 are specific markers for corneal epithelial cell differentiation and are expressed by all the layers of the central cornea and the superficial layers of the limbus (Chen, Mui, Kao, Liu, & Tseng, 1994; Schermer et al., 1986). CK15, which is considered as a positive marker for stem cells of the hair follicle, is also expressed by cells of the human and murine ocular surface. CK15 is expressed by basal cells of the conjunctiva but not by cells of the central corneal epithelium. In the limbus, CK15 expression was observed in both basal and supra-basal epithelial layers (Yoshida et al., 2006). CK14 is a positive marker for epidermal progenitors. It has been observed that CK14 was also expressed by highly proliferative LECs *in vitro* suggesting CK14 as a positive marker for LESCs and transient amplifying cells (TACs) (Figueira, Di Girolamo, Coroneo, & Wakefield, 2007). Cytokeratin 19 (CK19) is expressed by basal and suprabasal cells of the conjunctival epithelium. CK19 is also strongly expressed by basal cells of the limbus and has been suggested as a positive marker of LESCs (Yoshida et al., 2006). Chen et al. 2004, however reported that CK19 was also expressed by basal and suprabasal cells of the central corneal epithelium (Chen et al., 2004). The cytokeratin distribution profile of the human ocular surface is summarized in table 1.2.

	Central cornea		*Limbus*		*Conjunctiva*	
	B	SB	B	SB	B	SB
CK3	++	++	-	+	-	-
CK12	++	++	-	+	-	-
CK14	+	+	+++	++	++	+++
CK15	-	-	+++	++	-	+++
CK19	+	+	+++	++	+++	++

Table 1.2 Cytokeratin expression profile of the human ocular surface

B: basal epithelial layer; SB: suprabasal epithelial layers.

+++ Highly expressed, ++ Moderately expressed, + Weakly expressed, - No expression.

Integrins: Integrins are heterodimeric transmembrane glycoproteins involved in adhesion of epithelial cells to the underlying basement membrane and extracellular matrix. Integrin heterodimers consist of α and β subunits. Integrins β1 and α6 have been shown in epithelial stem cells of the human hair follicle (Jones & Watt, 1993). Immunohistochemical studies identified expression of several integrin subunits in the human cornea. Integrin β1 was abundantly expressed by cells from limbal and central corneal epithelium with a higher level in limbal basal cells. Integrin α9 was also detected at the surface of limbal basal cells, but not in suprabasal or cells from the central corneal epithelium. In contrast, integrin α6 was weakly expressed by cells from the limbal basal epithelium and is thus considered as a negative marker for the limbal progenitors (Chen et al., 2004). In 2013, Ordonez et al. identified integrins αvβ5

as new LESC marker. Integrin αvβ3 or β5 specifically binds vitronectin, a glycoprotein of the limbal basement membrane. It has been shown that integrin αvβ3/5 positive cells, that represent 4% of the total limbal epithelium, co-localized with N-cadherin and CK15 positive limbal basal cells. Moreover, integrin αvβ3/5 positive cells had the greatest proliferative potential in culture suggesting these cells as good candidates for limbal stem/progenitor cells (Ordonez, et al., 2013).

Connexin 43: Gap junctions are formed by four-pass transmembrane proteins called connexins. Connexins form connexons that together constitute a communicating channel between cells allowing the diffusion of low molecular weight metabolites and synchrony within a cell population. Connexin 43 is abundantly expressed by cells populating the central cornea. In contrast, connexin 43 expression is absent at the limbal basal epithelial layer suggesting the later as a marker of cell differentiation (Matic et al., 1997). However, in 2007 Shanmuganathan et al. reported that basal cells from the limbal epithelial crypts, that they believed correspond to a niche for LESC, were highly positive for the expression of Cx43. The authors suggested Cx43 as a positive marker for stem cells of the human ocular surface (Shanmuganathan et al., 2007).

Bmi-1: Barbaro et al. 2007, demonstrated co-localisation of the CCAAT enhancer-binding protein (C/EBPδ) with the oncogene Bmi1 in 10% of limbal basal epithelial cells that are able to generate holoclones in culture and that are mitotically quiescent during normal corneal maintenance (Barbaro et al., 2007).

Frizzled7: It has recently been observed that Wnt signaling receptor, Frizzled 7 (Fz7), was co-localized with limbal basal cell clusters that were positive for the expression of stem cell markers such as N-cadherin and p63α in the native niche.

Moreover, when Fz7 was knockdown in human LECs *in vitro*, the expression of the stem cell markers ABCG2 and ΔNp63α was significantly decreased suggesting the importance of Wnt signaling in the maintenance of the undifferentiated state and Fz7 as a marker of limbal stem/progenitors cells (Mei et al., 2014).

ABCB5: Recently, Ksander et al. observed that LECs positive for the expression of the ATP-binding cassette, sub-family B, member 5 (ABCB5) isolated from murine or human corneas were able to fully restore the cornea after Algerbrush II induced LSCD in NSG (NOD scid gamma) recipient mice. Murine ABCB5 +ve cells presented slow cycling properties as shown by BrdU label retaining and were also p63α positive (Ksander et al., 2014). Furthermore, ABCB5 expression appears to be frequently reduced in limbal biopsies of patients affected by limbal stem cell deficiency (LSCD). Taken together, these observations strongly suggest ABCB5 identifies mammalian limbal epithelial stem/progenitor cells and would thus be a promising marker for future LESC isolation and investigation.

Notch-1: It has been reported that Notch family members play a role in maintaining stem cells in hematopoietic and neural stem cells microenvironments (Varnum-Finney et al., 2000). Notch 1 plays a crucial role in controlling the cell fate during development through cell-to-cell interactions (Artavanis-Tsakonas et al., 1999). In the human ocular surface, Thomas et al. 2007 observed clusters of limbal basal epithelial cells mainly located within the palisades of Vogt (POV) that were positive for Notch-1 staining. Moreover, Notch-1 positive cells co-expressed ABCG2 suggesting that Notch-1 could be a possible marker for stem cells of the limbal basal epithelium (Thomas et al., 2007).

While no single marker for LESCs has been identified yet, a combination of different positive and negative markers is the best available method to identify limbal epithelial stem/progenitor cells *in vitro* and *in vivo*.

1.4 Stem cell niches

1.4.1 Background

"The cellular environment which retains the stem cell I shall call a stem cell 'niche' ". R. Schofield 1978.

Stem cells are characterized by their self-renewal properties and their ability to differentiate into a specific lineage or into several types of cells. Adult stem cells are found in specific areas of an organ. This specific anatomical location is commonly named the "stem cell niche". R. Schofield, 1978 first proposed the concept of a stem cell niche by describing hematopoietic stem cells in the bone marrow (Schofield, 1978). The niche can be considered as a specific and highly regulated unit of tissue or the microenvironment surrounding the stem cell. One piece of evidence supporting the importance of the niche in the control of the stem cell fate is attributed to Thomson et al. 1998. In their experiments, the authors isolated ESCs from murine blastocysts that they reintroduced into adult SCID (severe combined immunodeficiency) animals. Stem cells out of their native microenvironment generated multiple tumors called teratomas that contained multiple cell types from all three embryonic germ layers (Thomson et al., 1998). These observations highlighted the importance of the microenvironment and its impact on the stem cell behavior. The niche is not limited to anatomical

architecture. It also consists of a unique microenvironment involving multiple physicochemical factors summarized in figure 1.4. Direct interactions between stem cells and the surrounding niche cells appear to be crucial for maintaining the stem cell properties and for prevention of the differentiation process (figure 1.4A). The importance of these interactions has been clearly identified from studies on Drosophila germ stem cells (GSCs). In the female fly, GSCs are directly attached to the cap cells located at the anterior end of the ovariole. When GSCs divide, one of the daughter cell moves away from the cap and enters into the differentiation process. The other daughter cell remains in association with cap cells through DE-cadherin cell adhesion molecules. In this model, loss of E-cadherin expression results in detachment of the GSC from the cap cell and generates premature differentiation and loss of the germinal stem cell population (Song & Xie, 2002). Soluble mediators including cytokines and growth factors also influence stem cell behavior in the niche (figure 1.4B). The latter can be secreted by the stem cell (autocrine) or by the niche cells in proximity (paracrine). For example, multiple signaling pathways are involved in the continuous maintenance of intestinal stem cells in the niche. The interaction between the intestinal epithelial stem cell and the niche cell (mesenchymal cell) is mediated by soluble factors (cytokines or growth factors) from the Wnt, Shh, BMP and notch families that control mitosis, motility and stem cell differentiation (Scoville et al., 2008; Yeung, et al., 2011). *In vitro* or *in vivo*, cells are also exposed to mechanical forces generated by their surrounding environment. These external forces resulting from the compression exerted by neighboring cells and the local extracellular matrix (ECM) influence the stem cell behavior. Saha et al. 2008 observed that neural stem cells grown on hydrogels

with a stiffness comparable to the normal brain were more likely to generate neurons *in vitro* whereas harder matrices promoted glial differentiation (Saha et al., 2008).

The extracellular matrix (ECM) is a dynamic microenvironment surrounding the stem cell *in vivo* and plays an important role in maintaining the undifferentiated stem cell phenotype (figure 1.4D). The extracellular matrix and stem cell interactions can be mediated by receptors such as integrins. Integrins are heterodimeric transmembrane receptors connecting the extracellular matrix (laminins, tenascin, fibronectin, collagen) to the intracellular cytoskeleton. In the hematopoietic stem cell (HSC) niche, integrin $\alpha 9$ binds with high affinity the ECM protein tenascin-C and such interaction promotes HSC proliferation (Nakamura-Ishizu et al., 2012). Physicochemical aspects of the stem cell niche seem to be also involved in the control of stem cell fate (figure 1.4E). It has been reported that the level of oxygen to which stem cells are exposed could also promote self-renewal or differentiation. Wang et al. 2006, have indeed observed that the generation of murine ESC lines established from blastocysts was more likely to be successful and cells were more likely to express stem cell markers such as Nanog and Oct-4 when cultured under 5% O_2 compared to the 20% O_2 that is commonly used (Wang et al., 2006).

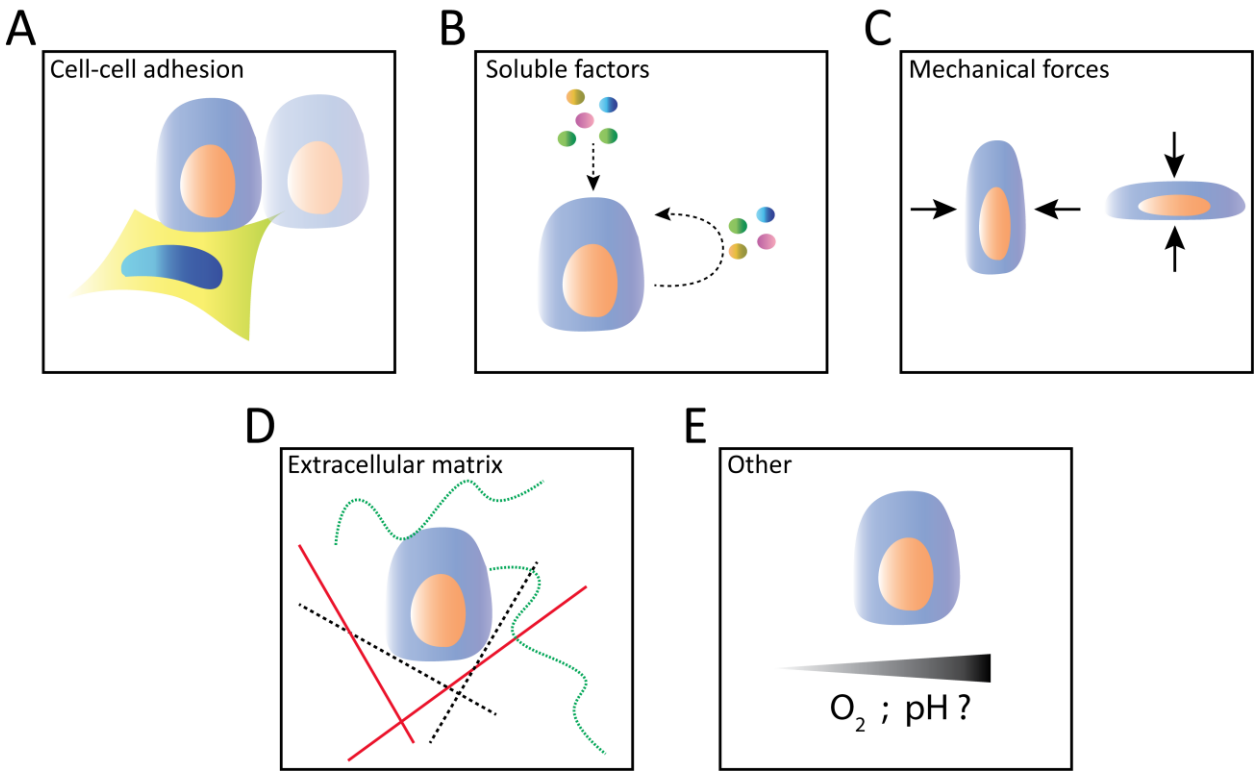

Figure 1.4 General concept and composition of the stem cell niche

A. Direct cell-cell interaction. B. Interaction mediated by soluble factors released by the stem cell itself (autocrine), niche cells in the vicinity (paracrine) or supplied by blood vessels (endocrine). C. Mechanical forces and rigidity of the local microenvironment can influence stem cell behavior in the niche. D. Interaction with the local extra-cellular matrix. E. Physicochemical features of the local microenvironment can influence the stem cell self-renewal and differentiation.

1.4.2 Human limbal epithelial stem cell niche

In mammals, epithelial stem cell niches have been successfully identified within the bulge of the hair follicle (Cotsarelis et al., 1990), the base of the crypt in the small intestine (Booth & Potten, 2000), the terminal bronchioles of the epithelial

airway (Giangreco et al., 2002) and within the limbus of the human cornea (Cotsarelis et al., 1989).

a) Corneal epithelial homeostasis: Thoft and Friend's XYZ hypothesis

Surface epithelia are constantly renewed throughout life. Whereas the human epidermis is regenerated approximately every month, it has been proposed that the half life of corneal epithelial replacement is about 9 weeks and that the whole corneal epithelium is renewed every 9 to 12 months (Sharma & Coles, 1989; Wagoner, 1997). Maintenance of the corneal epithelium is essential for vision and relies on LESCs located in the basal region of the limbus at the corneoscleral junction. LESCs have capacity for asymmetric division. Cells of the outer layers of the corneal epithelium are shed from the surface of the eye into the tear film and are continuously replenished by cells moving centripetally from the limbus (Figure 1.5).

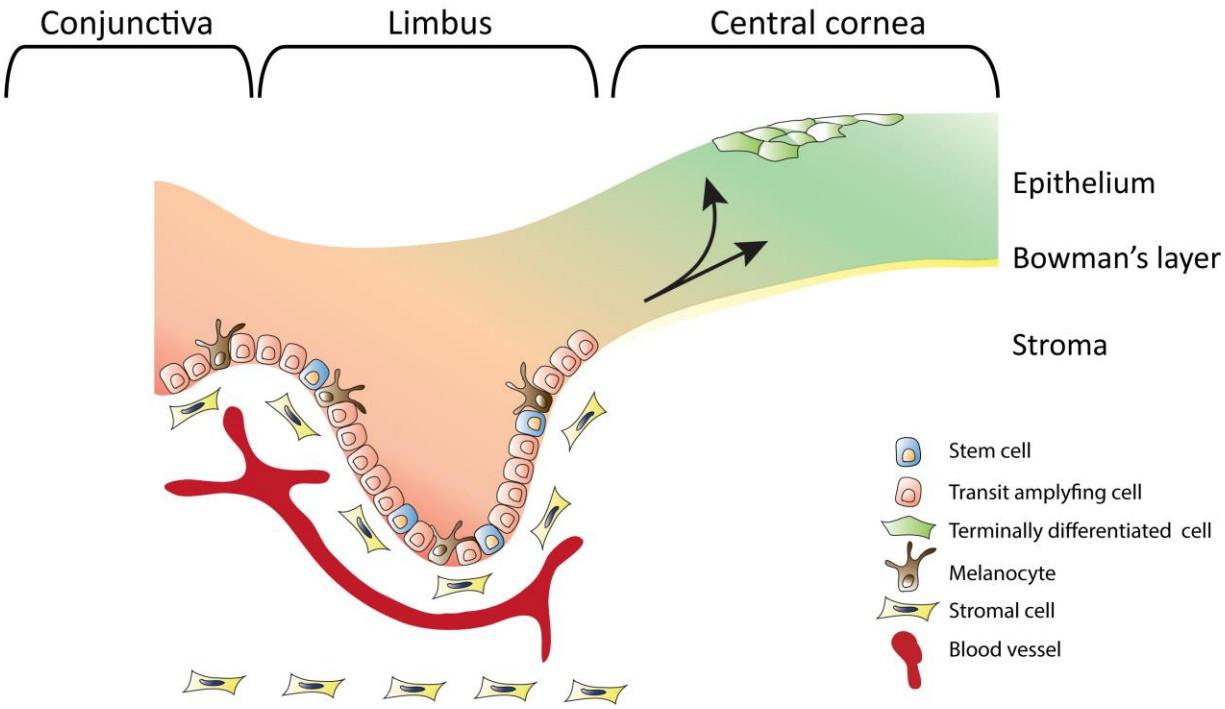

Figure 1.5 The human limbal stem cell niche

LESCs reside in the basal layer of the limbal epithelium. Daughter transient amplifying cells (TACs) divide and migrate centripetally towards the central cornea where they differentiate and slough from the ocular surface. The highly vascularized limbal niche is also populated with other cell types including stromal fibroblast-like cells and melanocytes.

In Thoft and Friend's model, the epithelial "cell mass" is maintained by three independent phenomena in which X describes the proliferation of the basal epithelial cells, Y the centripetal movement of the limbal (peripheral) cells and Z, cells shedding from the ocular surface representing the normal loss of cells (figure 1.6) (Thoft & Friend, 1983). LESCs self renew but also generate daughter TACs that have great proliferative potential. Transient amplifying cells migrate centripetally toward the central corneal epithelium. Once in the suprabasal layers, the TACs progressively become more differentiated, move vertically and

eventually become post-mitotic terminally differentiated cells and shed from the ocular surface (figure 1.6A).

b) New model of the corneal epithelial homeostasis.

In 2008, Majo et al. demonstrated that central corneal epithelial cells of mice and pigs contained cells exhibiting stem cell properties. Using the murine model, they observed that the transplant of a central corneal biopsy was sufficient to reconstruct the entire corneal epithelium of recipient mice in which portions of the limbus were excised. They also showed that cells from the central cornea were sufficient to maintain normal corneal homeostasis and that stem cells located at the limbus were only solicited after significant corneal damage or injury. Furthermore, the authors observed that porcine central corneal epithelial cells had the ability to generate holoclones *in vitro*. They finally concluded that corneal stem cells are distributed throughout the entire ocular surface in mammals and proposed a new model in which the limbus is a zone of equilibrium where stem cells extending from both conjunctival and central corneal epithelia are confronted in a mechanism reminiscent of tectonic plates (Majo et al., 2008) (figure 1.6B).

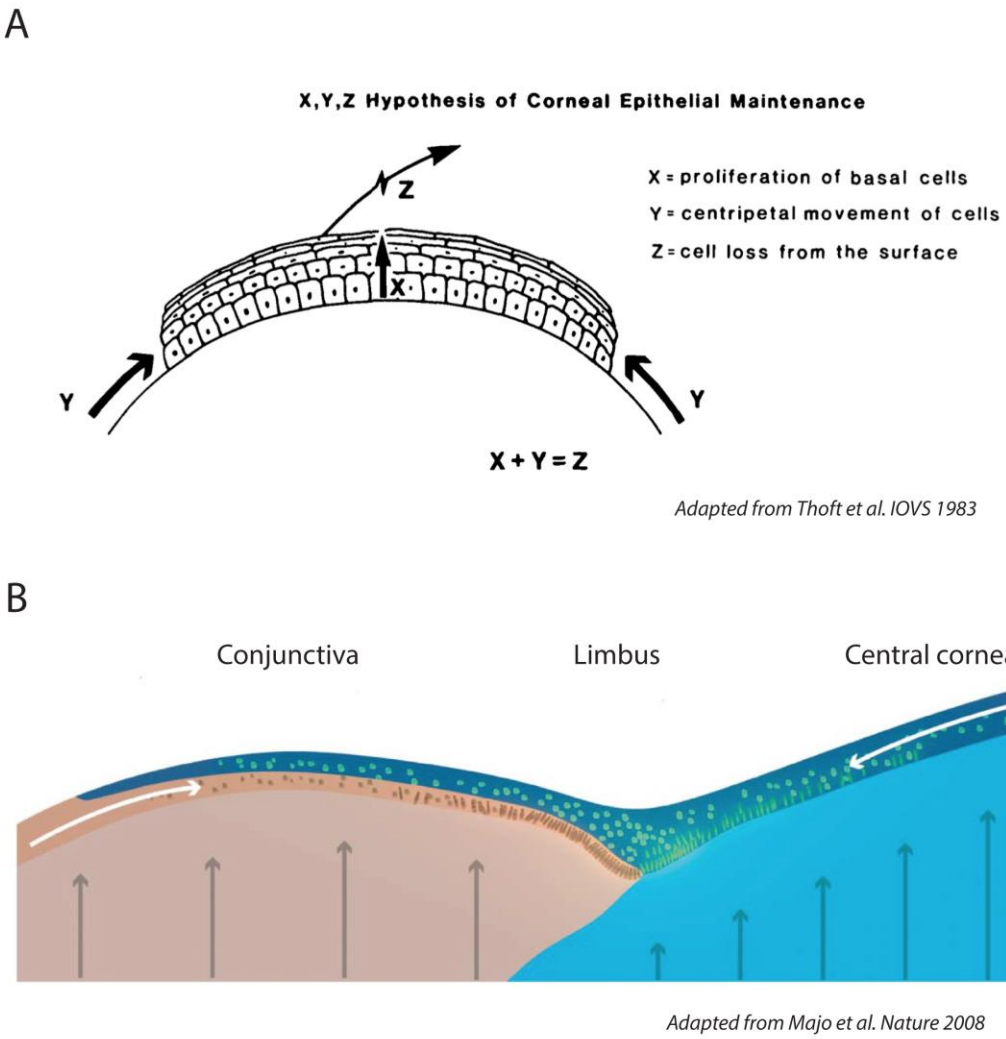

Figure 1.6 Corneal epithelial maintenance defined by two opposing models

A. Thoft and Friend's XYZ hypothesis of corneal maintenance. In this model, the corneal epithelial mass is maintained by three inter-related phenomena in which X corresponds to the proliferation of basal epithelial cells, Y the centripetal migration of peripheral cells, and Z cells shedding off the ocular surface.

B. The model described by Majo et al. implies the existence of stem cells within the central cornea that are sufficient to maintain normal tissue homeostasis. The limbus is proposed as a zone of confrontation between two opposite forces (white arrows) generated by the expansion of stem cells from both conjunctival and central corneal epithelia.

c) Cellular and molecular aspects of the limbal stem cell niche

The limbal stroma plays a critical role in down-regulating epithelial differentiation. Understanding the biology of the limbal stem cell niche is for this reason as important as understanding the biology of epithelial stem cell itself.. Espana et al. 2003, showed in the rabbit, that transplantation of epithelial sheets isolated from the central cornea onto the limbal stroma resulted in the loss of expression of the negative stem cell markers CK3 and connexin 43 normally present in the basal epithelial layer of the central cornea (Espana et al., 2003). Furthermore evidence of trans-differentiation of corneal epithelial cells into epithelial cells expressing markers of the hair follicle has also been suggested (Pearton et al., 2005). In this study, recombination of mouse embryonic dermis and rabbit central corneal epithelial cells has been performed. As a consequence, the authors observed repression of the transcription factor PAX6 in corneal epithelial cells responsible for the upregulation of critical signaling pathways such as Wnt, β-catenin and Lef-1. In addition, corneal cytokeratins 3 and 12 were progressively replaced by the skin cytokeratins, CK5 and CK14. These findings directly support the notion that the stem cell microenvironment is essential for the control and maintenance of the epithelial stem cell population.

Role of the extracellular matrix

The ECM composing the limbal stroma presents some unique features and is believed to be essential in maintaining limbal stem/progenitors in the niche. Ljubimov et al. 1995 observed heterogeneity in the composition of the epithelial basement membrane of the limbus and the central cornea. The basement

membrane of the central corneal epithelium was found to contain type IV collagen α3 and α5 chains whereas the limbal epithelium contained α1 and α2 collagen IV and α2, β2 laminin chains. Later, Shlötzer-Schrehardt et al. 2007, analyzed topographical variations of the basement membrane of the ocular surface by immunohistochemistry. Interestingly, the basement membrane of the limbal epithelium presented a patchy immunoreactivity for laminin γ3 chain, BM40/SPARC and tenascin C, which co-localized with ABCG2, p63, K19 positive and CK3, connexin 43, desmoglein, integrin α2 negative basal epithelial cell clusters. Vitronectin is a glycoprotein that is highly expressed within the limbal basement membrane but not in the central cornea or the conjunctiva. Echevarria et al. 2011, reported that limbal epithelial cells expanded on vitronectin-coated plates generated large holoclone like colonies and presented a higher colony forming efficiency than cells expanded on non-coated plates suggesting a potential role of vitronectin in supporting LESCs in the native niche.

Soluble factors and signaling pathways

LESCs communicate with their microenvironment in order to maintain self-renewal and direct cell fate. Different studies have shown that the cross-talk between LESCs and the surrounding niche cells involving paracrine factors and their receptors is crucial for maintenance of the stem cell phenotype. These include:

- Wnt canonical signaling pathway

The wnt signal transduction pathway regulates crucial aspects of cell fate such as migration, proliferation, differentiation and polarity. Wnt signaling plays a critical role in early stages of the embryonic development but also has a role in

the adult. Wnt are secreted glycoproteins that bind to the N-terminal extra cellular domain of the Frizzled (Fz) receptor family. Wnt binding to its receptor stimulates several intra-cellular transduction cascades including the Wnt/β-catenin canonical pathway. Upon activation, β-catenin is released by its inhibitory complex, accumulates and eventually translocates into the nucleus where it activates specific target genes. The Wnt signaling pathway has been demonstrated to be an important factor in various types of stem cells niches regulating stem cell proliferation and differentiation. In the intestinal stem cell niche, Wnt ligands are released by the myofibroblasts underlying the crypts where the epithelial stem cells reside. It has been observed that inhibition of Wnt signaling in this niche reduces proliferation of intestinal epithelial cells and induces loss of the crypts (Chen et al. 2011., ; Pinto et al., 2003). In the human ocular surface, Wnt2, Wnt6, Wnt11, Wnt16b are specific to the limbus where the LESC/progenitors are believed to reside. Moreover, nuclear localization of β-catenin has been observed in only a very small subset of basal cells at the limbus. *In vitro*, activation of wnt/β-catenin signaling increased the potential of LECs to generate secondary colonies that also maintained a stem cell phenotype as shown by high expression of ABCG2 and ΔNp63α (Nakatsu et al., 2011). Taking together, these findings strongly suggest that Wnt signaling is present in the human ocular surface and plays a potential role in regulation of LSCs/progenitors. Recently, it has been observed that Fz7 was preferably expressed by cells from the limbal basal epithelium and was co-localized with N-cadherin and p63α positive clusters. *In vitro*, when Fz7 was knocked down in LECs, the expression of the stem cell markers ABCG2 and ΔNp63α was reduced

significantly confirming the role of Fz7 in maintenance of the undifferentiated state of LESCs/progenitors (Mei et al., 2014).

- Stat3 and IL6 signaling pathway

In the human limbal crypts, limbal stromal fibroblast-like cells are localized immediately beneath the limbal epithelium in close proximity to the LESC/progenitors. In order to identify potential paracrine factors of epithelial/stromal interaction, Notara et al. developed an *in vitro* model of the limbal stem cell niche in which limbal fibroblasts were co-cultured with limbal epithelial cells in a serum free culture system. In this model, limbal fibroblasts were able to support expansion of LECs that maintained stem cell characteristics with the ability to generate large holoclone like colonies, a high secondary colony forming efficiency and the expression of stem cell markers such as p63α and ABCG2. Interestingly, it has been shown that Il6 expression was induced by LECs when co-cultured with limbal fibroblasts but decreased with LECs differentiation. In the native niche, immunohistochemistry revealed clusters of limbal epithelial cells and underlying stromal cells that were both positive for IL6, suggesting IL6 could potentially be involved in stromal/epithelial cell interaction *in vivo*. IL6 also induced Stat3 time dependent phosphorylation. When IL6 and Stat3 were separately inhibited, the secondary colony forming efficiency of LECs was considerably reduced confirming involvement of the IL6 Stat3 signaling pathway in maintenance of progenitor-like characteristics of LECs *in vitro* (Notara, Shortt, Galatowicz, Calder, & Daniels, 2010).

Cell-to-cell interaction

The limbal stroma is a complex environment that is highly vascularized, innervated but also populated by a mix of poorly characterized stromal cells. It is generally accepted that cells form the limbal stroma could have a potential role in the maintenance of LESC and are thus considered as important elements of the stem cell niche. In 2011, Chen et al. observed that epithelial cells isolated following collagenase digestion of human limbal biopsies maintained interaction with limbal stromal cells in culture. Interestingly, epithelial cells interacting with stromal cells *in vitro* were highly positive for the expression of stem cell markers such as p63α, had a small size and were able to generate large holoclone-like epithelial colonies. Moreover, epithelial cells isolated after collagenase digestion, which preserved the close interaction with the stromal cells, had the greatest potential to generate secondary colonies when reseeded and co-cultured on 3T3s compared to epithelial cells isolated with Dispase. Taking together, these observations suggest that epithelial-stromal cell interactions are an important factor for the maintenance of LESCs characteristics (Chen et al., 2011). In a further study, it has been shown that the attraction of PCK-/vimentin+ mesenchymal cells by PCK+/vimentin– limbal epithelial cells *in vitro* was mediated by SDF-1 and CXCR4 signaling and promoted sphere growth in matrigel. Interestingly, SDF-1 was highly expressed by limbal basal epithelial cells whereas limbal stromal cells located immediately beneath the limbal epithelium mostly expressed CXCR4 (Xie et al., 2011) . The authors suggested that the close contact between limbal epithelial and limbal stromal cells in the native niche is facilitated by SDF-1 CXCR4 signaling and that such interaction would support LESC function as observed during the “homing” phenomenon of

stem cells in other niches (Belmadani et al., 2005; Mazzinghi et al., 2008; Otsuru et al., 2008).

Melanocytes are neural crest-derived cells that have been intensively studied in the skin where they reside within the basal layer of the interfollicular epidermis and within the bulge of the hair follicle (Yamaguchi et al., 2007). To protect against ultraviolet radiation, melanocytes contain a specific organelle, the melanosome that contains melanin granules, a pigment that is delivered to the surrounding keratinocytes. Interestingly, melanocytes also localize within the limbal and conjunctival epithelium but are absent from the central cornea, possibly to preserve an optimal transparency of the tissue. It has been reported that in the human ocular surface, the ratio of melanocytes to CK19+ve limbal epithelial cells was about 1:10, which is approximately 3-fold higher than the average melanin unit of the skin (Hadley & Quevedo, 1966; Higa et al., 2005). This high population of melanocytes and the significance of a pigmented limbus still remain poorly understood. In addition to a protective role against UV radiation (Shimmura et al. 1996; Doutch et al. 2012), an emerging concept suggests that melanocytes could also potentially interact and maintain LESCs in the niche. In 2007, Hayashi et al. presented evidence that N-cadherin was expressed by a sub-population of melanocytes and limbal epithelial cells that were also positive for the expression of stem cell markers such as p63, Bmi-1, CK15 and ABCG2. Therefore, the authors suggested that LESCs could directly interact with melanocytes through N-cadherin homotypic adhesion and that such an interaction would maintain the slow cycling properties and stem cell characteristics of LESC in their niche (Hayashi et al., 2007). Homotypic N-cadherin cell-to-cell adhesion has been further investigated *in vitro*.

Interestingly, N-cadherin positive limbal epithelial cells in culture concentrate at the periphery of the epithelial colony, in close proximity to the 3T3 feeder fibroblasts whereas N-cadherin –ve cells are more likely located in the middle and present a more differentiated phenotype. In order to determine weather N-cadherin was functionally required to maintain progenitor cells, 3T3 cells transfected with N-cadherin siRNA were used as feeders for the expansion of limbal epithelial cells. When compared to untransfected 3T3s, limbal epithelial cells cultured with "N-cadherin low" 3T3s generated smaller epithelial colonies with significantly lower secondary colony forming potential. Taken together, these data demonstrate the requirement of N-cadherin in preserving the limbal epithelial phenotype *in vitro* suggesting a functional role for N-cadherin and the importance of direct cell-to-cell interaction in the native limbal stem cell niche.

d) Anatomical features of the LESC niche

Palisades of Vogt (POV)

The palisades is a term first used by Vogt to describe radial striae observed at the limbus. Despite considerable variations from one individual to the other, the limbal palisades usually measure between 0.5 and 0.9 mm in length (Graves, 1934; Townsend 1991) and are most frequently observed at the upper and lower limbal arcs (Goldberg & Bron, 1982). The palisades are easily identified in pigmented individuals because of a concentration of melanin-containing cells lining the interpalisade ridges. However, Goldberg and Bron 1982, reported that in some lightly pigmented individuals, limbal palisades could not observed. The authors also reported that the distribution of the palisades from one eye to the

other is symmetrical in the same individual. These structures appear more prominent in young individuals and become more discrete with age (Zheng & Xu, 2008). The shape of the palisades is also very varied: Golberg and Bron described them as long and narrow rectangles that sometimes appear as tiny circles and ovals. Histologically, the interpalisades appear as thick grooves filled by epithelial cells and correspond to the limbal crypts that will be discussed further in this chapter (Shortt et al., 2007). The palisades are highly populated by a radially oriented vascular complex. It has been proposed that the palisade vessels supply the metabolic needs of the large amount of epithelial cells populating the interpalisade grooves.

Limbal epithelial crypts

In 2005, Dua et al. described for the first time a novel anatomical structure of the human limbus that they named the "limbal epithelial crypt" and proposed it as a stem cell niche for the limbal epithelial progenitors. Five human cadaveric corneas aged between 17 and 75 years old were histologically serially sectioned and this unique anatomical structure was identified at the limbus of all specimens studied. Limbal epithelial crypts extended from the peripheral aspects of an interpalisade rete ridge and further extended into the conjunctival stroma as a solid chord of cells measuring up to 120 μm in length (Figure 1.7A and B). Immunohistochemical analysis revealed that all cells populating the limbal epithelial crypts were highly +ve for the expression of the stem cell marker ABCG2 (Dua, 2005). In 2007, Shanmuganathan et al. further characterized the anatomy of the LEC in the human eye. Among 8 human corneo-scleral rims analyzed, 74 limbal epithelial crypts were identified with an

occurrence that varied between donors ranging from 4 to 13 per cornea. The limbal epithelial crypts varied in size and seemed to be uniformly distributed around the corneal circumference. For this reason, these observations do not correlate with the distribution of the POV that are mainly present within the superior and inferior segments of the limbus. Immunohistochemistry revealed that cells populating the limbal epithelial crypts were mainly CK3 –ve, Ck19 +ve, CK14 +ve, CD34 –ve, Vimentin +ve, p63 +ve and connexin 43 (Cx43) +ve. Interestingly epithelial cells populating these structures expressed Cx43 that is believed to be a negative marker for LESCs whereas limbal areas devoid of these structures appeared Cx43 -ve (Shanmuganathan et al., 2007). They finally concluded that Cx43 could potentially be a marker for the real LESCs as other studies reported involvement of connexin43 in stromal support in the hematopoietic stem cell niche (Cancelas et al., 2000).

Limbal crypts

Limbal crypts (LCs) are another structure of the human limbus that has been proposed to be a niche for LESCs of the ocular surface. The following section will only discuss the morphological aspects of these structures as their functional properties as a stem cell niche will be covered in detail in the chapter 3 of this thesis.

In 2007, Shortt et al. characterized the interpalisadal grooves observed by Goldberg and Bron that they named “limbal crypts”. LCs have been described by the authors as “Distinct invaginations of epithelial cells extending from the peripheral corneal epithelium into the corneal limbal stroma”. These structures are similar to the rete pegs of the epidermis and correspond to downward

projections of the limbal epithelium into the limbal stroma (Figure 1.7 C and D). High-resolution microscopy including scanning electron microscopy (SEM) analysis on decellularized corneal limbal biopsies revealed the manner in which the limbal stroma encloses the limbal crypts laterally. Immunohistochemistry highlighted the presence of a complex vascular plexus that is intimately associated with the LCs. The limbal stroma that surrounds the LCs is also highly vascularized and contains a high population of stromal cells. Similarly to the limbal palisades, LCs seem to be predominantly located in the superior and inferior limbal quadrants and could not be observed in the horizontal meridian of all individuals studied (Shortt et al., 2007).

Focal stromal projections

Focal stromal projections (FSPs) have been described as finger-like projections of the limbal stroma into the limbal epithelium containing a central blood vessel. Unlike the LCs describing grooves extending radially through the limbus, FSPs correspond to a focal protrusion of the limbal stroma into the limbal epithelium (Figure 1.7 E and F). The authors observed that basal epithelial cells directly adherent to FSPs were significantly smaller in diameter and had a higher nucleus/cytoplasm ratio when compared to suprabasal cells immediately adjacent to them (Shortt et al., 2007).

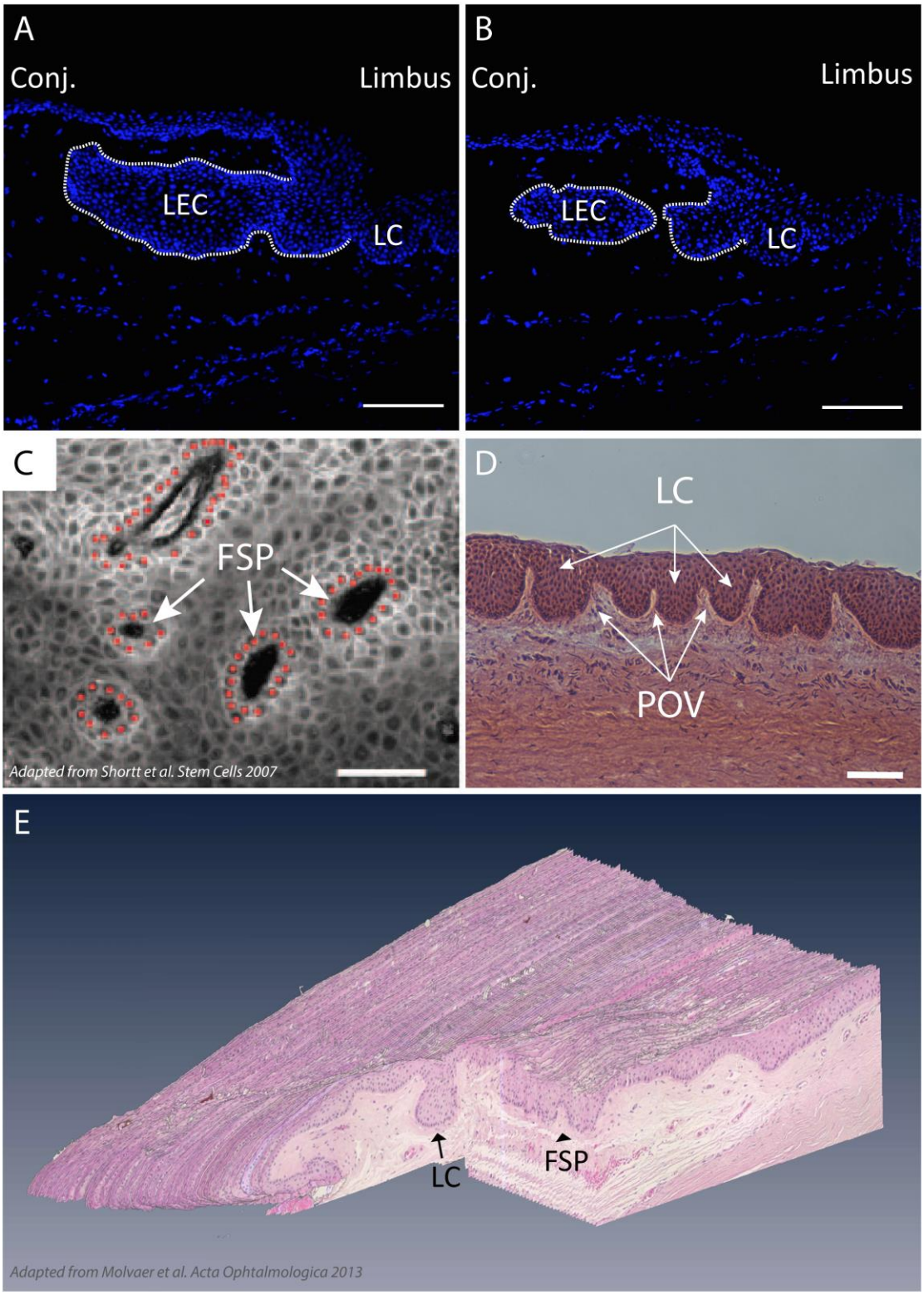

Figure 1.7. Anatomical features of the human limbal epithelium.

A. Limbal epithelial crypts appear as large extension of the limbal epithelium into the conjunctival stroma. Serial sectioning (B) reveals limbal epithelial crypts (labeled LEC) detach from the limbus as a solid

chord of epithelial cells as previously described by Dua et al. Note the presence of limbal crypts (LC) in the vicinity of the limbal epithelial crypt.
C and D. En face section of focal stromal projections (C) and tangential section of limbal crypts (D) described by Shortt et al.
E. 3D model of the limbal stem cell niche highlighting FSP and LC ultrastructure (Molvaer et al., 2013)**.**
Scale bars: 100μm A, B, D. 50μm C-F.

e) Stem cell activity in the developing human cornea

The human cornea starts to develop 6 weeks after gestation and its development involves the interaction of the lens vesicle with the overlying ectoderm. The cornea-scleral junction appears at the end of the embryonic development by gestational week 11. Immaturity of the fetal central corneal epithelium has been attributed to weak expression of CK3. Cells populating the fetal corneal epithelium are highly positive for Ki67 suggesting a rapid expansion of the tissue in early gestational age. The percentage of Ki67 +ve cells however decreases after 22 weeks gestation. Proliferative corneal epithelial cells are mainly confined in the limbal area but no specific "crypt-like structures" are identifiable at this stage. It has thus been proposed that the limbal POV are anatomical features that develop at least 4-months post-natally. These observations are consistent with previous studies suggesting that development of the human cornea continues until 6 months after birth (Lesueur et al., 1994). However, a ridge-like elevation circumscribing the fetal human cornea around 12 weeks gestation has been reported. If not a distortion artifact due to the dehydration of the tissue that involves SEM imaging, authors reported that these newly identified "limbal ridges" house most of the stem cells after 20 weeks gestation

as suggested by immunohistochemistry showing CK15 +ve clusters specifically populating this area. As shown in figure 1.8 they further suggested that these structures could potentially evolve into the limbal POV postnatally as a result of physical stress enforced by ocular and eyelid motion (Davies et al., 2009).

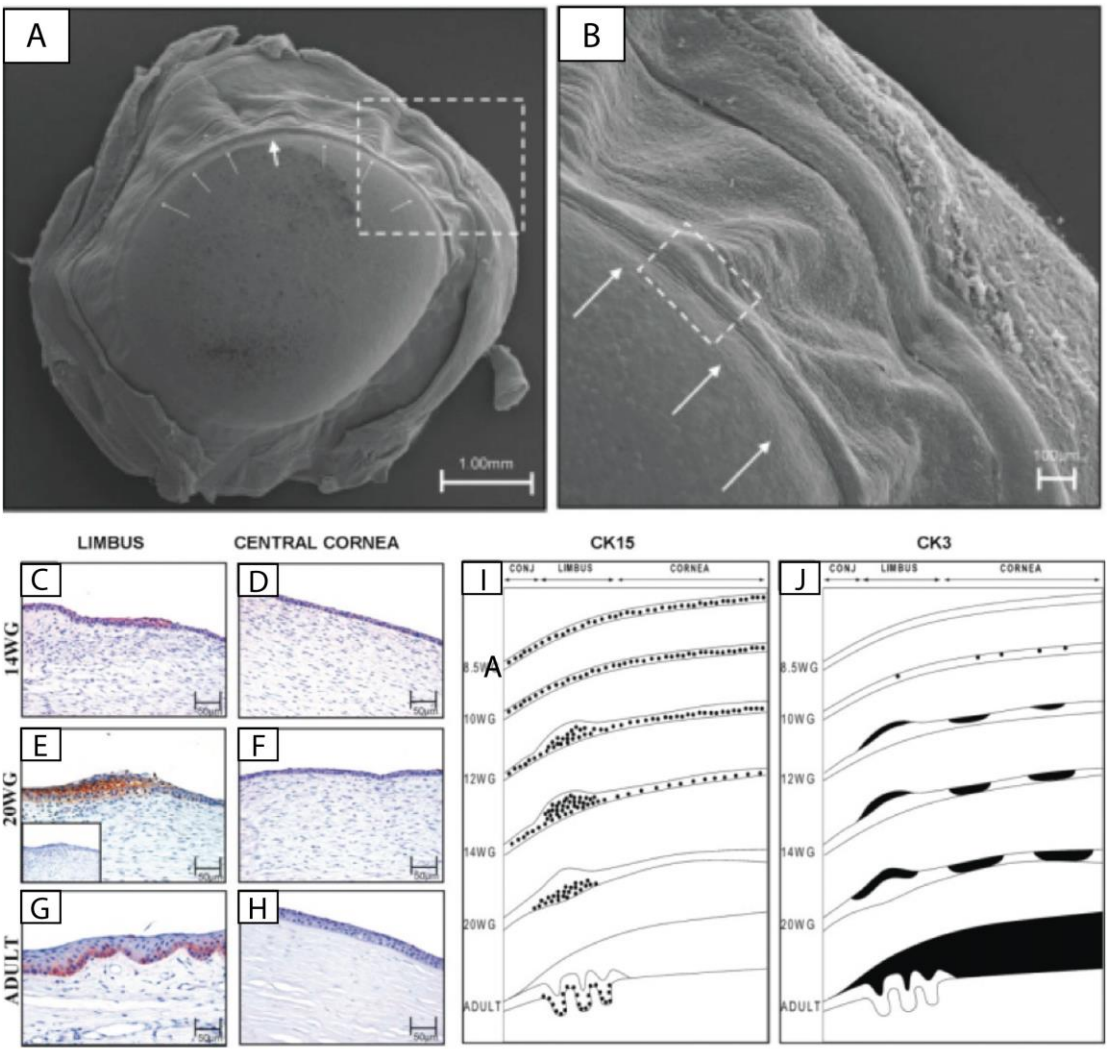

Adapted from Davies et al. 2009, Stem cells

Figure 1.8 Stem cells in the developing human cornea.

A and B, scanning electron micrographs illustrating limbal ridges observed at the limbus after 20 weeks gestation. C-H Immunohistological analysis of distribution of CK15 +ve cells in 14 weeks, 20 weeks gestation and adult limbus and corneas. I-J Model of formation of limbal ridges and POV from 8.5 weeks gestation to adult including distribution of CK15 and CK3 epithelial cells.

f) Limbal epithelial stem cells and ageing

The effect of age on stem cell niches has been reported in various human organs including the hematopoietic stem cell niche, the skin and the dental pulp stem cell niche (Gago et al., 2009; Wagner et al., 2008; Zheng et al., 2009). In the human ocular surface, Zheng and Xu, 2008, reported age-related changes in the POV. After slit-lamp examination of 160 healthy subjects, the limbal POV, in which limbal crypts are concentrated, could only be detected in 40% of the subjects aged 60 years and above whereas the presence of POV was above 97% in subjects aged between 0 and 19 years (Zheng & Xu, 2008). Further *in vitro* analysis revealed that the proliferative potential of limbal epithelial cells in culture significantly decreases with age suggesting that the loss of the limbal palisades and the limbal architecture is directly correlated to the loss of potency of the limbal progenitors (Notara, et al., 2012).

1.5 Consequences of limbal stem cell failure and stem cell therapy

1.5.1 Limbal stem cell deficiency

Failure of limbal stem cell function results in a disease state termed limbal stem cell deficiency (LSCD). LSCD can be partial or total and leads to loss of functional integrity of the corneal surface. LSCD can arise from chemical (alkali/acid) injuries, thermal burn or through diseases such as Steven Johnson syndrome and aniridia (Chen & Tseng, 1991). As a result, neighboring conjunctival epithelial cells, which normally are held at the limbal boundary, migrate over the corneal

surface. This conjunctivalisation is followed by neo-vascularization, inflammation and opacification of the central cornea eventually leading to blindness. One example of primary disorder leading to LSCD is the heritable eye disease aniridia that is genetically associated with mutations of PAX6. *Pax6* haploinsufficiency results in abnormal eye development including iris anatomy defects, foveal hypoplasia, optic nerve hypoplasia, nystagmus, glaucoma, cataracts and aniridic-related keratopathy (ARK). ARK occurs in 90% of individuals with aniridia by their early teenage years (Nishida et al., 1995) . The disease is manifested by a thick and irregular peripheral epithelium and is followed by a superficial neovascularization, sub-epithelial fibrosis and stromal scarring. The corneal stroma is infiltrated with inflammatory cells and destruction of the Bowman's layer is also observed. Conjunctival epithelial and goblet cells are observed on the corneal surface and these manifestations have lead to the consensus that limbal stem cell deficiency is responsible for the corneal abnormalities in aniridia (Secker & Daniels, 2008). Contact lens-associated limbal stem cell deficiency has also been reported and this could be either the result of cytotoxicity of the contact lens solution or the result of mechanical friction and inflammation of the limbus (Clinch et al., 1992).

1.5.2 Limbal epithelial stem cell therapy and tissue engineering

Traditional corneal transplantation cannot be used as a treatment to cure limbal stem cell deficiency due to the lack of stem cells in the epithelium of the transplanted central human corneal button. Allogeneic corneal transplantation can only restore the corneal transparency temporarily as conjunctival invasion

eventually resurfaces the corneal epithelium. Kenyon and Tseng, 1989, proposed that LSCD could be successfully treated using limbal tissue grafts. However, this procedure presented numerous disadvantages as it involves the use of a large sample of limbal tissue from the donor eye (in the case of unilateral LSCD) with the risk of causing LSCD at the source. For bilateral lesions, limbal transplantation requires long-term immunosuppression that involves risks of infection and systemic complications (Ilari & Daya, 2002). In 1997, Pellegrini et al. reported for the first time that for patients with unilateral burns smaller limbal biopsies could be removed from the healthy eye and limbal epithelial cells pre-expanded *in vitro* using growth arrested 3T3 feeder cells. The resulting epithelial sheet was then transplanted into the recipient eye after removal of the conjunctival tissue from the corneal surface and the outcome persisted after the initial engraftment with an up to 10 years follow-up (Pellegrini et al., 1997; Rama et al. 2010).

More recently, bioengineered carriers for the expansion of autologous LESCs *in vitro* have been developed. Bioengineered substrates must fulfill many criteria in order to be suitable for transplantation and corneal repair. The ideal substrate should be optically transparent, strong and flexible enough to be easily manipulated and set on the ocular surface, to be non-immunogenic and cytocompatible for the expansion of limbal epithelial progenitors maintaining stem cell properties.

a) Human amniotic membrane

The human amniotic membrane (hAM) is currently the most commonly used carrier for the cultivation of limbal epithelial cells prior to engraftment onto the

diseased eye. Amniotic membrane is the innermost layer of the placental membrane which consists of a monolayer of epithelial cells, a thick basement membrane and an avascular stroma (Grueterich, Espana, & Tseng, 2003). After being decellularized, the non-immunogenic amniotic membrane can be used as a biological substrate for the expansion of limbal epithelial cells in the presence or absence of 3T3 feeder cells (Mariappan et al., 2010; Tsai, Li, & Chen, 2000). The success of hAM for the culture and transplantation of limbal epithelial cells is not fully understood. It has been proposed that the hAM might provide cytokines and other growth factors or various anti-inflammatory proteins, which together could play a crucial role in maintaining limbal stem cell characteristics (Dua, Gomes, King, & Maharajan, 2004; Koizumi et al., 2000). Moreover, the hAM basement membrane contains type IV and type VII collagens, and fibronectin that play an important role for epithelial cell adhesion to the substrate and prevents epithelial apoptosis. Despite these favorable qualities, hAM also presents a number of drawbacks associated with its use including the lack of reliable supply of tissue, considerable donor variations and more importantly, a lack of optimal transparency that is directly correlated to the origin of the tissue (proximal or distal to the placenta) (Connon et al., 2010). For these reasons, many alternatives to hAM using bioengineered substrates for the culture of corneal epithelial cells have been investigated.

b) Fibrin scaffolds

Fibrin is a natural degradable substrate that can be fabricated into gels by combining fibrinogen and thrombin. Fibrin gel scaffolds have been successfully used as a carrier for epithelial cell expansion. Rama et al. 2001, reported that

fibrin gels could support the culture of limbal stem cells and that these constructs were used successfully to treat 14 of 18 patients who received a transplant (Rama et al., 2001 and 2010). Later, Talbot et al. observed that rabbit limbal epithelial cells isolated from small limbal biopsies generated epithelial sheets on fibrin gels that were suitable for transplantation after only two weeks; three Days after transplantation the fibrin gels were degraded and a complete functional epithelium was restored in one month (Talbot et al., 2006).

c) Collagen based carriers

Collagen-based carriers are potentially an ideal substrate for limbal epithelial cell expansion since collagen is a major constituent of native human cornea. Moreover, collagen presents various favorable properties such as a low immunogenicity, biocompatibility and is relatively inexpensive to isolate. Collagen hydrogels can be cross-linked to increase their resistance to degradation without affecting their transparency (Dravida et al., 2008). Griffith et al. successfully produced a whole human cornea equivalent by combining type I collagen-chondroitin sulfate with glutaraldehyde and by seeding epithelial cells on top of the construct, endothelial cells at the bottom and stromal cells within the construct (Griffith et al., 1999). Later, cross-linked collagen gels consisting of type III collagen blended with 1-ethyl-3 carbodiimide and N-hydroxysuccinimide were used for the culture of primary human limbal epithelial cells as a replacement for hAM. The scaffold was optically transparent and robust enough to withstand manipulation in culture and surgery and, more importantly,

supported epithelial cells expressing stem and differentiated cell markers in a similar fashion to cells grown on hAM (Dravida et al., 2008).

Collagen hydrogel could also be compressed by using highly hydrophilic absorbers. Removing water from the hydrogel increases the mechanical strength without the need for crosslinkers that could reduce biomimetic qualities of the construct and increase cytotoxicity. In 2010, Levis et al. showed that 100-150μm type I compressed collagen gels could support expansion and multilayering of limbal epithelial cells similar to the human corneal epithelium. Plastic compressed collagen tissue equivalents that mimic aspects of the natural corneal environment facilitated attachment of limbal epithelial cells onto the scaffold, were easy to handle and did not affect viability of the epithelial and stromal cells that remained functional in the construct. This process has been recently improved and is now referred as Real Architecture For 3D tissue or RAFT (Levis, Massie, Dziasko, Kaasi, & Daniels, 2013). RAFT collagen constructs provide a convenient tissue equivalent for culturing limbal epithelial cells and understanding behavior of the limbal progenitors in a 3D microenvironment in which fibroblasts or other 'niche cells' can be easily incorporated. However, without fibroblasts incorporated within the construct, RAFT tissue equivalents lack basement membrane components required for optimal epithelial cell adhesion and stem cell maintenance. The new collagen tissue equivalent model takes in consideration the compliance requirements for production in good manufacturing practice facilities and could in the future be suitable for transplantation for ocular surface repair.

1.6 Conclusion and aims

The cornea is an ideal model to study epithelial stem cell biology because it has a readily accessible source of progenitor cells located around the limbal circumference (Tseng, 1989). Despite great advances in our understanding of the limbal stem cell biology over the last decade, reliable markers that can differentiate stem cells from the early TACs have not yet been identified. For this reason, the exact location of the human LESC niche remains unclear and controversial (Dua, 2005; Shanmuganathan et al., 2007; Shortt et al., 2007). The advent of powerful high-resolution imaging techniques have led to discoveries of new limbal structures that have been suggested as physical niches carrying the limbal epithelial progenitors (Shortt et al., 2007). Among these structures, limbal crypts located between the limbal POV are easily observable under a dissecting microscope. Thus, crypt-rich limbal biopsies can be easily isolated and limbal epithelial cells from this area expanded *in vitro.*

If the LCs constitute a niche for LESCs, epithelial cells populating these structures should express the newly identified stem cell markers and show the highest clonogeneic potential, with the ability to generate holoclones when put in culture (Barrandon & Green, 1987).

Interaction between LESCs and their microenvironment (niche) are the subject of important investigations *in vitro.* It has been shown in culture that the association of epithelial and stromal cells enhances the stem cell properties of the epithelial progenitors. However, the existence of such association in the native niche has not been investigated yet. For this reason, high-resolution electron microscopy, which permits imaging beyond the limits imposed by the

wavelength of light, has been further applied to image the previously described limbal crypts. Despite a great resolution in X and Y reached by conventional transmission electron microscopy (TEM), defining the nature of the focal interactions between epithelial and stromal cells would be facilitated with a higher resolution imaging in the Z direction. Thus, volume electron microscopy has been further applied to image and reconstruct in 3D the putative interactions occurring between the epithelial progenitors and their surrounding niche cells. After observing a close association between basal limbal melanocytes and epithelial progenitors, it was hypothesized that in addition to their protective role against UV radiation by the release of melanin, limbal melanocytes could also act as niche cells preserving LESCs in an undifferentiated state (Hayashi et al., 2007). Therefore, isolation of limbal melanocytes from human cadaveric biopsies was performed and the isolated cells were further used as a feeder layer for the potential expansion of LECs *in vitro*.

Therefore aims of this thesis were:

- **To discover if the LCs constitute a niche or LESCs of the ocular surface**
- **To represent a 3D model at the cellular level of the LESC niche**
- **To investigate whether or not LESCs are physically associated with underlying stromal niche cells in the niche**
- **To examine the role of melanocytes as niche cells for the maintenance of LESCs**

Chapter 2: General material and methods

2.1 Human tissue and ethics statement

All human tissue was handled according to the tenets of the Declaration of Helsinki and written consent was acquired from next of kin of all deceased donors regarding eye donation for research. Research consent was obtained via the Moorfields Eye Hospital Lions Eye Bank (UK) http://www.moorfields.nhs.uk./Aboutus/Clinicalsupportservices/Eyebank and Lions Eye Institute (Florida, US) http://www.fleb.org/. All experiments were approved by the National Research Ethics Service, Southwest 3 REC, reference 10/H0106/57.

2.2 Cell culture

2.2.1 Culture and maintenance of 3T3 fibroblast feeder cells

3T3-J2 mouse irradiated embryonic fibroblasts were kindly provided by Prof. Fiona Watt and are referred to as 3T3 feeder cells. 3T3s were used as a feeder layer for the expansion of limbal epithelial cells. These fibroblasts were maintained in Dulbecco's modified Eagle medium (DMEM, Life Technologies, Paisley, UK) supplemented with 10% Adult Bovine Serum (ABS; Sigma-Aldrich, Dorset, UK) and 1% Antibiotic-antimycotic (Sigma-Aldrich, Dorset, UK). Culture medium was changed three times a week and the culture passaged upon reaching upon 90% of confluence. The cultures were maintained at 37^0C in an atmosphere containing 5% CO_2 in air.

a) Cryopreservation of 3T3 fibroblasts feeder cells

When reaching confluence, 3T3 feeder cells were detached using 0.05% Trypsin-0.02% EDTA, stained with trypan blue (Life Technologies, Paisley, UK) and counted. The cryopreservation medium consisted of 70%(v/v) 10%ABS-DMEM, 20% (v/v) FBS and 10% (v/v) dimethyl sulfoxide (DMSO). Cells were resuspended in cryopreservation medium and transferred into 1ml cryovials ($1x10^6$ cells/cryovial) (Fisher scientific, Loughborough Leicestershire, UK). Vials were transferred into a freezing container (Mr Frosty, Nalgene) at -80°C for optimal cryopreservation (-1°C per minute cooling rate) and stored in liquid nitrogen at -196°C.

b) Growth arrest of 3T3 feeder cells

When reaching 80% confluence, 3T3 feeder fibroblasts were incubated with mitomycin C (Sigma-Aldrich, Dorset, UK), at a concentration of 4μg/mL in 10% ABS-DMEM, for 2.5 hours at 37^0C. Growth arrested fibroblasts were then washed three times with Phosphate-Buffered Saline (PBS) and returned to 10% ABS-DMEM. Cells were detached in the next day by using 0.05% Trypsin-0.02% EDTA and seeded on a new culture plate/flask at a cell density of $2.4x10^4$ cells/cm^2. Cells were allowed to attach for at least for 3 hours prior to seeding LECs on top.

2.2.2 Cell counting with Neubauer hemocytometer

A hemocytometer (Neubauer chamber) was used to perform LECs or 3T3s cell counting. Cells were detached with the appropriate trypsin-EDTA concentration (0.05% for 3T3s and 0.5% for LECs), resuspended in 10 ml of culture medium

and centrifuged for 5 minutes at 100g. The cell pellet was then suspended in 1 ml of the appropriate culture medium and 10 μl of final cell suspension was mixed with 10 μl of trypan blue (for viability assessment) (0.4%, Life Technologies, Paisley, UK). All trypan-blue unstained cells in the central large square were counted. Neubauer chamber's counting grid is 3 mm x 3 mm in size. The grid has 9 square subdivisions of width 1mm. The central square is split in 25 squares of 0.2mm width containing each 16 squares and was used to perform cell counting. The central big square area is 0.1 cm x 0.1 cm = 0.01cm^2. Since the depth of the chamber is 0.1mm, the volume of one the central big square is 0.01 cm^2 x 0.1 cm = 0.0001 cm^3 = 0.0001 ml. As the trypan blue introduces a dilution factor of 2 to the cell suspension, the final cell concentration (Cells/mL) is determined by the formula:

$$Concentration\ (Cell/mL)$$
$$= Number\ of\ unstained\ cells\ (large\ central\ square) \times 10.000 \times 2$$

2.2.3 Isolation of human limbal epithelial cells

Human corneo-scleral rims were cut into four equal pieces and transferred into a solution containing 1.2 U/mL dispase II (Roche Diagnostics GmbH, Mannheim, Germany) in corneal epithelial culture medium (CECM) and incubated for 2 hours at 37°C or overnight at 4°C. Epithelial cells from the crypt-rich and non-crypt rich limbal tissues were then gently scraped with the point of thin forceps and transferred in small T25 cell culture flasks containing a feeder layer of growth arrested 3T3s at a density of 2x10^4 cells/cm^2. Co-cultures were maintained in corneal epithelial culture medium (CECM) (section 2.2.4).

2.2.4 Culture of primary human limbal epithelial cells

Limbal epithelial cells were seeded on top of growth arrested 3T3s and maintained in corneal epithelial cell culture medium (CECM) containing a 1:1 ratio of DMEM:F12, 10% (v/v) fetal bovine serum, 100 U/mL penicillin, 100 µg/mL streptomycin, 0.25 µg/mL Fungizone, epidermal growth factor (EGF) 10 ng/mL (Life technologies, Paisley, UK), hydrocortisone (0.4 µg/mL), insulin (5 µg/mL), adenine (0.18 mM), transferrin (5 µg/mL), T3 (2 nM), cholera toxin (0.1 nM) (Sigma-Aldrich, Dorset, UK) and incubated for 2 hours at 37°C. LECs were expanded in T25 flasks on a 3T3 feeder layer that had been previously growth arrested with 4µg/mL mitomycin C (Sigma-Aldrich, Dorset, UK) for 2 hours. CECM culture medium was changed three times a week and the co-cultures maintained at 37°C in a humidified atmosphere containing 5% CO_2 in air.

2.2.5 Routine visualization of cell morphology in culture

Epithelial cell morphology was imaged using an inverted phase contrast microscope (Nikon Eclipse TS100 inverted phase contrast microscope, Nikon Instruments Europe B. V., Surrey, UK)

2.2.6 Rhodamine staining of epithelial colonies

After being fixed with 4% paraformaldehyde (PFA) for 10 minutes, culture plates containing epithelial colonies were rinsed with PBS and stained with a solution containing 1% rhodamine (Sigma-Aldrich, Dorset, UK) for 10 minutes. Finally, culture plates were rinsed with dH_2O and imaged on a light box.

2.3 Measurement of epithelial colonies and statistical analysis

2.3.1 Colony forming efficiency assays

LECs were isolated and pre-expanded on either 3T3 fibroblasts or human limbal melanocytes. When reaching about 80% confluence, cells were washed with PBS and 3T3 feeder cells were detached using 0.05% Trypsin-0.02% EDTA and discarded. Then, limbal epithelial cells were detached using 0.5% Trypsin-0.2% EDTA for 4 min at 37°C in order to prepare a single cell suspension.

For secondary colony forming efficiency analysis, limbal epithelial cells were seeded at 1,000, 500 and 250 cells/well in six well plates containing growth arrested 3T3 feeder cells. Culture medium was changed every other day and cells were fixed when single colonies started to merge between 10 and 12 days of culture. Colonies were fixed for 10 min in 4% PFA washed and stained with 1% rhodamine. Plates were finally photographed on a light boxed and analyzed with ImageJ software. Proliferative colonies with a circular morphology and smooth borders were counted to determine the colony forming efficiency. The total colony forming efficiency was calculated using the equation:

$$CFE\ (\%) = \frac{Number\ of\ colonies}{Number\ of\ cells\ seeded} \times 100$$

2.3.2 Measurement of nucleus/cytoplasm ratio

The area of nucleus and cytoplasm of limbal epithelial cells in culture was determined using the free hand selection tool on epithelial culture images in ImageJ software. For one cell, nucleus/cytoplasm (NC) ratio was calculated by dividing the area of the nucleus by the area of the cytoplasm. For each

experiment, NC ratio was calculated in 200 randomly selected cells in 5 distinct areas of the culture plate.

2.3.3 Measurement of limbal epithelial colonies

The area of epithelial colonies stained with 1% rhodamine was measured using the freehand selection tool in ImageJ software. By knowing the exact diameter of the culture plate, it was possible to determine accurately the diameter of macroscopic epithelial colonies with imageJ.

2.3.4 Measurement of cell density

The number of cells/mm^2 were counted using ImageJ software. Phase contrast images with a confluent field of view of epithelial cells were randomly taken. A minimum of five images taken on different areas of the same culture plate was analyzed for each culture condition.

2.3.5 Statistical analysis

Student's t test was performed to analyze CFE, cell density and N/C ratio. Bar graphs representing mean $\pm$ standard error of the mean were plotted. A p value of $p < 0.05$ was considered to represent a statistically significant difference.

2.4 Preparation of collagen solution and RAFT collagen tissue equivalents

2.4.1 Preparation of collagen solution

The collagen solution was prepared by mixing 80% v/v sterile rat tail collagen type I at 2mg/ml; First link, Birmingham, UK) with 20% v/v 10x Minimum Essential Medium (MEM) (Life technologies, Paisley, UK). The collagen solution was then neutralized with 5M sodium hydroxide solution and set on ice for 30 min to prevent gelling while allowing dispersion of any small bubbles.

2.4.2 Preparation of RAFT tissue equivalents

A volume of 2.4 ml of the freshly prepared collagen solution was transferred into wells of 24 well plates and placed on a heater (TAP Biosystems, Royston, UK) set to 37°C for 30 min to allow fibrillogenesis. Once the collagen hydrogels were formed, highly hydrophilic porous absorbers (TAP Biosystems, Royston, UK) were applied to the surface of the hydrogels. The liquid in the collagen hydrogel was gently removed by capillary action during a 30 min absorption process.

2.5 Immunohistochemistry

2.5.1 OCT embedding, cryosectioning and histological analysis

Limbal biopsies or RAFT collagen tissue equivalents were rinsed 2x with PBS before being transferred into cryomoulds containing OCT (optimal cutting temperature) compound. Cryomoulds containing the samples in OCT were orientated and dipped in liquid nitrogen for 2-3 minutes. Once the blocks hardened, 7.5μm thick cryosections were cut using a Leica CM1850 cryostat (Leica microsystems, Milton Keynes, UK) and transferred onto superfrost plus microscope slides. Slides were allowed to dry at room temperature 45 minutes

and were eventually stored at -80°C until required for Immunostaining. When limbal biopsies were cut tangentially to the corneal circumference, haematoxylin and eosin staining was performed for every 5 slides in order to orientate the tissue prior to immunohistochemistry.

2.5.2 Immunostaining

Frozen sections were allowed to warm up 20 min at room temperature prior to being rinsed with PBS and fixed with 4% paraformaldehyde for 10 minutes. Slides were washed 3 times with PBS and cells were permeabilised with 0.5% Triton X-100 if the antigen targeted was intracellular. Following permeabilization, slides were washed with PBS and blocked for 90 minutes in PBS supplemented with 5% goat serum. Sections were then incubated with primary antibody (see table 2.1 for references and dilutions) in 5% goat serum PBS, in a wet chamber at 4°C, overnight. Sections were washed 3 times with PBS and incubated with the appropriate secondary antibody or counterstained with FITC conjugated phalloidin (1/500) in 5% goat serum PBS for 1 hour at room temperature. Slides were washed 3 times with PBS and mounted using Vectashield medium with DAPI (Vector laboratories Ltd. Peterborough, UK) and coverslipped.

Antibody	Concentration	Supplier	Reference
CD90	1/10	Abcam	Ab23894
CD105	1/40	Abcam	Ab44967
N-cadherin	1/100	Santacruz	SC-7939
ABCB5	1/100	Abcam	Ab140667
Frizzled 7	1/100	RD systems	Mab1981
MelanA	1/500	Abcam	Ab51061
MiTF	1/500	Abcam	Ab12039
CK3	1/100	Millipore	CBL-218
CK15	1/100	Santacruz	SC-47697
Bmi1	1/250	Abcam	Ab14389
p63α	1/100	Cell signaling	4892

Table 2.1 List of primary antibodies and dilution used for IHC.

2.5.3 Observations

Images were captured using a Zeiss 710 confocal microscope (Carl Zeiss, Hertfordshire, UK).

2.6 Transmission electron microscopy

2.6.1 Embedding

a) Fixation and post-fixation

Small limbal 3-5mm^3 limbal biopsies were cut under a dissecting microscope and transferred into Karnovsky's fixative for primary fixation. Karnovsky's fixative consists of 2.5% glutaraldehyde and 2% formaldehyde in 0.1M cacodylate buffered to pH 7.4. Samples were left overnight at 4°C for primary fixation. The next day, samples were washed with 0.1M cacodylate and post-fixed in 1%

aqueous osmium tetroxide (Agar scientific, Elektron Technology Ltd. Essex, UK) for 3 hours at room temperature. Following post-fixation, samples were washed 3x with distilled water and stepwise dehydrated using ascendant concentrations of ethanol.

Dehydration:

30% ethanol	15 minutes
50% ethanol	15 minutes
70% ethanol	3x 5 minutes
90% ethanol	15 minutes
100% ethanol	3x 10 minutes

b) Resin embedding

Samples were transferred into embedding moulds and put into propylene oxide for 2x15 minutes. Epoxy resin for embedding was prepared by mixing 50ml of Dodecenylsuccinic Anhydride (DDSA) hardener with 40ml araldite resin CY212 and 1.6ml DMP30 accelerator (Agar scientific, Elektron Technology Ltd. Essex, UK). Samples were transferred to the infiltration mixture consisting of epoxy resin: propylene oxide 50:50 overnight at room temperature. The next day, samples were transferred into new embedding moulds and put in full epoxy resin for 5 hours. Samples were finally put into fresh resin and placed in a dry oven set to 60°C for 24 hours.

2.6.2 Resin block trimming and sectioning

Resin block were trimmed into a trapezoidal shaped pyramid around the sample with a single edge razor blade (Figure 2.1 A and B) (Fisher scientific, Loughborough, Leicestershire, UK) and mounted onto the arm of a Leica utlracut S (Leica microsystems, Milton Keynes, UK) ultramicrotome. A dry glass knife was used to trim the surface of the resin block. Semi-thin sections of 750nm were cut every 100μm using a 45° histological diamond knife (dEYEmond, Scimed GmbH, Germany) (Figure 2.1 C). Sections were collected on superfrost microscope slides (VWR international Ltd, Lutterworth, Leicestershire, UK) and dried on a hot plate. Sections were then stained with 2% aqueous toluidine blue and left on a hot plate set to 90°C for 30sec. Slides were gently rinsed with dH2O and dried, mounted with Depex (Fisher scientific, Loughborough, Leicestershire, UK) and examined with a phase contrast histological microscope (Figure 2.1D). The trimming/semi-thin sectioning procedure was repeated until identification of the area of interest. Then, silver/gold (approximately 70nm) ultrathin ribbons were cut with a 45° ultra diamond knife (Diatome AG, Switzerland), stretched with chloroform and collected on copper grids (Agar scientific, Elektron Technology Ltd. Essex, UK) (Figure 2.1 E and F).

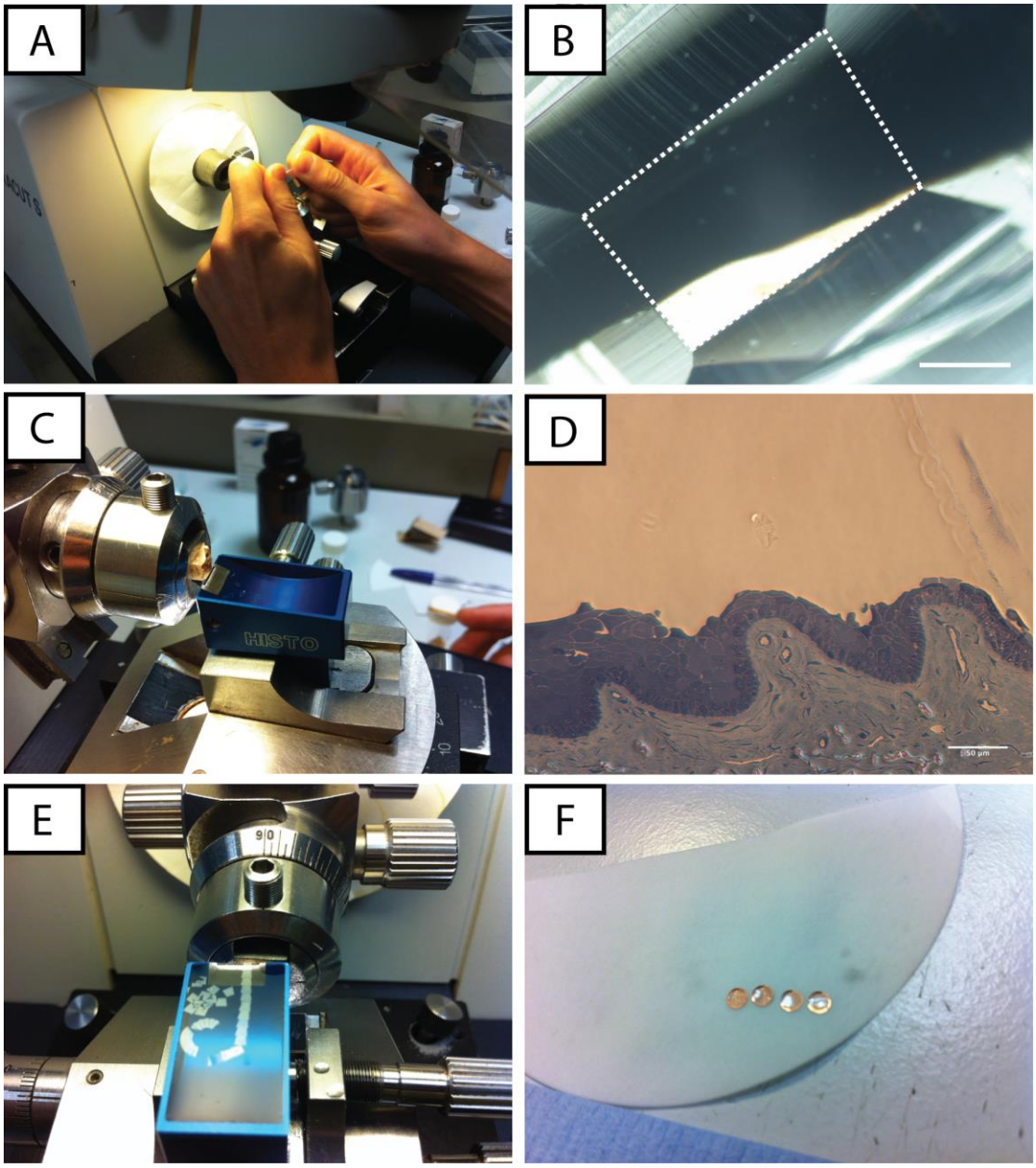

Figure 2.1 Trimming and sectioning of the resin block for transmission electron microscopy.

Resin blocks were trimmed with a single edge razor blade under the binocular of an ultramicrotome (A). Blocks were trimmed into a trapezoidal shape (B) and semi-thin sections were cut with a histo diamond knive (C). Semi thin sections were stained with 2% aqueous toluidine blue and imaged with a histological microscope (D). Once the area of interest was identified, ultrathin sections were cut with an ultra diamond knife (E) and ribbons of 70nm ultrathin sections were collected

on copper grids (F) prior to lead citrate staining. Scale bars: 500μm B, 50μm D. Box in B represents the surface of the block sectioned in E.

2.6.3 Staining of ultrathin sections

Lead citrate reacts with the reduced osmium used during the post-fixation process and enhances the contrasting effect for cellular structures such as cytoskeleton, ribosomes and lipid membranes.

Grids were inverted on top of a drop of lead citrate in a petri dish containing pellets of sodium hydroxide giving a CO_2 free atmosphere. Sections were stained for 5 minutes and washed in 10 successive changes of deionized water.

2.6.4 Observations

Sections were observed in a JEOL 1010 transmission electron microscope and imaged with an SC1000 Orius CCD camera (Gatan, Abingdon Oxon, UK).

2.7 Histological staining of cryosections

Thick frozen sections (7μm) tangential to corneal circumference from crypt rich and non-crypt rich limbal biopsies were fixed in 4% PFA before being stained with haematoxylin and eosin and mounted in DPX. Sections were imaged using a Nikon Eclipse TS100 inverted microscope.

Chapter 3: Localisation of the human limbal stem cell niche

3.1 Introduction

Adult stem cells reside in a specific microenvironment called the "niche" that preserves their properties. Within a tissue, the stem cell niche corresponds to a specific anatomical location where an appropriate interaction occurs between the stem cell and niche factors, which consist of other types of cells in the vicinity, a specific composition of the local extracellular matrix and the presence of soluble molecules such as cytokines and other growth factors (Scadden, 2006; 2014). Human adult stem cells have been successfully identified in various organs and the identification and characterization of niches has revealed conservation of many components that are just beginning to be uncovered.

Despite a readily accessible source of tissue, stem cells and the stem cell niche of the ocular surface are not well understood. It is generally accepted that stem cells of the ocular surface reside within the limbus, a 1.5-2mm wide ring of tissue at the interface between the transparent central cornea and the opaque (over the sclera) conjunctiva. However, until recently, it has been believed that stem cells of the ocular surface were uniformly distributed around the corneal circumference and previous investigations of the limbal stem cell niche were focused on random areas of the corneal limbus (Chen et al., 2004; Cotsarelis et al., 1989; Schermer et al., 1986). In 2005, Dua et al. described an epithelial cells filled crypt-like structure extending radially toward the conjunctiva they named "limbal epithelial crypt". Cells populating this structure were positive for the expression of stem cell markers, but the *in vitro* proliferative potential of epithelial cells populating these structures has not been assessed (Dua, 2005).

Later, Shortt et al. described distinct anatomical features of the limbal epithelium: the limbal crypts localized between the limbal POV and the FSP (Shortt et al., 2007). In this study, the authors rigorously characterized the limbal crypts by combining multiple imaging techniques including laser scanning and scanning electron microscopy. They observed that basal cells populating the crypts were smaller and highly positive for the expression of stem cell markers such as ABCG2 and p63α. Limbal crypts and focal stromal projections were distributed non-uniformly around the limbal circumference. These structures were indeed more likely to be observed within the superior and inferior limbal areas and, interestingly, were not be observed in patients affected by clinical limbal stem cell deficiency. *In vitro* analysis revealed that limbal epithelial cells isolated from the limbal crypts had the ability to generate "holoclone-like" colonies and had a higher proliferative potential in primary cultures than cells isolated from limbal areas devoid of these structures. The authors concluded that limbal crypts and focal stromal projections constitute a niche for epithelial stem cells of the ocular surface (Shortt et al., 2007)

Most of the studies that have focused on LESCs rely on the use of putative positive and negative stem cell markers. One limit of such investigations is that a single reliable marker has not been identified to discriminate the real stem cell from the early progenitors. For these reasons, the exact location of LESCs still creates debate and controversy. Initially developed by Barrandon and Green, 1897, single cell clonal analysis has been used to demonstrate the existence of stem cells in the human hair follicle (Rochat, Kobayashi, & Barrandon, 1994), the ocular surface (Pellegrini et al., 1999) and in the urinary tract (Larsson, Gorostidi, Hubbell, Barrandon, & Frey, 2014). Single cell clonal analysis remains

the gold standard *in vitro* technique to confirm the presence of stem cells isolated and cultured from an epithelial tissue. Despite the stem-like morphology and the high expression of p63α and ABCG2 of cells populating the limbal crypts, the growth potential of epithelial cells populating this area was limited to the characterization of epithelial colonies in early passages that was unable to discriminate stem cells from TACs. In fact, both cell types have the ability to generate epithelial colonies with similar aspects in primary cultures. In their initial study, Barrandon and Green observed that single epithelial cells isolated from the skin had the ability to generate 3 different types of clones when put in culture on a layer of 3T3 feeder fibroblasts. A single cell generating a "holoclone" had the greatest proliferative potential *in vitro* and has been designated as a stem cell. Whereas single cells generating "meroclones" or a "paraclones" correspond to either early or late progenitors respectively. In their study, Shortt et al. observed the generation of large epithelial colonies they described as "holoclones" by cells isolated from the limbal crypts. However, at this stage single cell clonal analysis was not rigorously performed and the colonies only had the morphology of holoclones rather than their proliferative properties. In fact, real holoclones cannot be generated in primary cultures, as it requires the tracking of one single epithelial cell and its direct progenies for at least two passages. For this reason the appellation "holoclone-like colony" could not refer to real stem cells in this context. Further experiments are required to demonstrate LCs as a niche for epithelial stem cells of the ocular surface.

If the LCs constitute a niche for LESCs of the human ocular surface, cells populating these structures should be highly positive for the expression of the

newly established stem cell markers, but also, have the greatest potential of holoclone generation *in vitro*.

In order to evaluate these hypotheses, we firstly compared expression of LESCs markers in crypt rich and non-crypt human limbal biopsies. We further analyzed the growth potential of single limbal epithelial cells isolated from both limbal areas and compared the distribution of 'real' stem cells upon their ability to generate holoclones in culture.

3.2 Materials and Methods

3.2.1 Human limbal biopsies

Fresh human corneas or corneo-sclera rims stored in Optisol were briefly rinsed with PBS and transferred from sterile pots into dissecting dishes and observed under a dissecting microscope. After identifying crypt-rich limbal quadrants under a dissecting microscope, human cadaveric corneas were cut into 4 equal quarters; 2 crypt-rich quarters (C+) and 2 non-crypt quarters (C-) but not following their orientation (superior, inferior, nasal and temporal). 1C+ and 1C- quarter were used for histological analysis and assessment of the quality of the epithelium. The remaining C+ and C- quarters were separately transferred into sterile tubes for dispase digestion and epithelial cell isolation and expansion as described in chapter 2.

3.2.2 Analysis of LESC markers of C+ and C- limbal biopsies by immunohistochemistry

Immunohistochemistry of crypt rich and non-crypt limbal biopsies has been performed as described in the general material and methods section (chapter 2)

3.2.3 Single cell clonal analysis of C+ and C- limbal biopsies

LECs isolated from either C+ or C- limbal biopsies were pre-expanded on a feeder layer of growth-arrested 3T3s as described in the general methods, section 2.2.1. When cultures reached approximately 70% of confluency, 3T3s feeder cells were detached from the cultures with 0.05% TE-EDTA. Remaining LECs were detached with 0.5X in order to prepare a single epithelial cell suspension. Single LECs (250-500) were seeded on to a new culture plate containing growth-arrested 3T3s. Cultures were maintained for approximately 5-7 days until small colonies of about 1mm were observed (Figure 3.1A). At this stage, all epithelial colonies were marked with a thin black marker and 6 colonies per culture dish were randomly selected for further clonal analysis. Culture plates were washed with PBS and 8mm glass cylinders (Sigma-Aldrich, Dorset, UK) were dipped into sterile vacuum grease (Sigma-Aldrich, Dorset, UK) and applied on top of the randomly selected colonies (figure 3.1B). 300μl of 0.5X TE-EDTA (Life Technologies, Paisley, UK) was introduced into the cylinder in order to detach and specifically isolate epithelial cells from the selected colonies. Cells were finally seeded in to a new culture plate containing a feeder layer of growth arrested 3T3s and expanded for further 12 days in 10% FBS-CECM. Cultures were finally washed and fixed with 4% PFA. Limbal epithelial colonies were stained with 2% rhodamine and scored as holoclones, meroclones or paraclones. When 0-5% of the total colonies were terminally differentiated, the

clone was scored as a holoclone. When more than 95% of colonies were terminally differentiated or aborted, the clone was scored as a paraclone. Finally, when >5% but <95% of colonies were terminally differentiated, the clone was scored as a meroclone. The experimental procedure used for single cell clonal analysis is illustrated in figure 3.2. In total, 124 clones isolated from the crypt-rich and non-crypt limbal biopsies from three donors were analyzed for their *in vitro* growth potential.

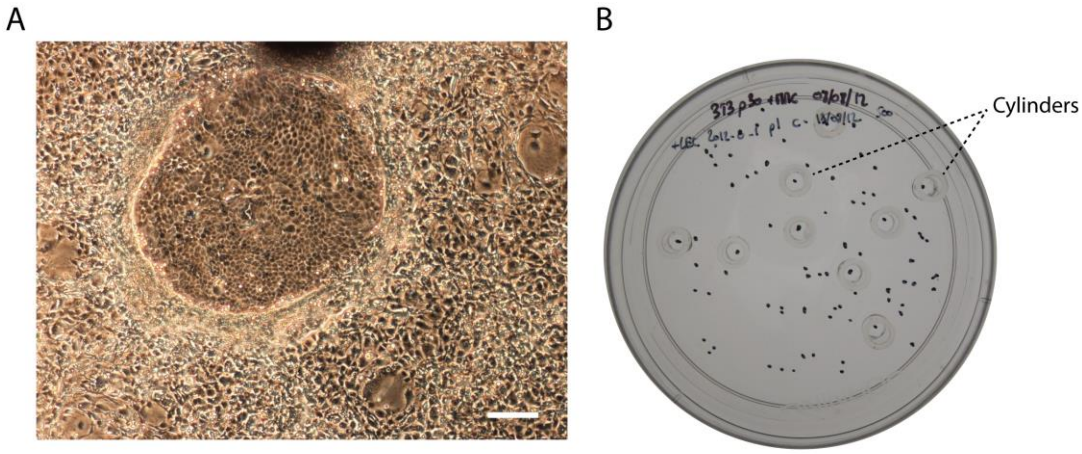

Figure 3.1 Isolation of epithelial cells from single colonies

A: Epithelial colony generated by one single epithelial cell at P1. B: Cloning cylinders placed on randomly selected epithelial colony marked with black dots. Scale bar: 200μm.

3.2.4 Statistical analysis

Statistical analysis was performed as described in the general method section. Fisher's exact test was used to compare frequencies of holoclones, meroclones and paraclones generated by epithelial cells isolated either the LCs or the non-crypt rich limbus.

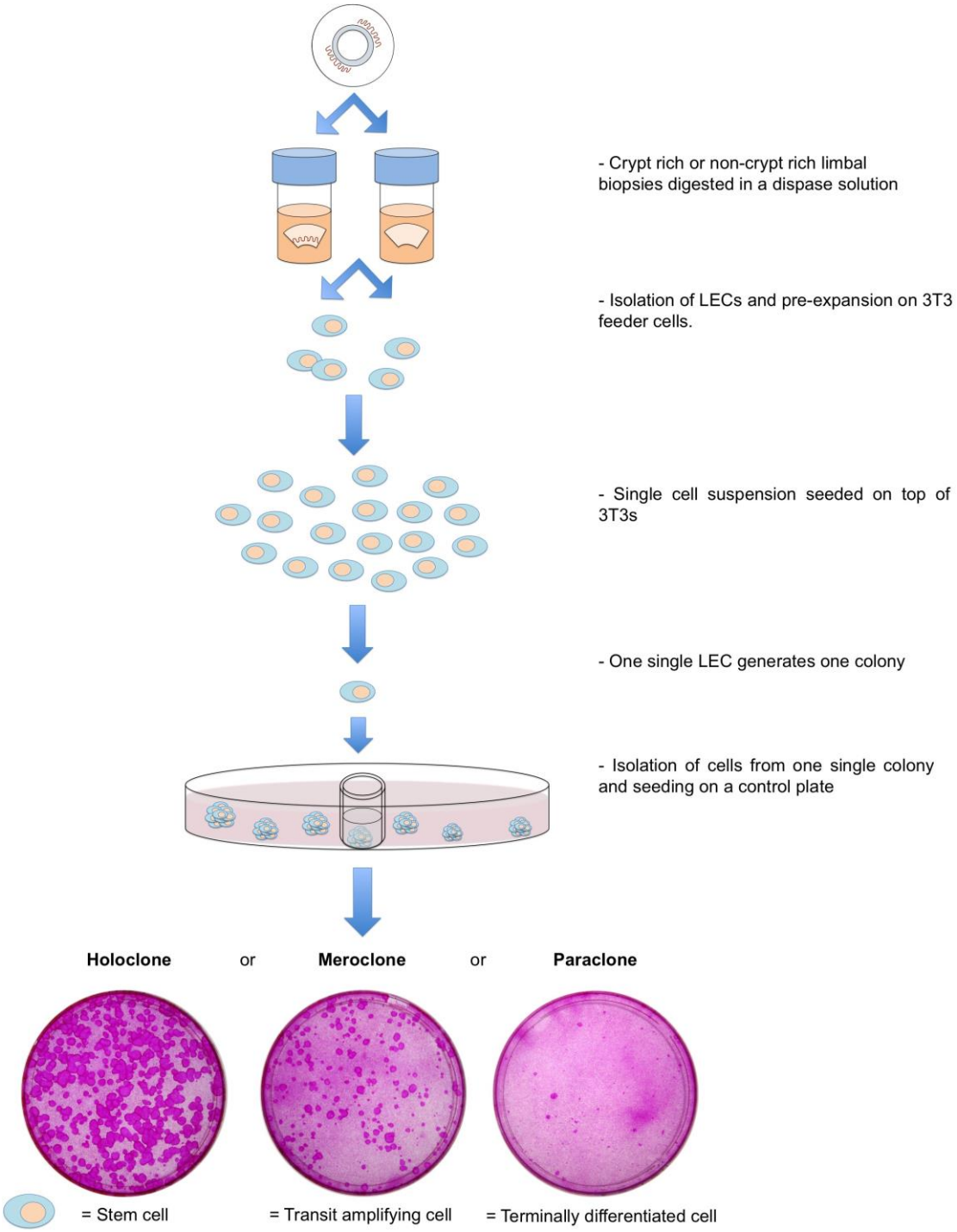

Figure 3.2 Description of the single cell clonal analysis procedure.

LECs were isolated from either crypt rich or non-crypt limbal biopsies and separately pre-expanded. At P1, single cell suspensions were seeded into a new culture plate and expanded for 7 days. When 1mm² colonies were

observed in the culture, single colonies generated by one single cell were isolated using cloning cylinder and expanded for further 12-14 days. Plates were scored as holoclone, meroclone and paraclone depending on the percentage of aborted colonies. If one single epithelial cell generated a holoclone, the cell was considered as a stem cell. If a meroclone or a paraclone was generated, the cell was considered as an early or late progenitor.

3.3 Results

3.3.1 Identification of crypt rich and non-crypt areas in human limbal biopsies

LCs but not focal stromal projections are easily observed at low magnification in the highly pigmented donors as shown in figure 3.3 and figure 3.4 left panels. Macroscopically, LCs are delimited by two highly pigmented lines that correspond to a superposition of melanocytes at the edge of the crypt (figure 3.3). POV are also easily observed between the LCs by a variation of contrast due to a difference of light transmission through the tissue. This is due to a difference in epithelial cell density between the limbal epithelium of the crypt that contains approximately 15 layers of cells and the epithelium covering the palisades that is only composed by 3-5 cell layers (figure 3.4 black arrows middle and right panels).

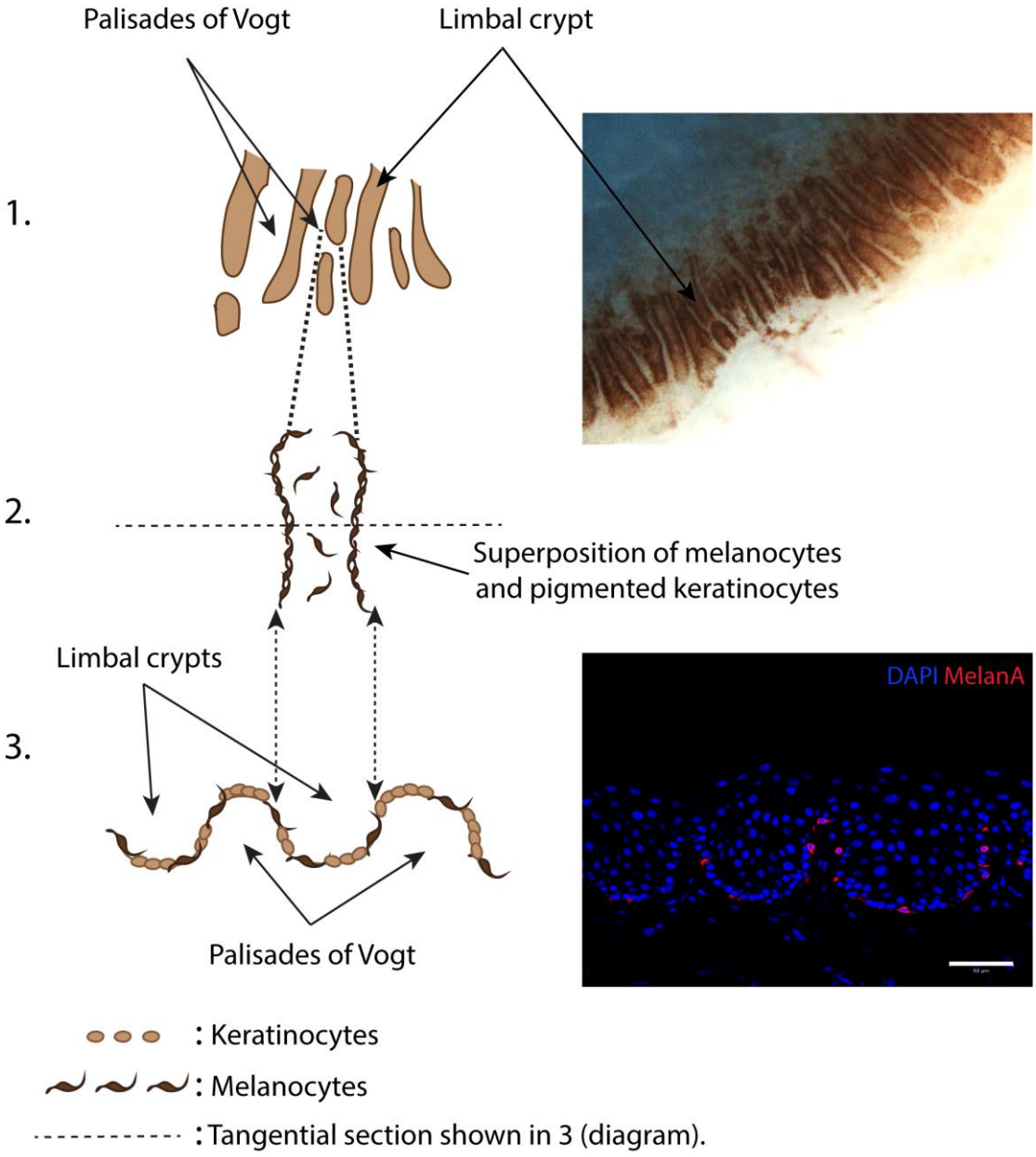

Figure 3.3 Localisation of limbal LCs in pigmented limbal biopsies.

(1) LCs can be identified under a dissecting microscope and are delimited by 2 highly pigmented lines. (2) Magnified area shown in (1). (3) Tangential section of (2) highlighting the superposition of melanocytes at the edge of the crypts observed macroscopically in (1) and (2). MelanA immunolabelling is specific for melanocytes and shows their distribution within the basal epithelial layer of the crypts. Scale bar: 50μm.

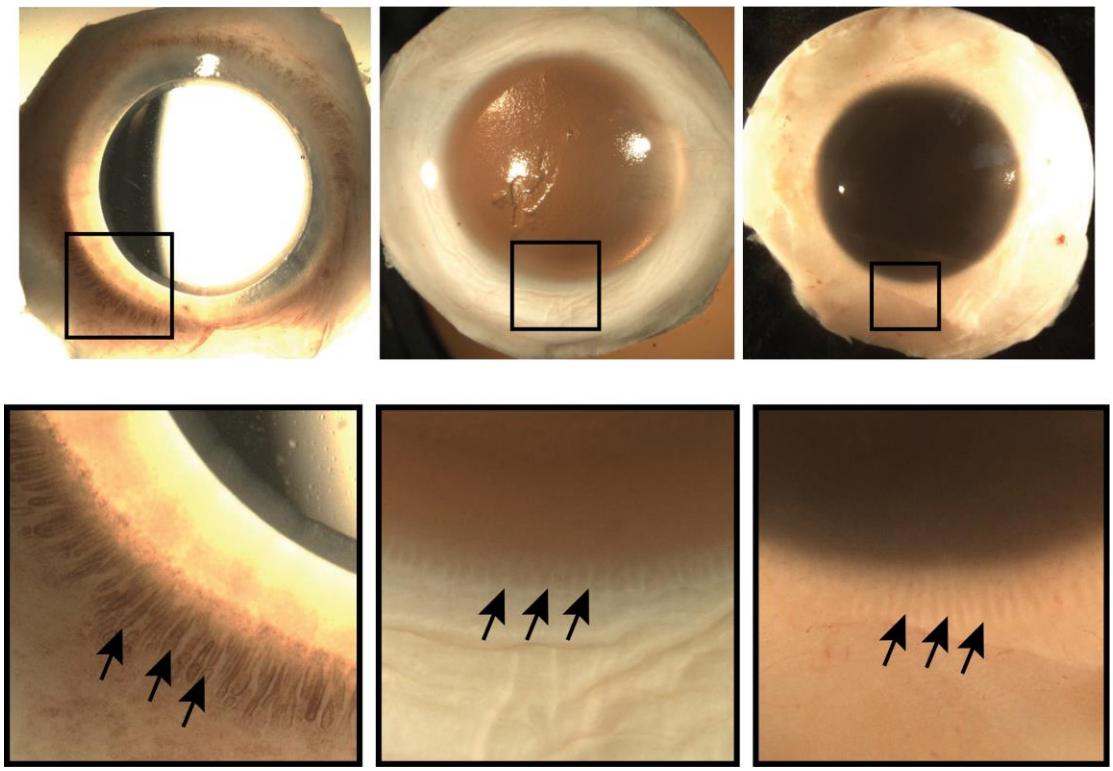

Figure 3.4 Identification of LCs under a dissecting microscope.

Left panel: pigmented donor. Middle and right panels: non-pigmented. Boxes in top panels correspond to bottom panels. Black arrows indicate the LCs between the limbal POV.

3.3.2 Localisation of LESCs markers in the human ocular surface

In order to determine whether the LCs house a higher population of epithelial stem cells than non-crypt limbal areas, the expression of the LESCs markers Frizzled7, ABCB5 and N-cadherin was evaluated in tissue sections isolated from central corneal, crypt-rich and non-crypt human limbal biopsies. As shown in figures 3.5 A and B, immunostaining for all markers analyzed appeared negative

in the central cornea and negative for both ABCB5 and Frizzled7 in basal cells population the non-crypt limbus. N-cadherin staining appeared positive for one single basal epithelial cell (white arrow) within the non-crypt limbus. On the other hand, expression of ABCB5, Frizzled7 and N-cadherin was markedly increased in epithelial cells populating the basal layer of the crypts. N-cadherin seems to be specifically expressed by basal cells of the crypt rich limbal epithelium whereas ABCB5 is expressed in clusters of small basal and suprabasal cells of the crypts (white arrowheads). Frizzled7 is another membrane antigen and seems to be specifically observed in the right place in basal cells of the crypt rich limbal epithelium (white arrowheads) but also by a subpopulation of cells from the limbal stroma. On the other hand, the positive signal observed within non-crypt epithelial cells lacks specificity and corresponds to a background staining.

A

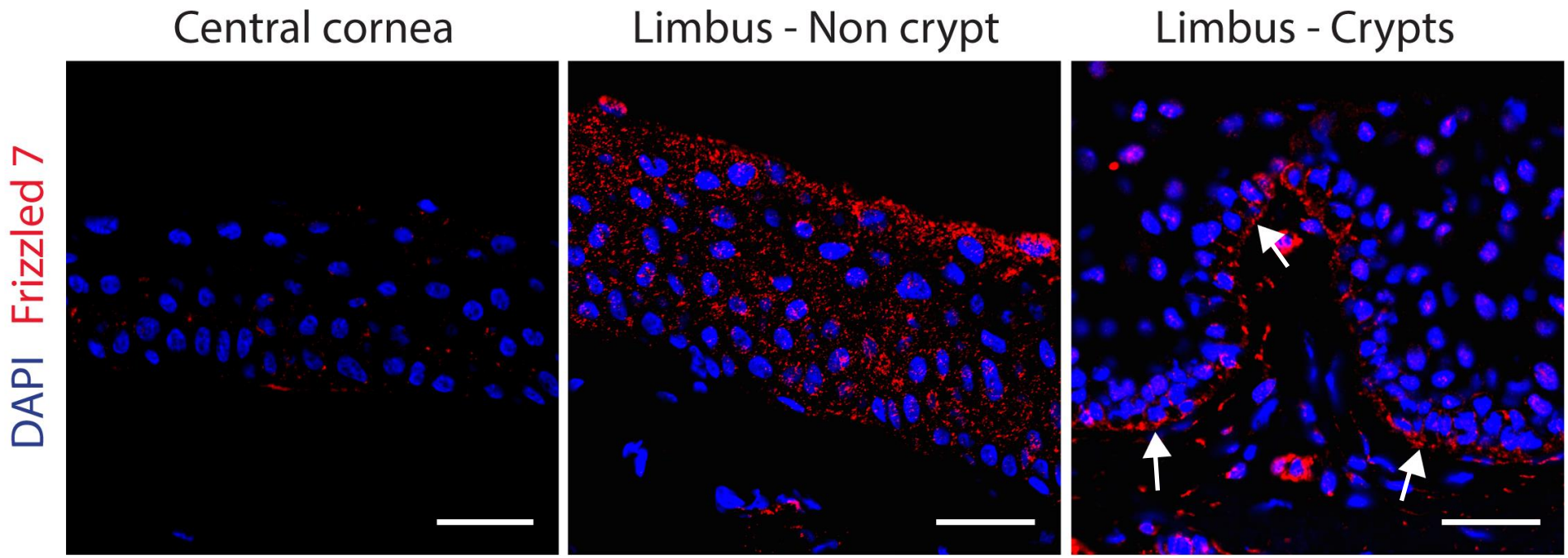
Central cornea
Limbus - Non crypt
Limbus - Crypts
DAPI Frizzled 7

B

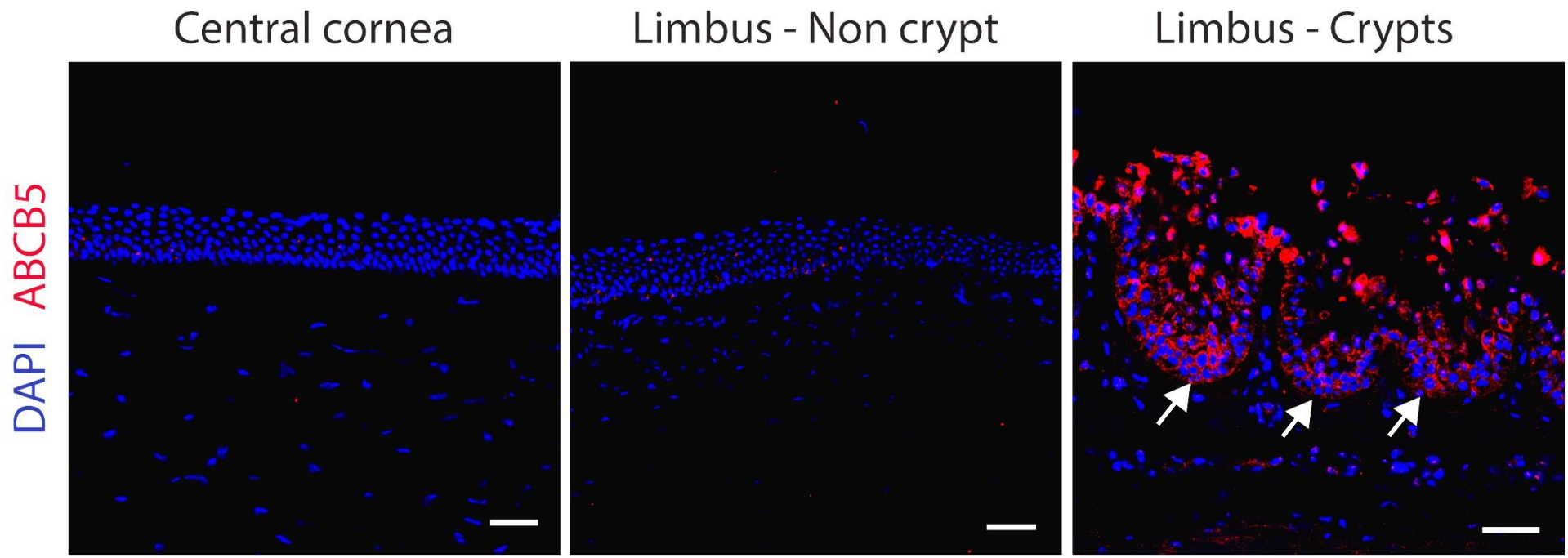

C

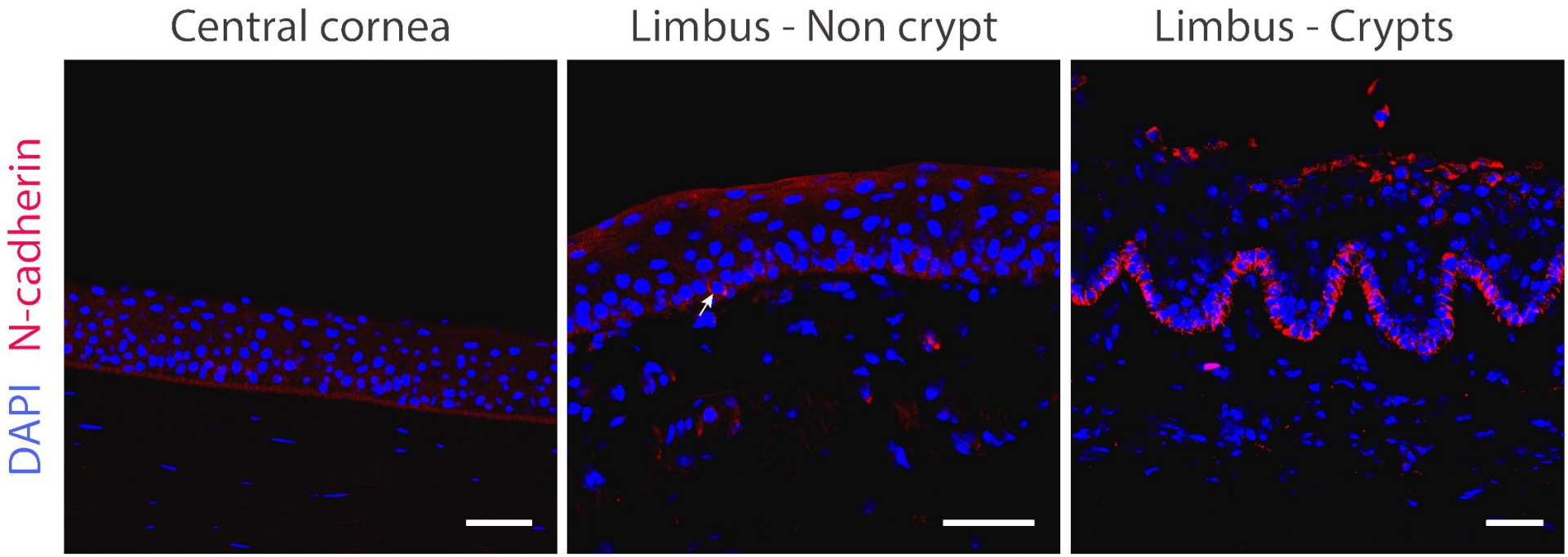

Figure 3.5 Results of immunofluorescence staining for the LESC markers Frizzled7 (A), ABCB5 (B) and N-cadherin (C).

No expression of LESC markers was detected within cells populating the central cornea. Expression of stem cell markers was markedly increased in cells lining the edges and bases of the LCs. White arrows indicate Frizzled 7 and ABCB5 positive clusters of epithelial cells. White arrow in C indicates the presence of a single basal epithelial cell positive for the expression of N-cadherin observed in a non-crypt limbal section. Scale bars: 50μm.

3.3.3 Proliferative potential of LECs isolated from C+ and C- biopsies in primary cultures

Crypt rich and non-crypt limbal biopsies used for single cells clonal analysis were successfully observed and isolated from 3 different donors. The quality of the limbal epithelium was assessed by HE staining of histological sections cut from control biopsies prior to performing single cell clonal analysis on the same tissue. Limbal tissues were classified as unacceptable and acceptable upon preservation of the limbal epithelium. A tissue was considered as unacceptable when 0-3 layers of epithelial cells were remaining on the limbal surface (figure 3.5). The quality of epithelium in corneal-scleral rims was dramatically decreased after 10 days post mortem. Poorly preserved tissues were not used for further cell culture experiments. Acceptable tissues in which at least 5 epithelial layers were remaining were used for cell culture and further clonal analysis (figure 3.5 and table 3.1).

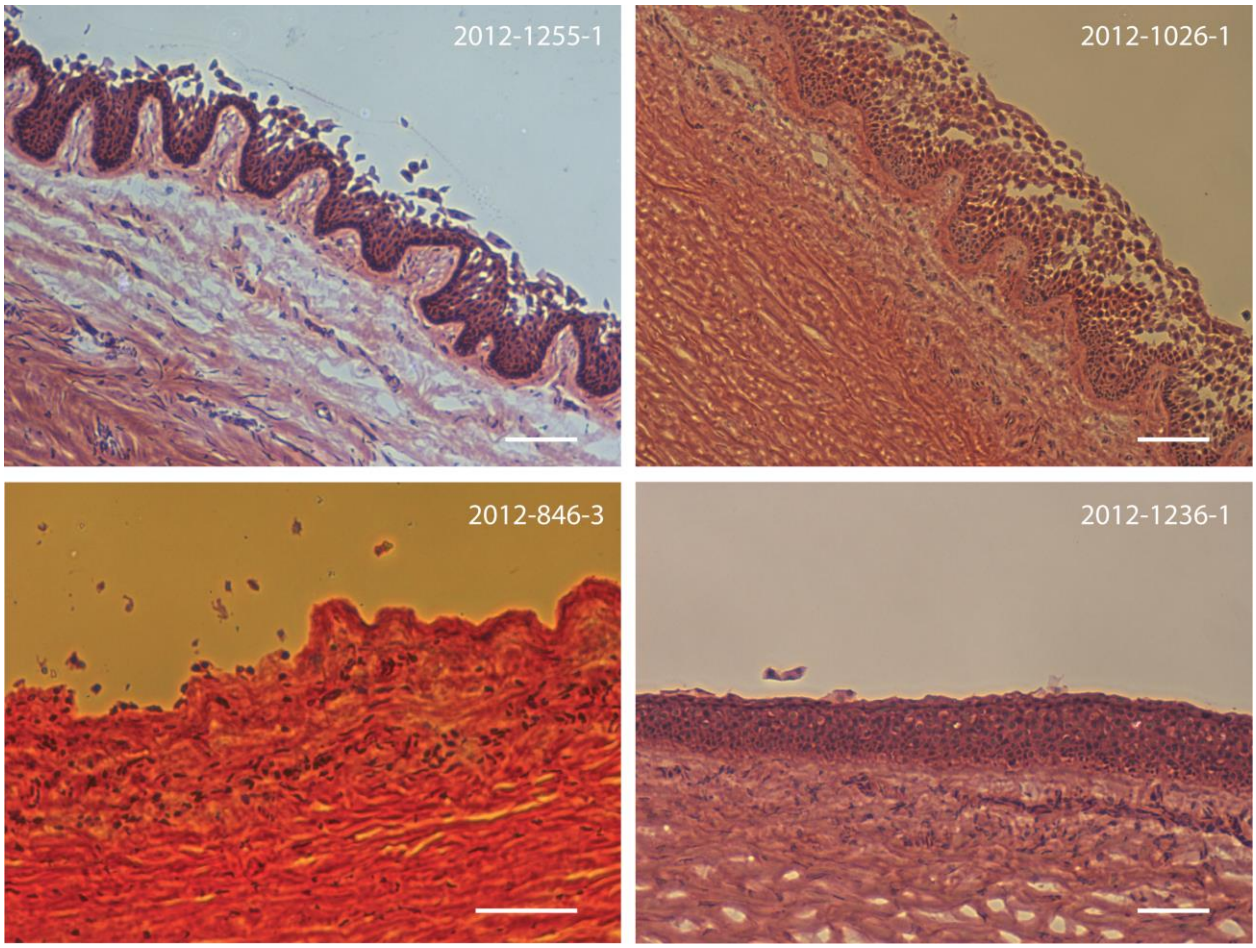

Figure 3.6 Histological analysis of the limbal epithelium prior to cell culture.

Single cell clonal analysis has been performed using cells isolated from donors 2012-1026-1, 2012-1255-1, and 2012-1236-1. As shown on histological control sections, most of epithelial layers were still present in these tissues. Histological analysis of 2012-846-3 shows a poorly preserved biopsy with a desquamated epithelium that was not suitable for cell culture (classified as "not acceptable" in table 3.1) Scale bars: 50μm.

Tissue number	Age of donor	Time between enucleation and experiment (days)	Storage	Quality
2012-846-3	45	11	Optisol	Not acceptable
2012-898-1	89	1	Fresh	Acceptable
2012-971-1	61	6	Optisol	Acceptable
2012-799-3	58	10	Optisol	Not acceptable
2012-1026-1	34	4	Optisol	Acceptable
2012-1255-1	51	6	Optisol	Acceptable
2012-1236-1	53	1	Fresh	Acceptable
2012-1144-1	65	11	Optisol	Not acceptable

Table 3.1 Tissue quality assessment

The quality of human corneal-scleral rims was assessed by histological analysis. Tissues classified as "acceptable" were used for primary cultures and clonal analysis.

Limbal epithelial cells were successfully expanded in primary cultures and rapidly reached 70% of confluency. As shown in figure 3.6 A and B, morphology of the epithelial colonies was similar when cells were isolated from either crypt rich or non-crypt limbal biopsies. LECs isolated from crypt rich and non-crypt limbal biopsies (C+ and C- respectively) were small, circular with a poorly differentiated general appearance (figure 3.6B). The average nucleus to cytoplasm (NC) ratio and cell density was high and similar for both crypt and

non-crypt isolated LECs. The number of colonies generated was slightly higher for cells isolated from the LCs but these observations could not be compared as the exact numbers of epithelial cells isolated from C+ and C- limbal biopsies and seeded for primary cultures could not be controlled after isolation from limbal biopsies.

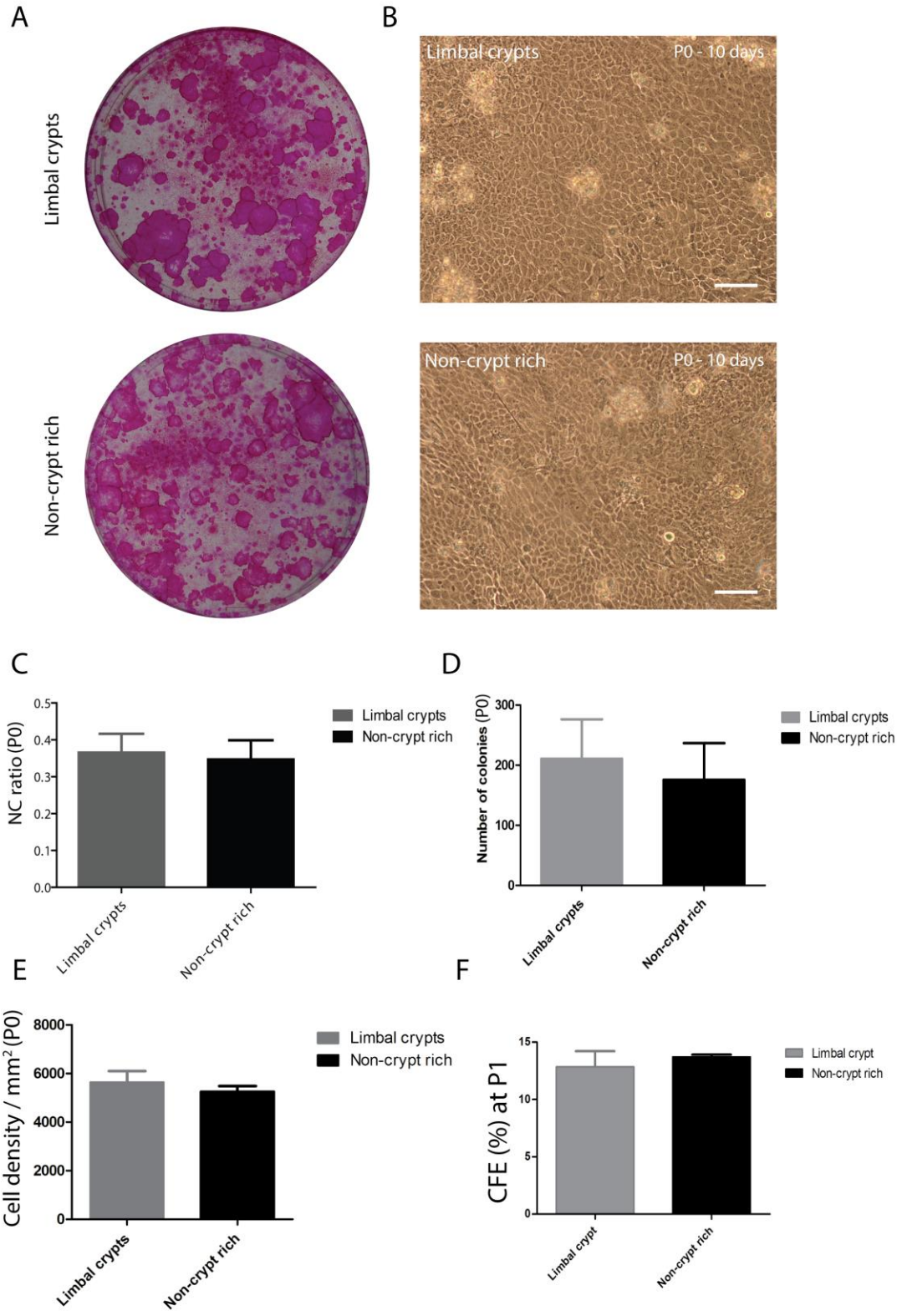
A
B
Limbal crypts
Non-crypt rich
Limbal crypts
P0 - 10 days
Non-crypt rich
P0 - 10 days
C
D
NC ratio (P0)
0.5
0.4
0.3
0.2
0.1
0.0
Limbal crypts
Non-crypt rich
Limbal crypts
Non-crypt rich
Number of colonies (P0)
300
200
100
0
Limbal crypts
Non-crypt rich
Limbal crypts
Non-crypt rich
E
F
Cell density / mm² (P0)
8000
6000
4000
2000
0
Limbal crypts
Non-crypt rich
Limbal crypts
Non-crypt rich
CFE (%) at P1
15
10
5
0
Limbal crypt
Non-crypt rich
Limbal crypt
Non-crypt rich

Figure 3.7 Proliferative potential of limbal epithelial cells isolated from crypt-rich and non-crypt limbal biopsies in early passages

Primary limbal epithelial cultures stained with rhodamine B (A). Morphology of the epithelial sheet generated by C+ and C- LECs in primary cultures (B). Numbers of colonies generated, cell density, NC ratio and secondary colony forming efficiency did not vary significantly between C+ and C- primary cultures.

3.3.4 Single limbal epithelial cells have the ability to generate 3 different types of colonies

After being successfully pre-expanded, single LECs seeded at low density on standard petri dishes containing growth-arrested 3T3s generated single colonies or 'clones'. Epithelial cells specifically isolated from one single clone and seeded on a control plate generated 3 types of progeny (Barrandon & Green, 1987): The "holoclone like" colony is a large colony (usually around 10mm^2) with a high circularity (circularity is equal to one if the shaped measured is a perfect circle) and smooth borders (figure 3.8 A, B and C). The high circularity of the "holoclone like colony" is explained by the circular and compact morphology of cells populating these types of colonies. When the cells at the edge of the colony differentiate (holoclone and meroclone), they tend to spread out and stop their proliferation. These colonies exhibit a lower circularity (figure 3.8 A). As shown on figure 3.8A (bottom left panel), cells populating the "holoclone like" colony appear small, tightly packed and have a poorly differentiated appearance. These cells are identified by a high nucleus cytoplasm ratio and the cell density in this

type of colony is very high (≈10.000 cells/mm^2). More than 95% of colonies of this type are observed in holoclones. The “paraclone” like colony is a small, irregular and aborted colony (figure 3.8A) (Barrandon & Green, 1987). Cells populating these colonies are large, flattened and terminally differentiated (figure 3.8A). The cells of a paraclone typically form colonies of this type. The “meroclone” colony grows to macroscopic size but remains smaller than the “holoclone” (figure 3.8A and B). This type of colony is irregular and presents wrinkled borders (figure 3.8A and C). Cells populating these colonies are heterogeneous. Some cells are small and tightly packed whereas others are flattened and terminally differentiated (black arrows in 3.8 A). For this reason, the average NC ratio and cell density of epithelial cells populating these colonies is lower than in holoclone like colonies. Such colonies will soon abort and are typically formed by meroclones.

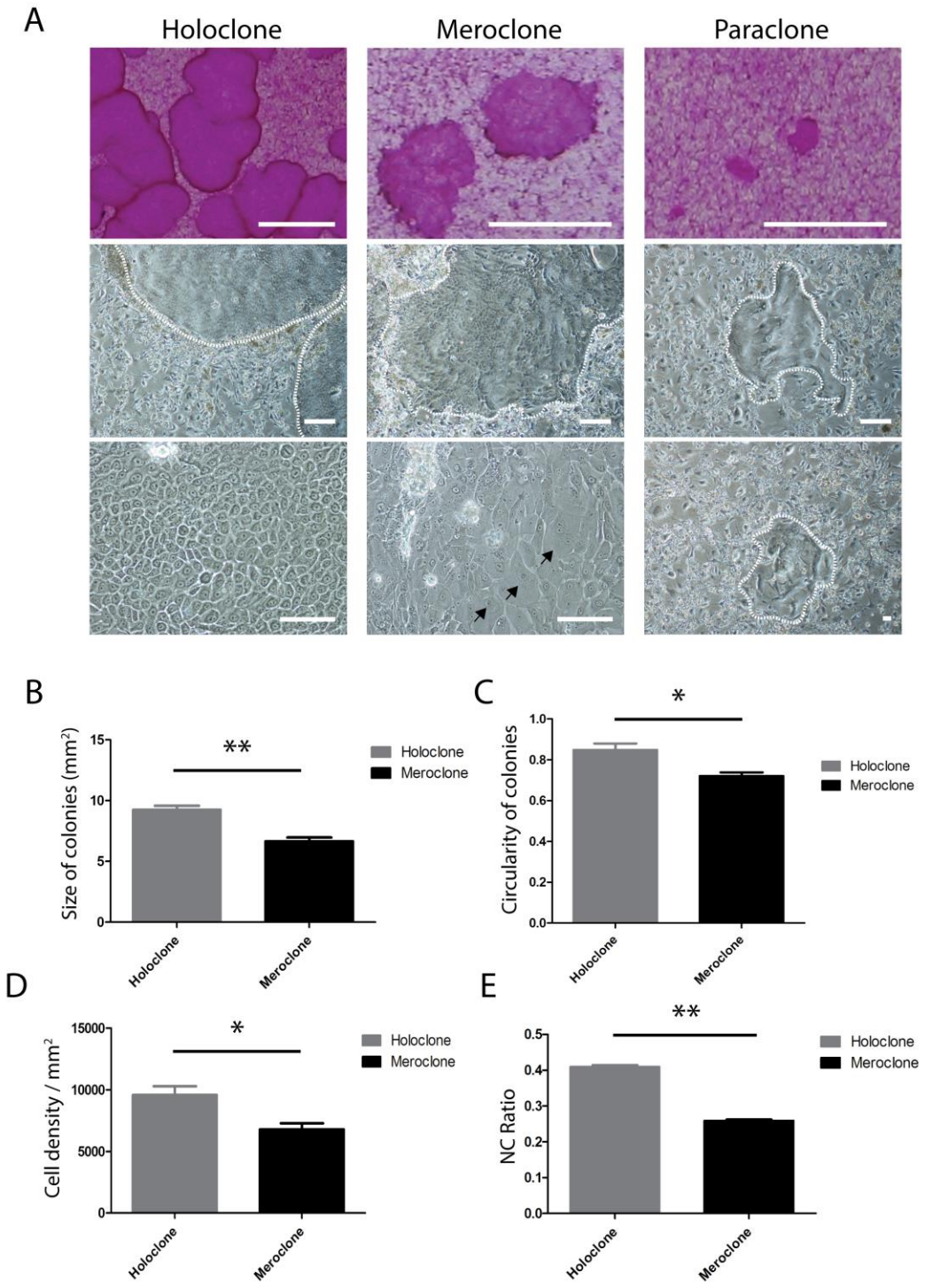

Figure 3.8 LECs have the ability to generate 3 types of colonies

A, top panels: rhodamine staining of epithelial colonies observed in middle and bottom panels.

The "holoclone like" colony (left panels in A) appears macroscopically large (generally around 10mm^2), circular with smooth borders (B and C).

Cells populating these colonies are small with a high NC ratio and tightly packed (D and E). Colonies of this type are typically formed by cells of a holoclone. The "meroclone like" colony (middle panel in A) is macroscopically large but generally smaller than the holoclone type. These colonies have a wrinkled perimeter and are typically formed by meroclones. These colonies contain a mixed population of epithelial cells that could be either small and circular or large and flattened (black arrows). The "paraclone like" colony (right panel A) is aborted and appears macroscopically small and irregular. Cells populating these colonies are flattened and terminally differentiated. This type of colony is mainly observed in paraclones.

Scale bars, top: 5mm, middle: 200μm, bottom: 50μm. Dashed lines: borders of epithelial colonies.

***: p<0.05, **: p<0.01**

3.3.5 Limbal crypts support a greater number of stem cells than non-crypt limbal areas

Among three different human donors and 124 clones analyzed, limbal epithelial cells isolated from the LCs had the greatest proliferative potential compared to cells isolated from non-crypt limbal areas. In fact, LECs isolated from the crypts showed the highest holoclone generation: Among 62 clones analysed, 11 generated holoclones (17.14%) when cells were isolated from C+ limbal biopsies while only one holoclone (1.61%) was generated when cells were isolated from C- limbal areas. Cells isolated from the non-crypt regions showed a lower growth potential when compared to those isolated from the crypt-rich limbus (56.45% paraclones cf. 38.71% paraclones respectively). The number of meroclones (43.55% for cells isolated from the crypts and 41.94% from the non crypt-rich) was similar for both limbal areas. (Figure 3.8 and table 3.2).

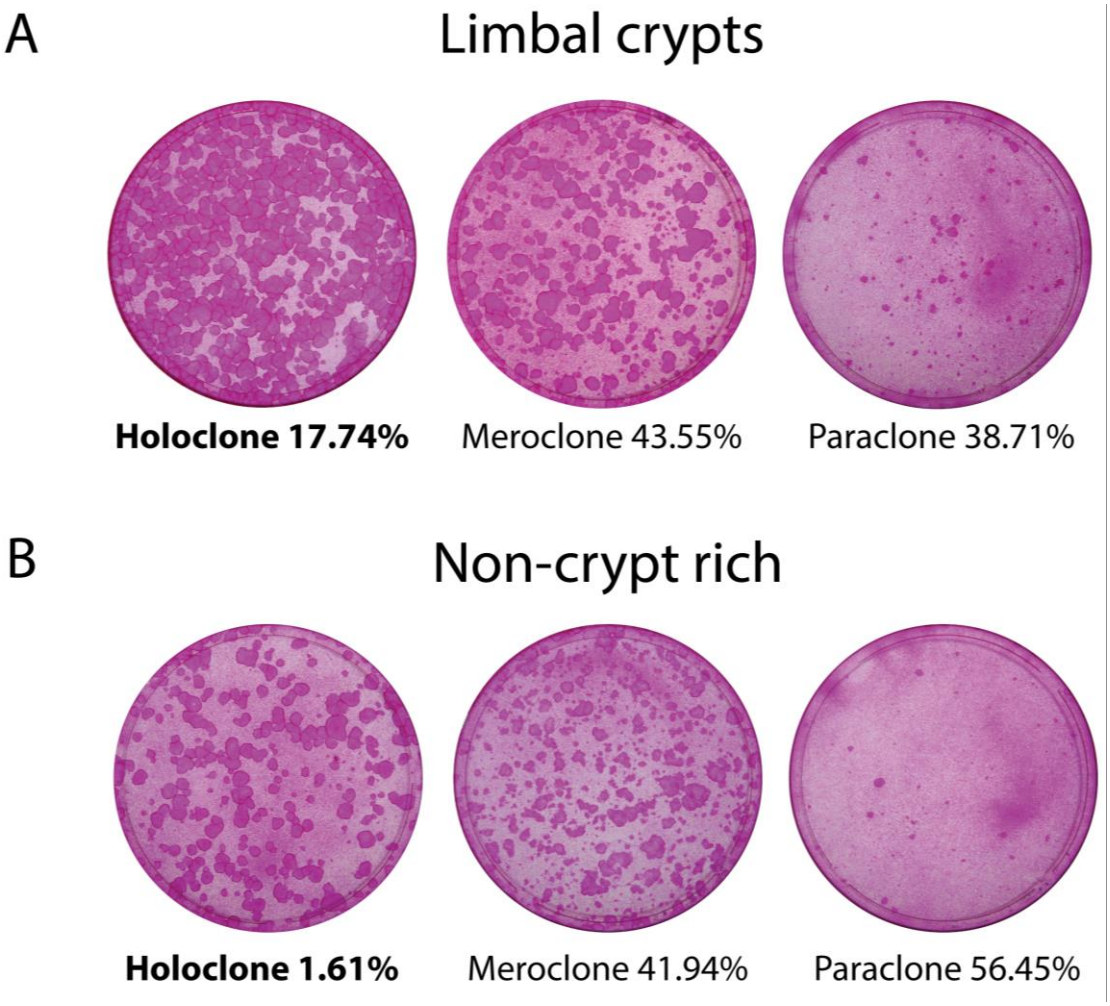

Figure 3.9 Single cell clonal analysis of epithelial cells isolated from crypt-rich or non-crypt rich limbal biopsies

Colonies of limbal epithelial cells grown in Petri dishes and stained with 2% rhodamine. Growth potential of single epithelial cells isolated from crypt-rich (A) and non-crypt rich limbal biopsies was characterized by the generation of holoclones, meroclones and paraclones. LECs isolated from limbal crypts generated the highest proportion of holoclones demonstrating their stem characteristics and the LCs as a stem cell niche.

Table 3.2 Clonal analysis

Origin of tissue	Number of donors	Age of donors	Number of holoclones	Number of meroclones	Number of paraclones	Total
Limbal crypts	3	51-71	**11**	27	24	62
Non-crypt rich	3	51-71	**1**	26	35	62
P-value	$p \leq 0.005^*$					

Table 3.2 Clonal analysis.

Single limbal epithelial cells were isolated from 6 primary co-cultures originated from crypt-rich and non-crypt rich limbal biopsies of three human donors. After 7 days, single clones were isolated and transferred to a new culture dish and expanded for 12 days prior to fixation and rhodamine staining. Clones were finally classified as holoclones, meroclones or paraclones depending on the percentage of aborted colonies. *represents statistical significance (Fisher's exact test p<0.005).

3.4 Discussion

The aim of this chapter was to compare the distribution of LESC markers from different regions of the human limbus and to further analyze, for the first time, the proliferative potential and holoclone generation abilities of single epithelial cells isolated from these different limbal areas. LCs, located between the POVs are easily observable at low magnification under a dissecting microscope. For this reason, it was possible to accurately cut crypt rich and non-crypt limbal biopsies from corneo-scleral rims and specifically isolate epithelial cells from

both limbal areas. Interestingly, both C+ and C- LECs presented high proliferative potential in primary cultures. Epithelial cells from both limbal regions generated large epithelial colonies 7 days after isolation. Cells within the colonies did not present significant morphological variations: LECs were tightly packed, had a small size, a high circularity and a high nucleus cytoplasm/ratio. All of these morphological aspects characterize epithelial progenitors in culture but cannot in this context discriminate stem cells from the TACs (or early progenitors). Our observations are however in direct contradiction with previous findings showing that non-crypt limbal epithelial cells had a very limited proliferative potential in primary cultures (Shortt et al., 2007). This might be due to the fact that the limbal epithelial cells were isolated from relatively fresh tissues in our experiments. In fact, it has been reported that the proliferative potential and maintenance of stem cell activity in stored human limbal tissues correlates with the preservation time and considerably decreased after the 4^{th} day despite maintenance of the limbal structure integrity and expression of stem cell markers (Liu et al., 2012). In this context, secondary CFE assays and single cell clonal analysis have only been performed with LECs isolated from human tissues preserved for a maximum of 4 days. Longer preservation times of tissues and thus rapid exhaustion of epithelial progenitor cells could explain the differences noticed in the proliferative potential of LECs in primary cultures and why authors did not performed further secondary CFE assays and single cell clonal analysis in their study (Shortt et al., 2007).

In the present study, secondary colony forming efficiency was similar for both crypts and non-crypt isolated LECs in both culture conditions suggesting that

both LCs and non-crypt limbal areas contain cells with important proliferative potential. These primary observations support the concept of a random distribution of the limbal epithelial progenitors around the corneal circumference as observed in rodents (Mort et al., 2009). By seeding a small number of cells in the culture plate and using cloning cylinders it was possible to isolate epithelial cells from one single colony generated by one single epithelial cell. After seeding all epithelial progenies isolated from one single colony into a control plate the generation of 3 types of clones was observed as previously reported by Barrandon and Green (Barrandon & Green, 1987). Limbal epithelial cells have the ability to generate holoclones, meroclones and paraclones. Macroscopic morphology of the 3 types of clones was similar to the description of Barrandon and Green in their protocol. Holoclones mostly contained large epithelial proliferative colonies with smooth borders in which epithelial cells were tightly packed and presented morphology consistent with stem cells. Meroclone presented large epithelial colonies that contained a mixed population of compact and circular or large and elongated epithelial cells whereas some colonies were aborted and contained terminally differentiated epithelial cells. Finally, some single epithelial cells generated paraclones, which consist of epithelial colonies that were mostly aborted and terminally differentiated. Despite similar growing potential in primary cultures, there was a substantial difference in the number of holoclones generated, with a significantly higher number observed when epithelial cells were isolated from the crypts. These results demonstrate for the first time that LCs constitute a reservoir for LESCs. The generation of just one holoclone from the non-crypt limbus suggests that stem cells could also be localized outside the crypts but in smaller numbers. LCs

located between the POV are more likely observed in the superior and inferior limbus where the eyelids and melanocytes provide protection to the limbal epithelial progenitors against ultraviolet radiations (Ahmad, 2012; Dua et al., 1994; Ordonez & Di Girolamo, 2012).

In their study, Pellegrini et al. 1999, observed that epithelial cells from the 4 limbal quadrants had the potential to generate holoclones *in vitro* (Pellegrini et al., 1999). The difference with our study is that authors focused on the orientation of the tissue rather than considering the anatomical features of the limbus. Even if it has been reported that LCs mostly concentrate at superior and inferior parts of the limbus (Townsend, 1991), the distribution of these structures is highly variable from one donor to the next and crypt extensions on the nasal and temporal sides of the limbus are frequently observed.

In 2008, Majo et al. challenged the concept of a limbal location for the epithelial stem cells that maintain the ocular surface. In their study, the authors observed that murine limbal epithelial cells expressing β-gal and transplanted into the limbal area of a recipient mouse did not migrate out of the transplant and only slightly contributed to normal homeostasis of the corneal epithelium. Transplanted limbal cells only became active when the central cornea was extensively wounded. They also observed that epithelial cells from the central cornea and transplanted at the limbus of a recipient mouse could completely restore the conjunctival and central corneal epithelium upon injury. Taking together, these results suggest that mouse central corneal epithelium contain cells exhibiting stem cell properties that are self-sufficient during natural tissue homeostasis. In the same study, the authors observed that central corneal

epithelial cells of the pig have the ability to generate holoclones by single cell clonal analysis suggesting the existence of stem cells outside of the limbus. These cells had the ability to differentiate into either epithelial or goblet cells, thus demonstrating their oligopotency. They finally proposed a new model of the ocular surface self-renewal in mammals in which stem cells, of equal potency are distributed throughout the entire ocular surface, expand in opposite directions and confront at the limbus. On the other hand, two recent studies used confetti reporter transgene in combination with tamoxifen inductible keratin14 CreER to investigate cell lineages in the mice limbal and central corneal epithelium (Amitai-Lange et al., 2014; Di Girolamo et al., 2014). In their study, Di Girolamo et al. 2014 tracked the growth of the same fluorescent clones for up to 21 weeks and observed that labeled cells emerged from the limbus and extended centripetally to reach the center of the cornea by 21 weeks. Authors of both studies also identified small patches of labeled epithelial cells in the corneal epithelium. The latter could correlate with the long-term epithelial progenitors of the central cornea identified by Majo et al. However, these latest lineage-tracing studies demonstrate that the unwounded rodent corneal epithelium is largely maintained by epithelial stem cells uniformly distributed around the limbal circumference. In human, no evidence of the presence of epithelial progenitors in the central cornea have been reported suggesting that species-specific differences exist in the localisation of the epithelial stem cells of the ocular surface.

In conclusion, it has been demonstrated in the present chapter that the LCs, localized between the limbal POV constitute a reservoir for LESCs. In the next chapters, LCs were specifically targeted to image the limbal epithelial

progenitors and to identify cell interactions occurring in this specific area by using state-of-the-art imaging techniques.

Chapter 4: Optimization of a protocol for high-resolution imaging of the human limbal stem cell niche by serial-block face scanning electron microscopy

4.1 Introduction

4.1.1 New advances in volume electron microscopy

Light microscopy (LM) is an essential tool for modern biological research as it allows imaging and identification of molecules inside living cells, tissues or whole organisms, with specific labeling strategies and minimal specimen preparation. Spatial resolution of light microscopy is limited by the wavelength of light to 200nm in lateral direction and 500nm in the axial direction. On the other hand, transmission electron microscopy (TEM) offers much greater resolution due to shorter wavelengths of electrons allowing imaging of fine intracellular details of cells and tissues. Despite a greater resolution, TEM also has some limitations such as a lengthy preparation of specimens, the introduction of artifacts during the dehydration and fixation processes and limited capabilities of antigen recognition and immunolabeling. Moreover, conventional TEM techniques rely on observation of ultrathin sections that strongly limits resolution in z direction that could potentially mask cell interactions and other cellular phenomena. Recent developments of super-resolution fluorescence microscopy has allowed imaging of biological structures beyond the diffraction of light, three-dimensional reconstructions, multicolor live cell imaging and cell-cell or protein interactions. In this context, Knott and Genoud have raised the legitimate concern asked at a biological workshop: “Is EM dead?” (Knott & Genoud, 2013). Despite great recent advances in super-resolution LM, electron microscopy (EM) is currently undergoing a revival with significant improvement in the rapidity and quality of specimen preparation and

the development of new imaging instruments. One area of growing interest in EM focuses on improvement of axial (z) resolution and is termed volume electron microscopy. Volume EM regroups emerging imaging techniques such as electron tomography (ET), serial block-face scanning electron microscopy (SBFSEM) and focused ion beam scanning electron microscopy (FIBSEM). These emerging techniques permit an analysis of volumes and thus, improve the very limited resolution in z that is achieved with conventional EM techniques.

4.1.2 Electron tomography

Electron tomography allows visualization of the three-dimensional architecture of organelles and small subcellular structures as small as ribosomes with a lateral resolution that can reach 4-5nm. Electron tomography has been used for understanding protein complexes such as the structure of nuclear pores, microtubules, the golgi apparatus and the trans-golgi network, clathrin coated vesicles and viruses (Cheng et al., 2007; Cyrklaff et al., 2007; Han et al., 2013; Koning et al., 2008; Maimon et al., 2012). The technique relies on sectioning thicker sections (generally ranged between 200nm and 1μm) and tilting the sample at different angles (between -70 and +70 degrees) inside the chamber of the TEM in order to collect information through the entire thickness of the section. The resulting data stack can be realigned and the volume of the structure of interest manually segmented and three-dimensionally reconstructed. This process can be repeated across several serial sections allowing a complete reconstruction of larger volumes (Henderson et al., 2007). Electron tomography however has significant disadvantages. Despite the great resolution achieved, the

procedure for a complete data collection is long and laborious but also presents fundamental limitations when it comes to larger volumes, as sections must remain transparent to the electron beam. Moreover, the field of view is very limited making it impossible to reconstruct the larger volumes of multicellular organisms or tissues. Finally, tilting the sample in one axis introduces the missing edge, an artifact generated by the lack of information that cannot be collected beyond +/- 70 degrees. For these reasons, more straightforward techniques are currently being developed and adapted for SEM serial imaging.

In the last years, significant improvements have been made in the context of 3D reconstructions using laser-scanning microscopy. The current interest is to develop new volume EM techniques that would improve axial (z) resolution and would be applicable for larger pieces of tissues or whole multicellular organisms providing imaging and reconstruction of volumes that can reach up to thousands of cubic micrometers with a resolution comparable to what is routinely achieved with transmission electron microscopy. For this purpose, SEM based serial block face imaging techniques have recently emerged and appear as a promising approach to bridge the gap between 3D LSM and electron tomography.

4.1.3 Introduction to serial block face imaging

Volume electron microscopy was initially developed for the examination of large pieces of nervous tissues in order to explore the connectivity of local networks of neurons by maintaining a resolution high enough to visualize neural vesicles and synapses (Denk & Horstmann, 2004). Serial block-face encompasses two similar but complementary techniques that are SBFSEM and FIBSEM. These volume EM

techniques involve imaging of the surface of a resin block inside the chamber of a SEM rather than imaging ultrathin sections observed by conventional TEM (Peddie & Collinson, 2014). Therefore, common artifacts due to compression and distortion of ultrathin sections encountered during the sectioning process are avoided. The principle of sample preparation (resin embedding) remains similar to conventional TEM imaging but multiple staining steps with heavy metals (osmium, lead, uranium) are recommended as the signal generated relies on backscattered electrons that are readily emitted from elements with high atomic numbers (Tapia et al., 2012).

4.1.4 Focused ion beam scanning electron microscopy

FIBSEM has been introduced in the field of neurobiology in 2008 and has now been used in several studies for the reconstruction at high resolution of several cellular and sub-cellular structures (Armer et al., 2009; De Winter et al., 2009; Felts et al., 2010; Heymann et al., 2009; Knott et al., 2008; Murphy et al., 2010; Schneider et al., 2011; Steinmann et al., 2013; Villinger et al., 2012; Wei et al., 2012; Wierzbicki et al., 2013). The technique relies on a destructive gallium ion beam that 'mills' the surface of the sample inside the SEM. Once the surface of the specimen is milled, the electron beam scans the freshly exposed surface and the backscattered electrons detected to generate an image. The procedure is automatically repeated allowing acquisition of a large stack of data. FIBSEM can serially 'slice' a sample of a thickness down to approximately 10nm. This technique has been used for serial imaging and 3D reconstruction of numerous mammalian cells such as keratocytes, melanocytes, 3T3 fibroblasts but also

viruses in infected cells, small organelles and larger pieces of brain tissue of up to 290μm^3 and preserving a lateral resolution that allowed identification of synapses and neurovesicles (Young et al., 2014; Felts et al., 2010; Heymann et al., 2009; Knott et al., 2008; Murphy et al., 2010; Wierzbicki et al., 2013). Despite a great axial resolution, FIBSEM has however a restricted imaging field of view to approximately 20μm^2. This renders imaging of a specimen at medium/low magnification limited. Moreover, milling the surface of the specimen by the ion beam is a long process rending the automated procedure time consuming for larger pieces of tissue (Peddie & Collinson, 2014). Therefore, FIBSEM is an ideal technique for imaging specimen at cellular scale when the area of interest is known and easy to target within the sample.

4.1.5 Serial block face scanning electron microscopy

Similarly to FIBSEM, SBFSEM is a volume imaging technique, which consists of imaging the surface of a resin embedded specimen with a scanning electron microscope. The SEM is here combined with an ultramicrotome inside the chamber of the microscope (Figure 4.4A). The electron beam scans the surface of the resin block and the generated backscattered electrons are detected. Conventional SEM relies on detection of secondary electrons generated by variation of the texture and orientation of the surface of the sample. Since the microtome produces a 'flat' surface of the block without any specific topography, the images produced are very poorly contrasted. For this reason, backscattered electrons that give a better contrast are used for imaging the 'flat' cut block faces. Once the surface is imaged, an ultrathin section is cut off the resin block exposing

the fresh surface for another round of scanning and imaging. The procedure is completely automated and can be repeated over and over until the required volume of tissue has been imaged. Practically, about 3.000 images can be captured in 24h generating a large stack of serial images of the area of interest (figure 4.1).

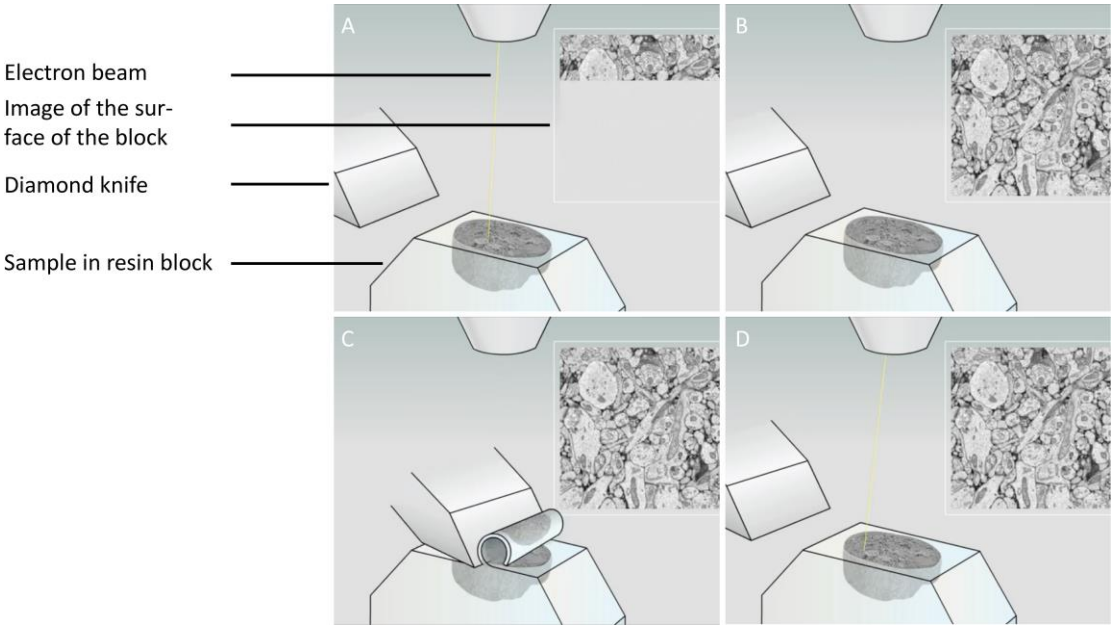

Courtesy of Julia Kuhl prepared for Denk laboratory – Max Planck Institute.

Figure 4.1 General principle of automated serial block-face SEM. Surface of the resin block is scanned (A) by the electron beam and back scattered electrons detected and imaged (B). Once imaged, ultrathin sections are cut off the surface of the block (C). The freshly exposed surface is scanned and imaged. The cycle can be repeated over 3000 times allowing acquisition of a large data stack of serial images.

Denk and Horstmann first described SBFSEM in 2004. Initially developed to image and reconstruct large volumes of neural tissues, the technique has been applied for imaging various non-brain specimen such as collagen fibrils, cardiac sarcoplasmic reticulum, zebrafish dorsal lateral vessels and mouse retina (Armer et al., 2009; Briggman et al., 2011; Pinali et al., 2013; Starborg et al., 2013).

Current research interests in the field of limbal stem cell biology are focused on cell interactions occurring between stromal niche cells and epithelial progenitors in the limbal stem cell niche. Recent findings suggest that LESC/progenitors cells might physically connect or interact with cells from the underlying stroma (Chen et al., 2011). However, such cell-to-cell interactions could only be observed in culture but not in the native niche.

Despite the great lateral resolution reached by conventional TEM, the technique relies on the imaging of ultrathin sections limiting the z resolution to its thickness ranging between 50 to 200 nm. For this reason, focal contacts between stem cells and their underlying stromal cells becomes extremely difficult to image. On the other hand, SBFSEM that maintains a high lateral resolution but also offers serial sectioning and imaging of the area of interest is an ideal technique for tracking a whole single cell within a large dataset and eventually highlight such putative focal contacts.

Despite progresses in automated SBF imaging in the last years, the method is still not commonly used in laboratories and generally needs to be adapted according to the nature of the specimen. In the present study, we employed for the first time SBF imaging to observe the human limbus. This chapter will, for this reason, cover multiple methodological aspects of sample preparation such as fixation

and resin embedding, targeting the area of interest, optimal microscope settings, data collection, segmentation and volume reconstruction.

4.2 Methodology and optimization of SBF imaging for the human limbus

4.2.1 Resin embedding of limbal biopsies

Despite similarities with the routine TEM embedding protocol, sample preparation for SBFSEM requires a few additional staining steps in order to enhance the contrast of the generated image. SBF imaging relies on the emission of backscattered electrons that provide the greatest contrast of the flattest surfaces such as a trimmed resin block in which the sample is embedded. However, the signal generated by backscattered electron must be enhanced by additional staining steps to generate micrographs with a higher contrast.

Crypt-rich human limbal biopsies were fixed in 2.5% glutaraldehyde and 2% paraformaldehyde in 0.08M sodium cacodylate buffered to pH 7.4. Tissues were washed in cold cacodylate buffer containing 2mM calcium chloride and incubated in a solution containing an equal volume of 2% aqueous osmium tetroxide and 3% potassium ferrocyanide in 0.3M cacodylate buffered with 4mM calcium chloride. The use of osmium tetroxide which binds at double bounds of unsaturated lipids is commonly used in electron microscopy and stains nuclear, plasma and mitochondrial double membranes whereas potassium ferrocyanide reduces the osmium causing it to be more reactive (Schnepf, Hausmann, & Herth, 1982; White, Mazurkiewicz, & Barrnett, 1979). Following osmication, tissues

were washed with double distilled water (ddH_20) and placed in a freshly prepared and filtered thiocarbohydrazide solution (0.01g/mL in ddH_20) in order to stain cellular carbohydrates molecules. After being rinsed with ddH2O, tissues were again placed in 2% osmium tetroxide in ddH_2O for 30 minutes at room temperature, washed in ddH_2O and placed in 1% uranyl acetate overnight at 4°C. The ferrocyanide-reduced-osmium-thiocarbohydrazide-osmium (R-OTO) staining method yields to enhanced preservation and contrast of subcellular structure and also makes the sample conductive permitting the reduction of the charging effect that introduces artifacts during the process of SEM imaging (Tapia et al., 2012; Willingham & Rutherford, 1984). Due to high atomic weight of 238 of uranium, uranyl acetate produces a high electron density around proteins, glycoproteins and nucleic acid phosphate groups of DNA and RNA increasing the contrast of these subcellular structures. After a rinse with ddH_20, tissues were placed in freshly prepared Walton's lead aspartate solution and placed in a 60°C oven for 30 minutes. In fact, it has been reported that R-OTO and lead aspartate association increases even more the contrast for EM imaging (Kopriwa, 1984). Tissues were finally washed with ddH_20 and dehydrated through increasing concentrations of ethanol (20%, 50%, 70%, 90% and 100%) similarly to resin embedding of samples prepared for routine TEM imaging. After dehydration, tissues were transferred to acetone before being infiltrated in mixtures of resin:acetone 25%, 50%, 75% respectively. Acetone is miscible with the resin used for embedding and such gradual impregnation mixture enhances infiltration of the hydrophobic resin into the sample. Tissues were finally placed in 100% resin (Durcupan ACM Epoxy kit, TAAB Laboratories Equipment Ltd) for

2 hours before being embedded in a fresh resin and polymerized in a dry oven set to 60°C for 48 hours.

4.2.2 Resin block trimming, assessment of tissue quality and mounting on cryopin

Once embedded in resin, tissues were trimmed with single edge razor blades under the binocular of an ultramicrotome as described in the general methods section. Quality of limbal biopsies was assessed after cutting and imaging semi-thin sections. As shown in figure 4.2, quality of the epithelium varied between donors. A and B show very poorly preserved tissues were the epithelium is totally lost. Moreover, cells of the limbal stroma and blood vessels were barely identifiable. Due to such poor preservation, this kind of tissue was not used for further electron microscopy analysis. Generally, rims stored in Optisol (+5 days post enucleation) had the poorest preservation (Figure 4.2A and B). These rims were potentially suitable for cell culture as few progenitors might still remain in the tissue but not for high-resolution imaging. As shown in figure 4.2C, fresh tissues, (24-48h post enucleation) had a much better preserved ultrastructure. Such tissues had a multilayered epithelium and a well-preserved basal epithelial layer. Stromal cell and blood vessels were also easily identified. Despite of desquamation of the top layers of the epithelium, tissues shown in figure 4.2D were still suitable for EM analysis as the area of interest, localized at the interface between the limbal epithelium and the limbal stroma remained in a good state of preservation.

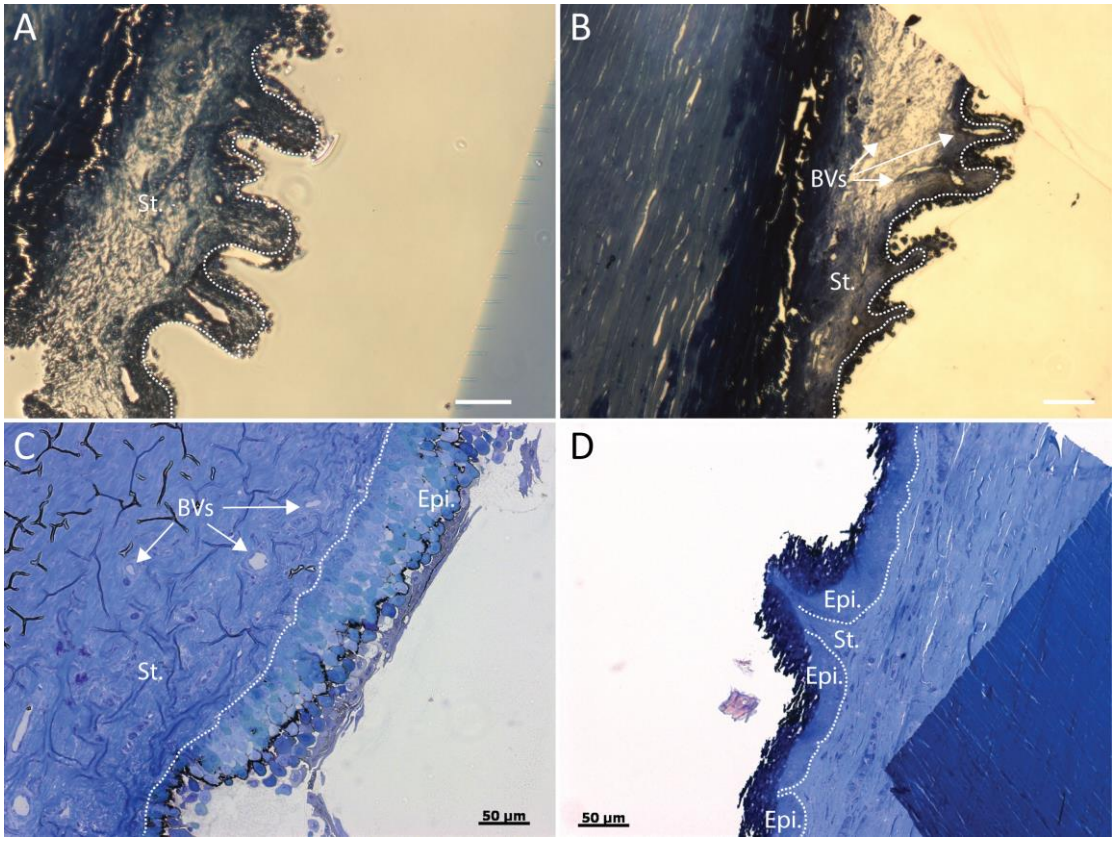

Figure 4.2. Assessment of tissue quality on semi-thin sections prior to SBFSEM.

Toluidine-blue stained semi-thin (750µm) sections of limbal biopsies embedded in resin. A and B show poorly preserved limbal epithelium and stroma that are not suitable for further SBFSEM analysis. C shows a well-preserved tissue where 7-10 layers of the limbal epithelium are preserved. Basal layer of the limbal epithelium is preserved in D. This tissue is acceptable for high-magnification SBFSEM imaging focused at the interface between the basal epithelium and the stroma. Dashed line: interface between limbal epithelium and stroma. Epi.: epithelium, St.: stroma, BVs: Blood vessels. Scale bars: 50µm.

Once the quality of limbal biopsies has been confirmed on semi-thin sections, any excess resin was further trimmed and the area of interest drastically reduced to

a 0.5mm square in order to fit the cutting window of the diamond knife in the chamber of the SEM (Figure 4.3). Sliver epoxy conductive glue (Agar Scientific) was then prepared by mixing an equal volume of the two components and used to attach the small resin blocks on SEM cryopins (Agar Scientific). Because of its conductivity, this glue limits accumulation of electrons at the surface of the sample and thus reducing the charging effect, an artifact generated by the accumulation of electrons at the surface of the sample inside the chamber of the microscope.

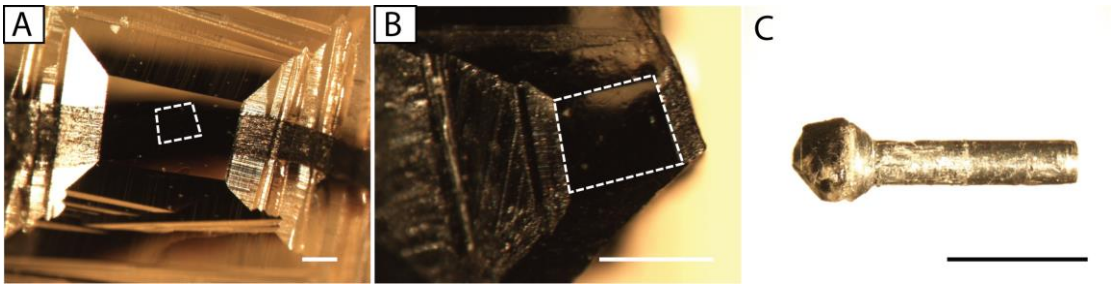

Figure 4.3 Comparison of resin blocks used for conventional TEM and SBFSEM

A represents the surface of a resin block used for ultrathin sectioning and TEM imaging.

B and C represent a resin block mounted on a cryopin (view from top in B) for SBF imaging. Dashed box in B highlight the surface of the resin block. Dashed box in B has the same size as the dashed box in A. Note that the area imaged by SBFSEM is greatly inferior to what is achievable by TEM where the area of the section is limited by the size of the grid (approximately 3mm in diameter). Bars: 0.5mm in A and B; 5mm in C.

4.2.3 Sample loading, serial block-face imaging and data analysis

Once mounted on cryopins, the surface of resin blocks was sputter coated with a thin layer of gold palladium in order to generate a conductive surface and limit the charging effect. Samples were then carefully inserted on the ultramicrotome of the 3view system (Figure 4.4A) and loaded inside the chamber of a Zeiss Zigma scanning electron microscope. Approach of the diamond knife to the sample was initially made manually using a binocular and the light reflection at the surface of the resin block and then automatically by making a 100nm step-by-step approach.

Numerous settings can be adjusted in order to obtain the best imaging quality. Typically, acceleration voltages (AVs) ranging between 2kV and 20kV are used for SEM imaging. For biological samples, more details are visible when using a high AV as more BSEs are generated from the sample. However, a high AV involves an increased interaction of the electron beam with the specimen and can be at the origin of melting of the surface of the resin block. Magnification is set by the size of the raster of the electron beam on the sample surface and is typically ranging between 30X and 30,000X. High magnification gives better details of what is seen but reduces the field of view and might generate resin softening. The pressure inside the chamber of the SEM is maintained by nitrogen and is also adjustable. A better signal to noise is generally obtained with a higher vacuum. However, a higher vacuum generates more charging and thus affects the quality of the micrograph. The dwell time corresponds to the length of time the electron beam dwells on one pixel of the sample. A long dwell time increases the

amount of BSEs that can be collected and thus increases quality of the image. However, a long dwell time involves a longer 'scanning' time that is directly associated with charging and melting of sample. Dwell time is a setting to consider when larger pieces of tissue are analyzed as it could drastically increase duration of the imaging run. Diameter of the aperture controls the amount of electrons hitting the surface of the sample. A high aperture is proportional to the amount of BSEs emitted and thus to the quality of the image generated. A high aperture however also increases the risk of charging and resin softening. Resolution of the image generated can also be adjusted and reach up to 4K x 4K. However, the amounts of details observed on the final image mostly depend on the quality of the sample (preservation, embedding, staining…). Using the highest resolution generates fundamental problem in the storage and subsequent analysis of large amounts of data that can routinely reach hundreds of gigabytes in one single overnight run. For this reason, setting a reasonable resolution for the amount of details required is essential when considering the storage of the vast amounts of data that volume EM involves. Advantages and disadvantages of changing settings of the 3View imaging are summarized in table 4.1.

	Description	Increasing		Decreasing	
		Advantage	Disadvantage	Advantage	Disadvantage
Acceleration voltage	The voltage at which electrons are pulled from the anode	More backscattered electrons (BSEs) therefore better signal to noise ratio	Increased interaction volume can mean more melting of sample, but also possible over sampling of image	Smaller interaction volume – can cut thinner sections	Fewer BSEs so signal to noise can be poor
Magnification	Set by the size of the raster area of the electron beam on the sample surface	Increases the detail of what is seen	Decreases the field of view. Because of nature of SEM the electron beam is now scanning over a smaller area and melting can occur.	Increases field of view	Decreases the detail/ resolution
Variable Pressure	Use of a gas (in our VP SEM this is nitrogen) within the chamber of the SEM	Decreasing the vacuum, decreases the charging	Decreases signal to noise ratio, thus interference and noisy image.	Increases charging	Better signal to noise
Dwell time	Length of time the electron beam dwells on one pixel worth of sample.	Increases the number of BSEs that can be collected = better image	Increases the chance of charging and melting of sample. Longer acquisition time.	Shorter acquisition time =more sections cut in same number of hours.	Fewer BSE collected = image could be noisy
Aperture	The final aperture of the SEM	Increasing the diameter increases the width of the electron beam and thus the number of electrons hitting the sample. = more BSEs	More electrons = more charging and heating of sample = chance of melting	Smaller beam diameter = better resolution	Fewer BSEs, lower signal to noise ratio
Resolution	By this we mean pixel resolution of the image, not actual resolution of the sample	Depending on sample may get more details within the sample	Larger file sizes	Less interaction of electron beam with sample = less charging/heating/melting	Fewer details within sample

e.g. the same sort of data could conceivably be obtained from these 2 scenarios (with the other parameters staying the same):
(1) High accelerating voltage Low vacuum (more gas) Short dwell time;
(2) Low voltage High vacuum (less gas) Long dwell time;
For the sake of time, if the sample can stand the parameters without melting then (1) would be a good option.

Table 4.1 Advantages/disadvantages of increasing or decreasing settings in the 3View.

The table illustrates what would happen when one parameter is changed and the others kept the same. Thus there is a fine balance for the setting of all the parameters to retrieve the information wanted from of a sample. Note that to make the point with each of these, the worst-case outcome was put in and the increase/decrease may have to be considerable (depending on the sample) to visualise the change.

For imaging of the limbal basal epithelial layer shown in chapter 5, the following settings were used:

- Magnification: x6.000.
- Accelerating voltage: 4 kV.
- Dwell time: 2 μs.
- Pressure: 20 Pa.
- Aperture: 60 mm.
- Resolution: 4k x 4k.
- Slice thickness 100 nm.

Because the sectioning process of SBF imaging takes approximately 30sec; with a dwell time set to 2μs at a resolution of 4k x4k, the total duration of an imaging-sectioning cycle is about 1min. The total duration time of SBFSEM imaging would be thus about 16-17 hours to cover 100μm of the sample in Z direction with an ultrathin sectioning thickness set to 100nm.

The automated process of sectioning-imaging was repeated for up to 999 cycles generating a large data stack of 999 serial images (figure 4.4B). Serial images were collected as .Dm3 file format and converted into .tiff files using Digital Micrograph™ (Gatan, UK). The complete data stack was then transferred into a Wacom Cintiq workstation and loaded into AMIRA 3D Software for Life Sciences for conversion into voxels (volumetric picture elements). Noise reduction median filter was applied to the entire data stack, and area of interest manually segmented on every single slice using the interactive pen (figure 4.4C). Finally, once the area of interest was entirely manually segmented, 3D volumes were generated (figure 4.4D).

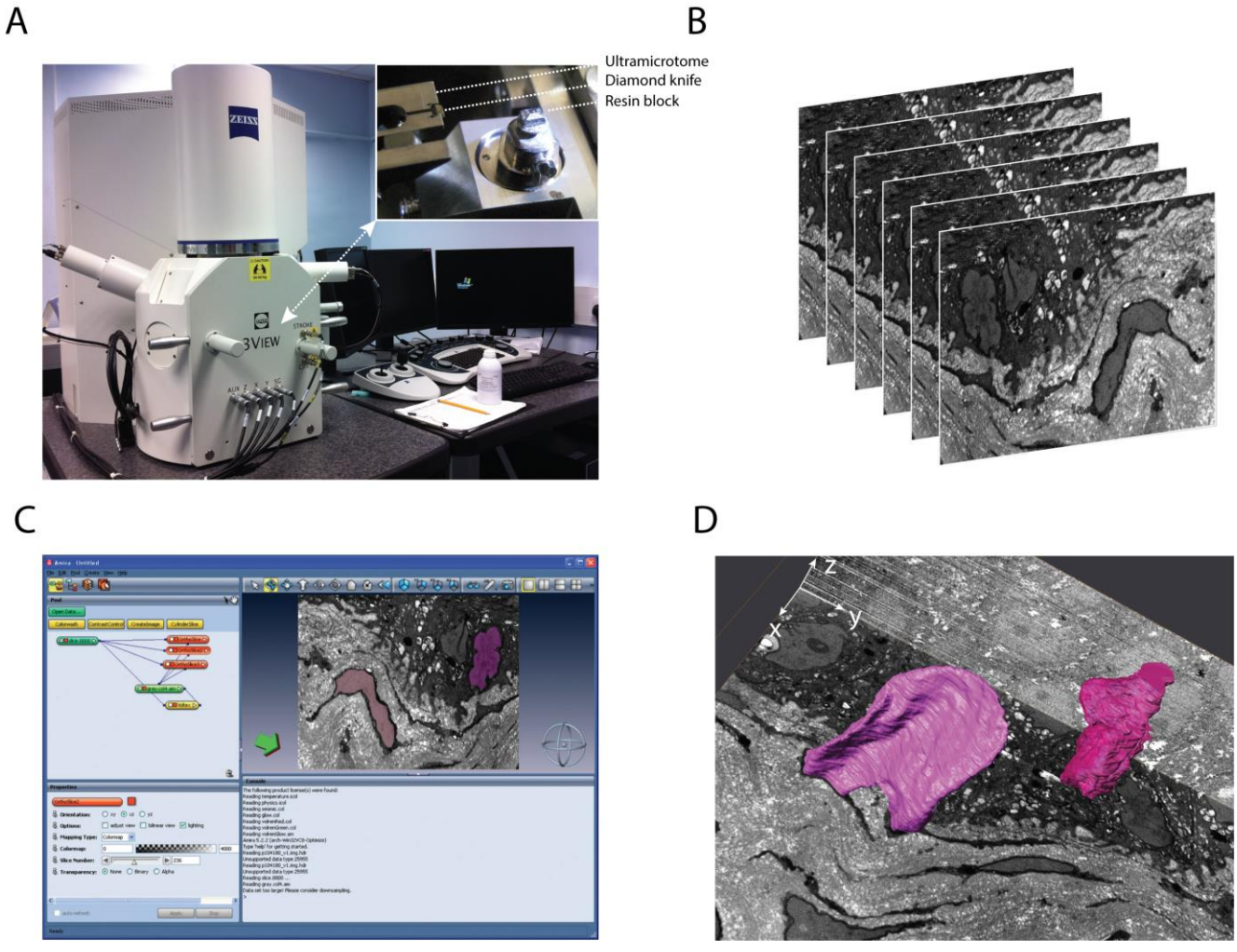

Figure 4.4 Serial block face imaging, manual segmentation and 3D reconstruction.

A. Gatan 3view serial block face imaging system within the specimen chamber of a Zeiss Sigma FESEM. Inbox shows the ultramicrotome, the diamond knife and the specimen loaded inside the chamber of the microscope.

B. Serial imaging and sectioning generate a large data stack of the area of interest. Here, the interface is between the limbal basal epithelial layer and the limbal stroma.

C. Converted files were transferred into a workstation and converted into voxels using AMIRA imaging software. Area of interest was manually segmented (purple and pink areas).

D. Manual segmentation of the area of interest on the entire data stack generated 3D volumes in x, y and z directions.

Serial block face imaging theoretically allows 3D reconstruction of a specimen in great detail, including subcellular structures as small as collagen fibrils. In practice, the resolution of images collected was affected by the quality of limbal biopsies prior to fixation. As discussed previously, rims stored in Optisol were generally not suitable for EM imaging, as these tissues were usually only available between 5 and 10 days post mortem. Fresh tissues unsuitable for corneal transplantation and usually available within 48 hours post mortem had a greater preservation as seen on semi-thin and hematoxylin-eosin sections. However, at very high-magnification, these tissues could also show some artifacts that limited imaging of small organelles and subcellular structures. Even if considered as relatively fresh, these tissues were not immediately fixed post enucleation, as it is the case for animal tissues, cells in culture or other model organisms. For this reason, the amount of details observed was limited when

imaging at a magnification higher than x6.000. Figure 4.5 compares the interface between the limbal basal epithelial layer and the limbal stroma imaged by both TEM and SBFSEM. Details of the limbal epithelium, limbal stromal cells and the basement membrane are clearly revealed by both imaging techniques. However, resolution of SBF imaging is marked by the absence of details of the collagen network within the limbal stroma. The resolution of SBF imaging however remains sufficient to image the basement membrane at the interface between the basal epithelial layer and the limbal stroma and also cell-to-cell interactions that might occur in this specific area.

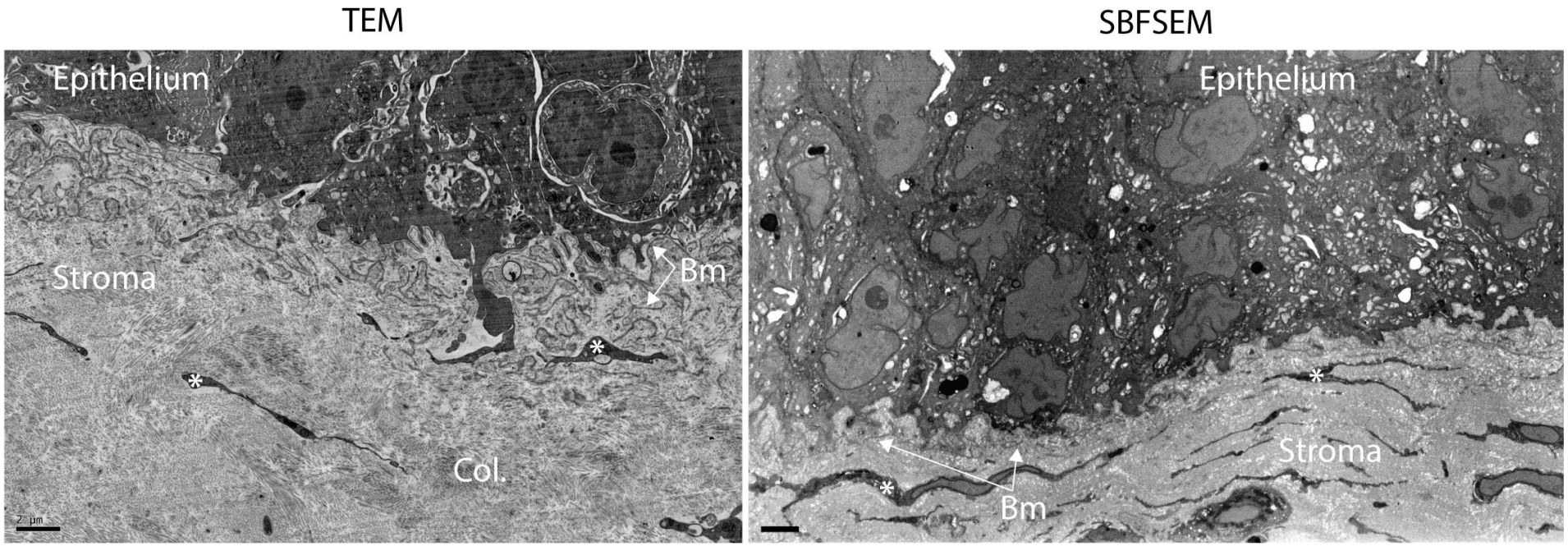

Figure 4.5. Limbal basal epithelial layer imaged by transmission (TEM) and serial block-face scanning electron microscopy (SBFSEM).

Transmission electron microscopy reveals ultrastructure of the limbal basal epithelium, the limbal stroma, the basement membrane and details of the collagen network.

Serial block-face imaging shows similar ultrastructure of the area of interest despite lower details of the basement membrane and limited details of collagen fibers.

Scale bars: 2μm. Col.: collagen fibers, Bm: basement membrane, *: limbal stromal cell extensions

4.2.4 Limits of SBF imaging

As discussed previously, serial block face imaging can introduce several artifacts that can limit high-resolution imaging of the specimen. Artifacts can be formed during the preliminary preparation steps or during the observation under the effect of the electron beam hitting the sample. The specimen is embedded in a hard resin that maintains the sample stable under the electron beam but with also a minimum of softness to allow diamond knife ultrathin sectioning. Longer exposition time (dwell time) increases the number of electrons interacting with the sample at the surface softening and melting the resin. As a consequence, the surface of the resin block becomes cracked and irregular as shown in figure 4.6A. Changing the setting such as the accelerating voltage, aperture, dwell time and pressure could limit this artifact but reduce the signal to noise ratio and thus the amount of details seen on the image. Knife marks are a common issue in TEM imaging and are generally inevitable. These marks might be due to damages of the diamond knife or due to the presence of resin particles remaining on the cutting edge of the knife. The same issues are encountered with SBF imaging and the resulting image presents “wheel marks” artifacts as seen in figure 4.5B. Serial block face imaging involves serial sectioning and imaging of the surface of the resin block. Normally, sections shed off the surface of the specimen after sectioning. In some cases, however, sections remain attached at the cutting edge of the diamond knife and redeposit at the surface of the block when the knife retracts. When the specimen is imaged, a folded section appears at the surface of block as shown in figure 4.6C. This artifact will disappear with the next sectioning cycle. One of the major issues encountered with scanning electron

microscopy imaging is termed the charging effect. This artifact is the consequence of the accumulation of electrons at the surface of the specimen. As shown in table 4.1, the charging effect increases with the acceleration voltage, low pressure and a large aperture. Despite the greater generation of back-scattered electrons and thus a higher signal to noise ratio, charging of the specimen is typically manifested by a bright spot artifact on the image as shown in figure 4.6D. The charging effect can be limited by reducing the number of electrons hitting the sample (table 4.1) but also by increasing conductivity of the sample during the preparation by sputter coating the surface of the specimen with gold-palladium and using silver epoxy glue for binding the resin block on the pin.

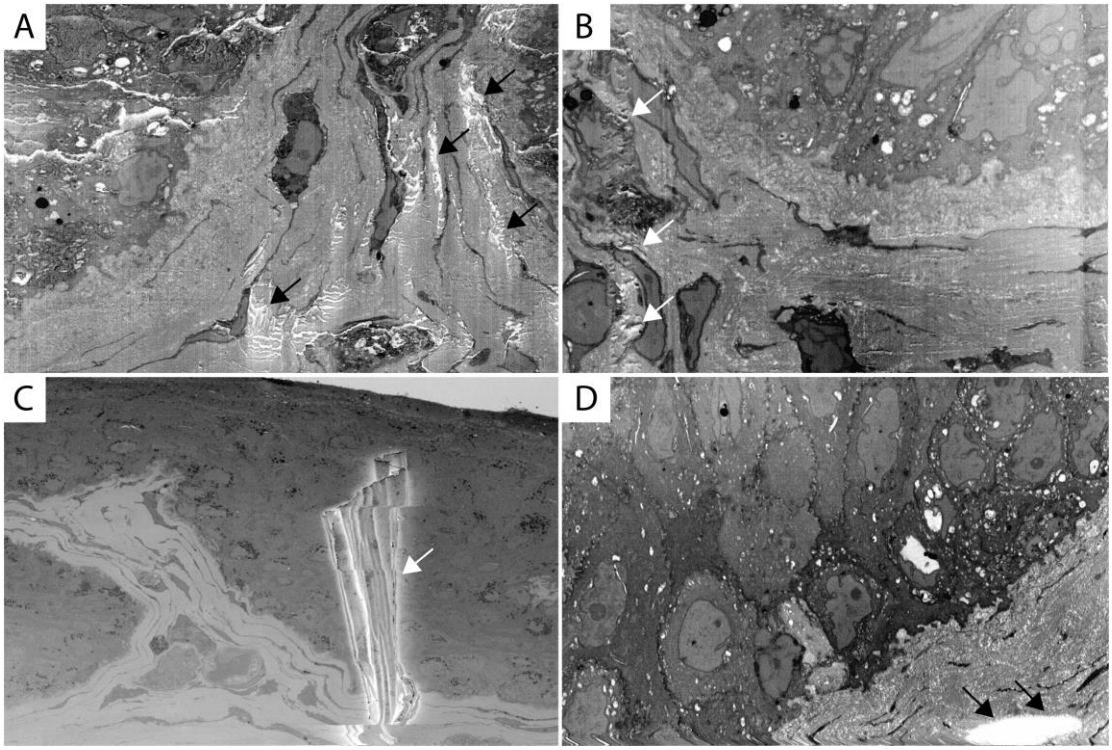

Figure 4.6 Artifacts commonly observed with serial block-face imaging.

A. Resin softening and melting (black arrows) occurs when the number of electron hitting and interacting with the sample is too high.
B. Knife marks (white arrows) are also a common artifact generally observed with TEM imaging and are the result of either damages, or particles remaining at the cutting edge of the diamond knife.
C. A folded section cut off the resin block in the previous cycle is sometimes deposited at the surface of the block (white arrow).
D. Accumulation of electrons at the surface of the sample is at the origin of the charging effect manifested by a bright spot artifact on the image (black arrows).

4.3 Discussion

Electron microscopy is currently undergoing a revival with the emergence of new volume EM techniques that enable the collection of large amounts of data and the imaging of tissues, cells and sub-cellular structures with unprecedented detail. Serial block-face imaging is still a recent innovation but the number of publications referring to this emerging imaging technique is constantly increasing and the technology has now been applied to a wide type of organisms, tissues and cells (Peddie & Collinson, 2014).

SBFSEM records serial images of the surface of a specimen in a process that is completely automated. The process generates a large data stack of serial images with a resolution approaching that of transmission electron microscopy for the imaging of biological samples. Initially developed for imaging and volume

reconstruction of the neuronal network of the central nervous system, SBFSEM has now been applied to image numerous tissues, organs and cell types (Peddie & Collinson, 2014). Because of the large volume of tissue that can be imaged in one run, SBF imaging appears as a powerful tool for the observation of multicellular structures such as LESCs and LCs. However, segmentation of the data stack by hand is time-consuming and tedious as there is no reliable software capable of automatic segmentation of membranes and volume rendering. For this reason, manual segmentation is often focused on a very specific type of cell or organelle and requires a precise preliminary analysis of the collected data stack. In the present chapter a protocol has been developed to image for the first time the limbal basal epithelial layer and the limbal stroma by SBFSEM. The main issue encountered in the preparation of human limbal biopsies for SBF imaging was the poor preservation of the specimen prior to fixation. This was due to the post mortem degenerative and release of intracellular enzymes as organelles breakdown, which irreversibly affects the quality of corneal biopsies. However, even if the lateral resolution reached in this study was lower than has been reported in other tissues and model organisms, it was sufficient to characterize cell-to-cell interactions that are present in the human limbal stem cell niche. This is the subject of the following chapter.

Chapter 5: High-resolution imaging techniques for investigation of cell-to-cell interactions in the human limbal stem cell niche

5.1 Introduction

The past decade has seen an important and growing interest in understanding the limbal stem cell niche as well as the LESC themselves. The limbal niche has a specific composition of the local extracellular matrix, a mixed population of poorly characterized stromal supporting cells, soluble factors and an important vasculature network that together provide the environment maintaining the limbal epithelial progenitors in an undifferentiated state (Klenkler & Sheardown, 2004; Notara et al., 2010; Pinnamaneni & Funderburgh, 2012; Schlötzer-Schrehardt et al., 2007; Schrader et al., 2010; Shimmura et al., 2006). The importance of the stem cell microenvironment has been rigorously investigated in the rabbit by Espana et al. (2003). In their study, the authors observed that central corneal epithelial cells transferred onto a decellularized limbal stroma, generated an epithelial sheet that did not express negative stem cell markers such as CK3 and connexin 43. On the other hand, limbal epithelial cells transferred onto central corneal stroma generated a differentiated epithelial sheet as shown by the expression of markers of corneal epithelial differentiation. Together, these results indicated that the limbal stroma and cells modulate limbal epithelial differentiation and proliferation in a direction favoring stemness whereas the central corneal stroma seems to promote terminal epithelial cell differentiation. Nevertheless, the exact function of these components and the identity of cells populating the limbal stroma remain poorly characterized and are the object of intense investigations. In chapter 3, we demonstrated using single cell clonal analysis that the LCs constitute a niche for LESCs (Dziasko et al., 2014). Human limbal epithelial progenitors are thus not

uniformly distributed around the limbus. In the present chapter, investigation is focused on the cells populating the limbal stroma immediately beneath the LCs. Attempts were made to identify putative interactions between LESCs and niche cells, but evidence of such interactions is currently limited and it has not yet been shown as in other stem cell compartments (Li & Xie, 2005). In 2011, Chen et al. demonstrated that the use of collagenase on limbal biopsies preserved some basement membrane proteins but cleaved the interstitial stromal collagen. Such digestion allowed the authors to not only isolate epithelial cells but also their associated mesenchymal cells. Interestingly, epithelial cells that were directly interacting with those 'niche' cells *in vitro* were highly positive for the expression of LESCs markers and had the greatest proliferative potential. Indeed, they showed that collagenase digestion maintained a close association between LECs and mesenchymal cells and that such interaction was sufficient to generate holoclone like colonies *in vitro* (Chen et al., 2011). Those observations suggest that LECs might directly interact with limbal stromal cells in the native niche and that such interaction is also important to maintain the potential of the epithelial progenitors. However, the evidence for such interactions in the native niche is currently limited and is the object of the present chapter. In the past, Gipson et al. showed using transmission electron microscopy that the basement membrane underlying the limbal epithelium was interrupted and fenestrated (Gipson, 1989). In the present chapter, we aimed to demonstrate by combining various high-resolution imaging techniques that such epithelial-stromal cell interaction might exist in the native niche and could be facilitated by these focal interruptions of the local basement membrane. Transmission electron microscopy was firstly used to image and compare the morphology of epithelial

cells composing the basal layer of either the LCs or the non-crypt rich limbus. Basal epithelial cells were considered as LESCs when they were small, compact and non-columnar on the electron micrographs. After optimizing the protocol of SBFSEM applied to the human cornea as described in chapter 4, we used this powerful volume imaging technique to highlight and identify for the first time direct cell-to-cell interactions between limbal epithelial cells and limbal stromal/mesenchymal cells. We further attempted to identify the stromal cells involved in the interaction with the limbal epithelial progenitors by targeting mesenchymal antigens by immunohistochemistry. We finally proposed the first 3D reconstruction at cellular scale of the limbal stem cell niche where limbal epithelial progenitors were unexpectedly closely maintained by both limbal stromal cells and limbal melanocytes.

5.2 Material and methods

5.2.1 Human tissue

All human tissue was handled according to the tenets of the Declaration of Helsinki and written consent was acquired from next of kin of all deceased donors regarding eye donation for research. Research consent was obtained via the Moorfields Eye Hospital Lions Eye Bank (U.K) and Lions Eye Institute (Florida, U.S). All experiments were approved by the National Research Ethics Service, South West 3 REC, reference 10/H0106/57.

5.2.2 Transmission electron microscopy

Human limbal biopsies were isolated from cadaveric corneas under a dissecting microscope and stored in Karnovsky's fixative prior to post-fixation and resin embedding. Embedding of the limbal biopsies has been done as described in the chapter 2 (general material and methods). Once the area of interest has been identified on semi thin toluidine blue stained sections, ultrathin sections were cut off the resin block, observed under a Jeol 1010 transmission electron microscope and imaged with an SC1000 Orius CCD camera (Gatan, Abingdon Oxon, UK).

5.2.3 Serial block-face scanning electron microscopy

Crypt rich limbal biopsies isolated from 3 different donors were embedded and imaged by serial block-face SEM as described in chapter 4.

5.2.4 Manual segmentation and volume reconstruction

For low magnification imaging (figures 5.3 and 5.4), the limbal epithelium was reconstructed in yellow and stromal cells in blue. At higher magnification, LESCs that were directly connecting cells from the underlying stroma were manually segmented in green. Stromal cells were segmented in yellow and nuclei in pink (figure 5.5). The area of epithelial-stromal junction was segmented and reconstructed in orange in the second experiment (figure 5.6). For the last 3D reconstruction, the limbal melanocyte was segmented in red, the LESC in green and the stromal cell in yellow. Nuclei are shown in blue (figure 5.9).

5.2.5 Immunohistochemistry

Crypt-rich (n=3) and non-crypt (n=3) limbal biopsies were isolated from fresh cadaveric corneas. Immunohistochemistry was performed on frozen sections as described in the general methods (chapter 2). Images were captured using a Carl Zeiss 710 laser-scanning microscope (Carl Zeiss, Hertfordshire, UK).

5.3 Results

5.3.1 Limbal epithelial and limbal stromal interface topography imaged by TEM

Figure 5.1 shows the general aspect of the limbal basal epithelial layer within the non-crypt rich limbus observed by TEM. As shown in 5.1 A and B, cells populating the basal layer are morphologically similar. The cells appear columnar and elongated and contain a dense network of intermediate filaments. Cells present on the basal side display finger like projections and highly express hemidesmosomes (white arrowhead in 5.1 D) to facilitate anchorage to the underlying basement membrane. The basement membrane appeared thick and perfectly aligned with cells of the basal epithelial layer (black arrows figure 5.1 D). Fibroblastic extensions were observed within the non-crypt limbal stroma but not in the direct vicinity of the limbal basal epithelium.

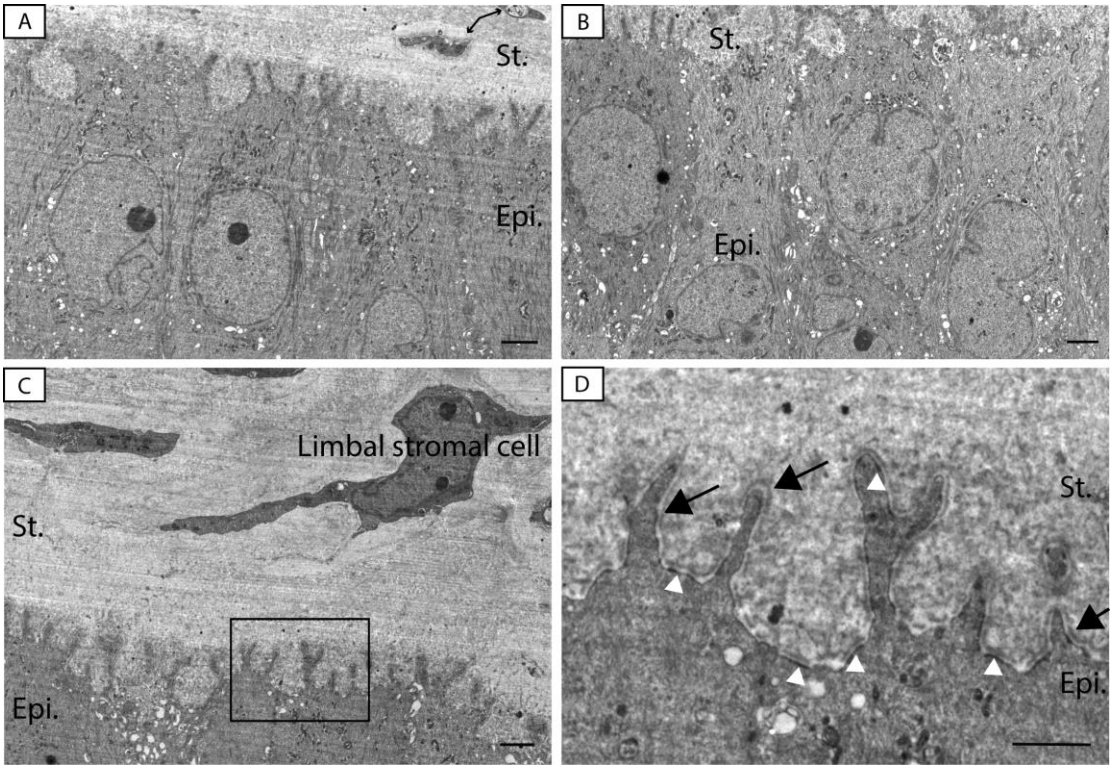

Figure 5.1 Interface of the limbal basal epithelial layer and the limbal stroma within the non-crypt limbus imaged by TEM.

Limbal basal cells appeared large and elongated (A and B). Intermediate filaments and hemidesmosomes were highly expressed (White arrowheads in D). Digitations on the basal side and a thick and regular basement membrane were also observed (Black arrows in D).

The box in C represents the area in D. Scale bars: 2μm. Epi: epithelium; St: stroma. Black arrows in A: limbal stromal cell extensions.

In contrast, basal epithelial cells at the edge of the limbal crypts contained a mixed population of epithelial cells. Most of the cells observed had the same morphological aspect as basal epithelial cells populating the non-crypt rich limbus. However, a population of small, circular, basal cells characterized by a high nucleus/cytoplasm ratio that were mainly located on the edges of the crypt, close to blood vessels of the underlying stroma (white asterisks in figure 5.2)

were also observed. These cells had a morphology consistent with stem cells; they were almost devoid of hemidesmosomes and rested upon a thin basement membrane. Moreover, these cells appeared to be in close proximity to limbal stromal cell extensions (black arrowheads in 5.2) suggesting a possible route for crosstalk or direct cell-to-cell interaction.

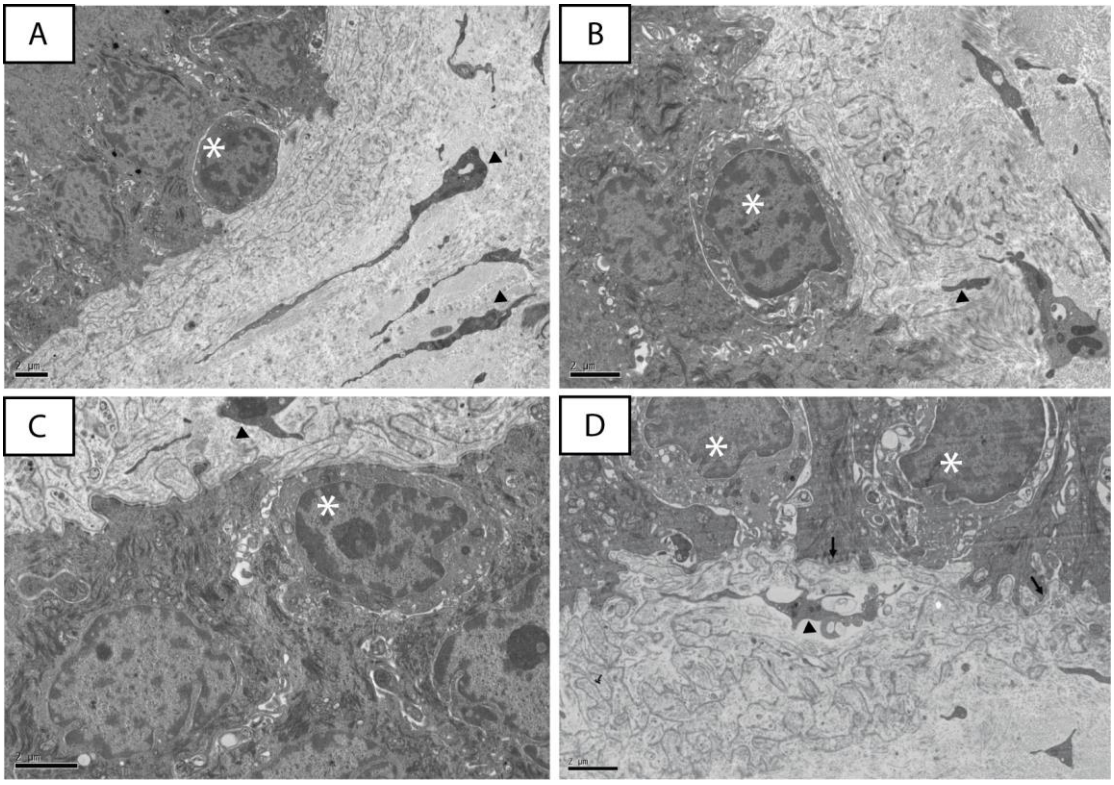

Figure 5.2 Interface of the limbal basal epithelial layer and the limbal stroma within the LCs observed by TEM.

LESCs marked with a white asterisk lay on a thin basement membrane. These cells were of small size, circular morphology and had a high NC ratio. Limbal stromal cell extensions (Black arrowhead) were in very close vicinity to the LESC and suggest a direct route for epithelial-stromal cell-to-cell interaction. Bars: 2μm; Black arrows: hemidesmosomes; White asterisks: LESCs.

5.3.2 Limbal crypt epithelial/stromal interface imaged by SBFSEM at medium-low magnification

Despite the great resolution reached by TEM, focal contacts between LECs and limbal stromal cells are extremely difficult to image as the resolution in z is strongly limited to the thickness of the section as discussed in chapter 4. For this reason, SBF imaging appears as an ideal technique for tracking, slice by slice, cells of interest and to highlight putative focal contacts.

Figure 5.3 reveals the proximity of limbal stromal cells (segmented in blue) with the limbal epithelium (segmented in yellow). Manual segmentation of the data stack and 3D reconstruction confirms the extensions pointed in figure 5.2 belong indeed to stromal cells in close vicinity with the limbal epithelium. Moreover, 3D reconstruction reveals how stromal cells shape the basal epithelium at the edge of the crypt (figure 5.3B and C). Such close interaction could not be observed within the non-crypt rich limbus where fibroblast-like cells and their extensions localize deeper in the stroma (figure 5.1C).

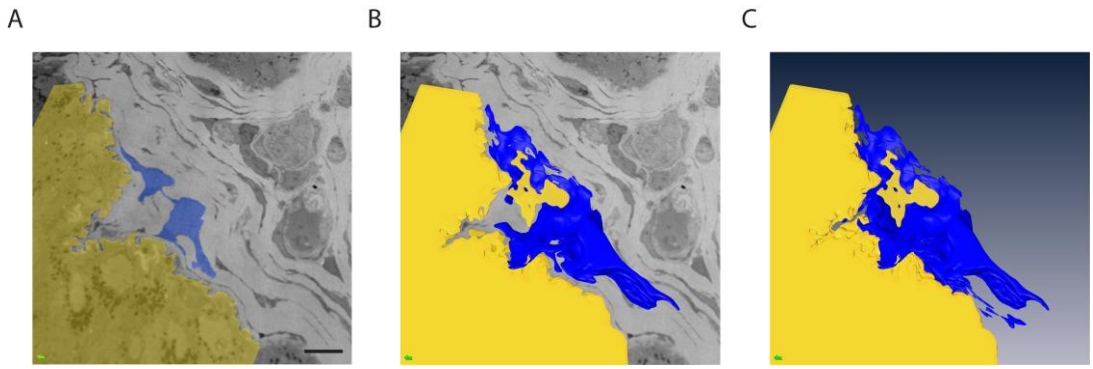

Figure 5.3 LC ultrastructure observed by SBFSEM at medium magnification.

3D reconstruction of the interface of the limbal basal epithelium and the limbal stroma imaged by SBFSEM.

Yellow area in A and yellow volumes in B and C represent the limbal basal epithelium at the interface with the limbal stroma; Blue area and blue volumes represent a limbal stromal cell before (A) and after 3D reconstruction (B and C). Note the close association between the basal epithelium and the stromal cell and the abundance of blood vessels in this specific area. Scale bar: 2μm

3D reconstruction highlights the proximity of the limbal epithelium with the limbal stroma and suggests direct cell-to-cell contacts. Scale bar: 5μm.

Figure 5.4 shows the general aspect of sections of the same LC imaged by SBFSEM at low magnification (200x). A, B, C and D correspond to non sequential images of the same data stack and give an overview of the area of interest that has been further imaged with a higher magnification (800x). Low magnification SBFSEM imaging revealed the complexity of the stroma beneath the limbal epithelium (Fig. 5.4 A-C and supplementary videos S1 and S2). Again, this area was characterized by an abundance of stromal cells and their extensions localized immediately beneath the epithelium (White asterisks in 5.4 B) and by the presence of blood vessels labeled Bv in 5.4A. Within the epithelium, some cells contained abundant electron dense cytoplasmic granules that had the potential to be melanosomes observed in limbal melanocytes (white arrowheads in 5.4B). 3D reconstruction revealed the proximity of the limbal stromal cells localized immediately beneath the limbal basal epithelium although direct contact could not be confirmed at this magnification (Blue and yellow volumes in

Fig. 5.4D and supplementary online videos 1 and 2).

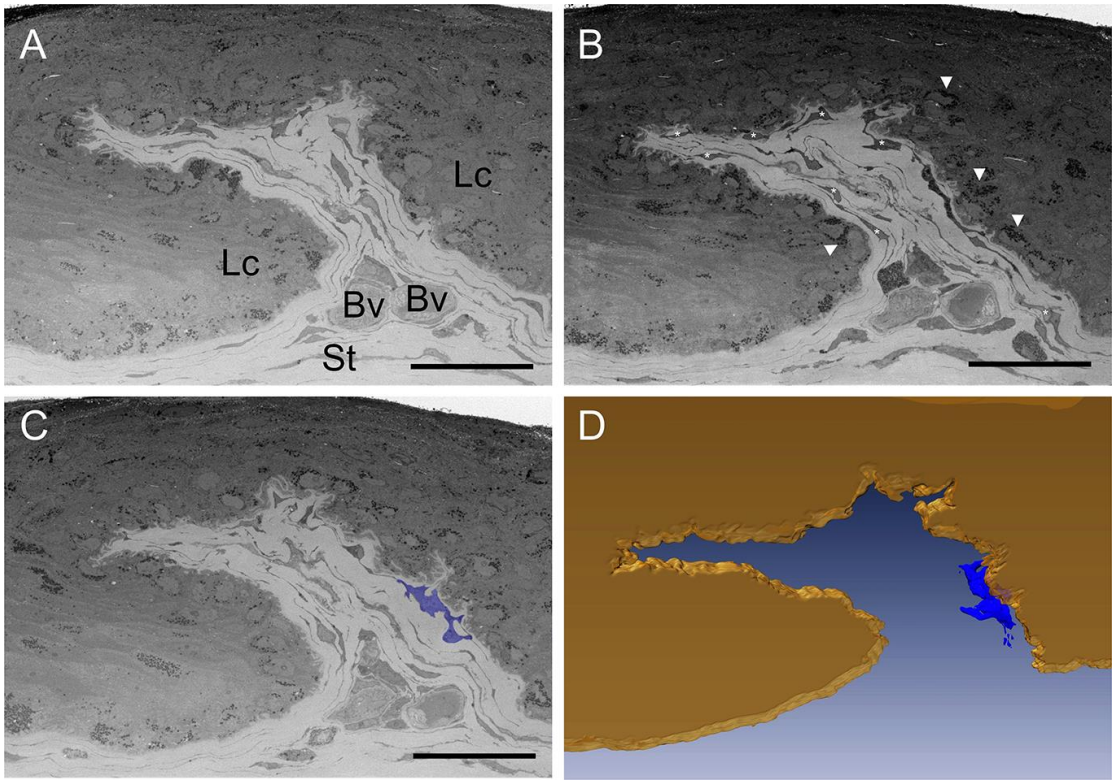

Figure 5.4 Limbal crypt ultrastructure observed by SBFSEM at low magnification.

LC tangentially imaged through 70 µm from the corneal to the conjunctival side of the limbus. A, B and C represent non-sequential micrographs of the same 3D dataset. Manual segmentation followed by 3D reconstruction highlights the close proximity between the limbal epithelium (yellow volume in D) and a limbal stromal cell (white asterisks in B, blue area in C and blue volume in D) within the limbal crypt (Lc) suggesting putative cell-to-cell contact. Lc: limbal crypt; Bv: blood vessel; St: Stroma. Arrowheads: melanocytes. Scale bars: 50 µm.

5.3.3 Limbal crypt epithelial/stromal interface imaged by SBFSEM at high magnification

High-magnification SBF imaging (800x) focused at the interface between the limbal basal epithelium and the limbal stroma within the LCs reveals that stromal fibroblast-like cells (yellow segmentation in 5.5A) have the potential to directly connect small basal epithelial cells (green segmentation in 5.5A). Manual segmentation and 3D reconstruction of nuclei (pink segmentations and volumes) confirms that the cells of interest are distinguished after reconstruction of two distinct nuclei (figure 5.5B). Figure 5.5B shows the morphological aspect of the LESC (green) and the stromal cell (yellow) after 3D reconstruction. The LESC could be tracked in 40 sequential images for a total thickness of approximately 4μm whereas the stromal cells, that could be tracked in more than 130 sequential micrographs, measured for this reason approximately 13μm.

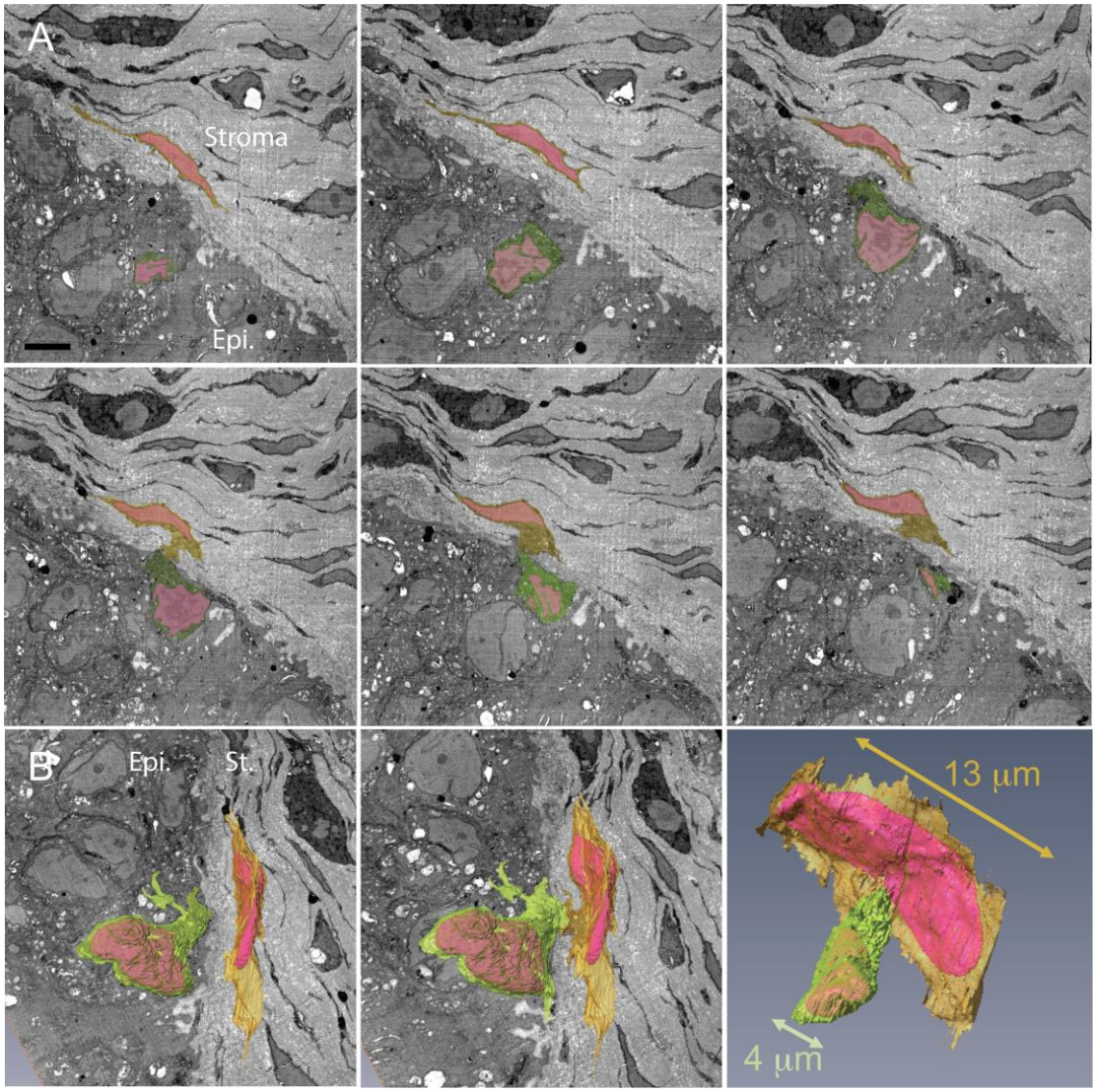

Figure 5.5 High magnification SBFSEM imaging of the limbal stromal and limbal basal epithelial layer interface at the edge of a limbal crypt.

A. Non-sequential serial images of SBF data stack showing focal connection between a small basal epithelial (green) cell and a stromal cell (yellow). Nuclei are segmented in pink.

B. 3D reconstruction of cells segmented in A showing focal connection of a LESC (green) and a large and elongated stromal cell (yellow). 3D reconstruction is aligned to the data stack (left and middle panels). The right panel represents the same cells rotated and highlights the difference in size between the LESC and the stromal cell. Scale bar: 5µm.

Such direct stromal-epithelial cell-to-cell interaction has been observed in all donors analyzed (n=3) and more frequently at the edge of the LC. Figure 5.6 shows a stromal-epithelial cell contact observed in a limbal biopsy coming from another donor. The small basal epithelial cell (putative LESC) is represented in green and stromal cell extensions in yellow. After 3D reconstruction, (figure 5.6B) it appeared that yellow stromal cell extensions segmented in A belonged to the same stromal cell. The area reconstructed in orange corresponds to the area of interaction that was seen in 5 sequential images of the data stack. As thickness of the sections cut off the surface of the resin bloc is about 100nm and that the direct contact could be seen in 5 sequential micrographs, the focal stromal-epithelial contact was maintained for approximately 0.5μm. For this reason such stromal/epithelial contacts are not frequently observed with conventional EM techniques.

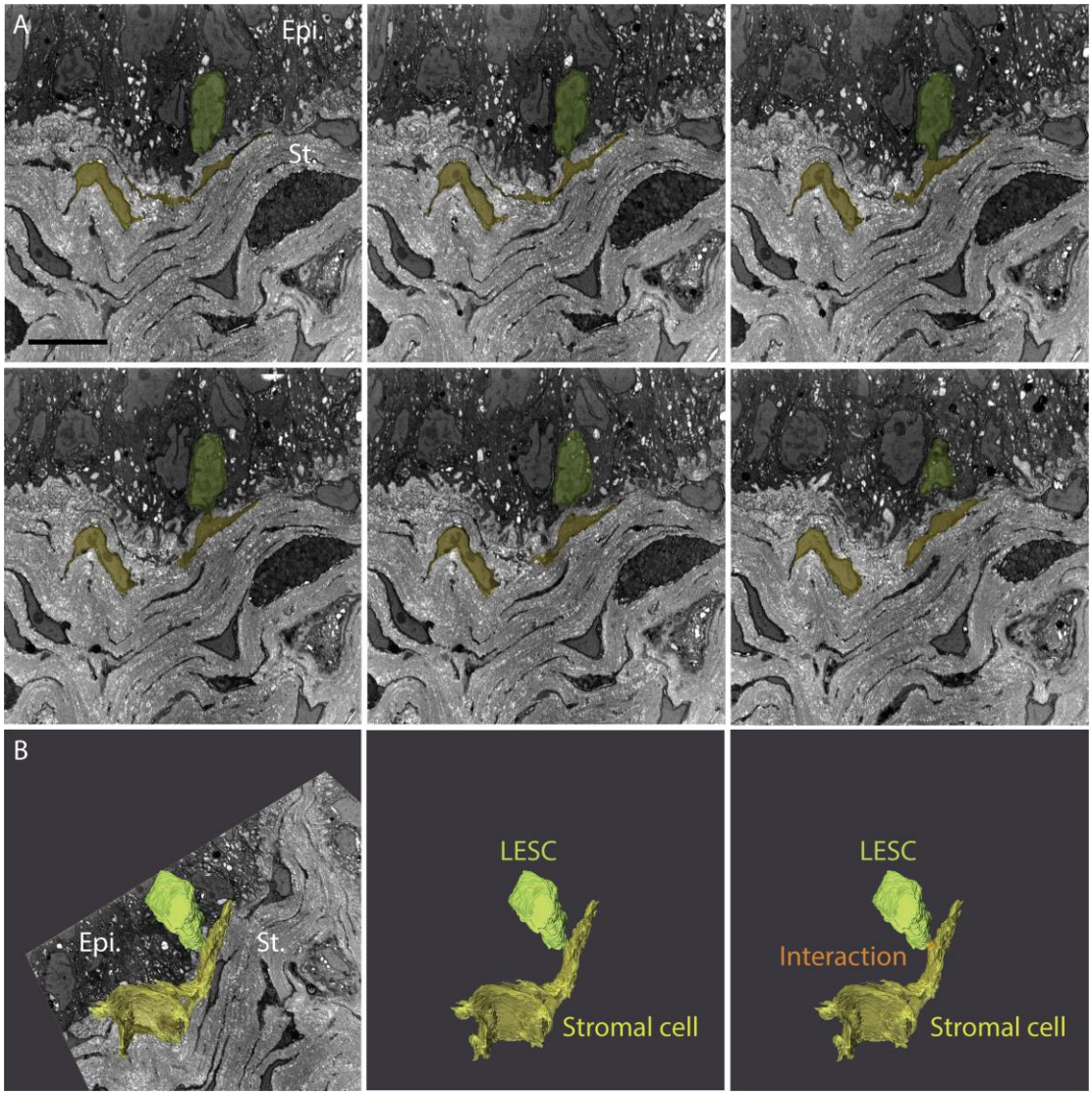

Figure 5.6 High magnification SBFSEM imaging of the limbal stromal and limbal basal epithelial layer interface at the edge of a limbal crypt.

A. Direct cell-to-cell interaction between a LESC segmented in green and limbal stromal cell extensions segmented in yellow. 3D reconstruction (B) shows that the yellow extensions segmented in A belonged to the same stromal cell. Area of interaction is represented in orange (right panel). Scale bar: 10μm.

5.3.4 Topographical analysis of the basement membrane at the edge of the limbal crypt

SBF imaging revealed unexpected focal contacts between small basal epithelial cells and elongated stromal cells. However, the resolution reached was not sufficient to analyze the basement membrane ultrastructure that should normally prevent such interaction. For this reason, the topography of the BM was further analyzed at high magnification by conventional TEM. Analysis of the BM was made at the edge of the LC where stromal/epithelial cell-to-cell interactions were previously been identified. As shown in figure 5.7 A, B and D, the BM appeared as a thin gray line supporting the basal epithelium. However, it appeared that the BM was interrupted in some locations allowing direct cell-to-cell contacts between the basal epithelium and stromal cell extensions (black arrowheads in 5.7 A and D).

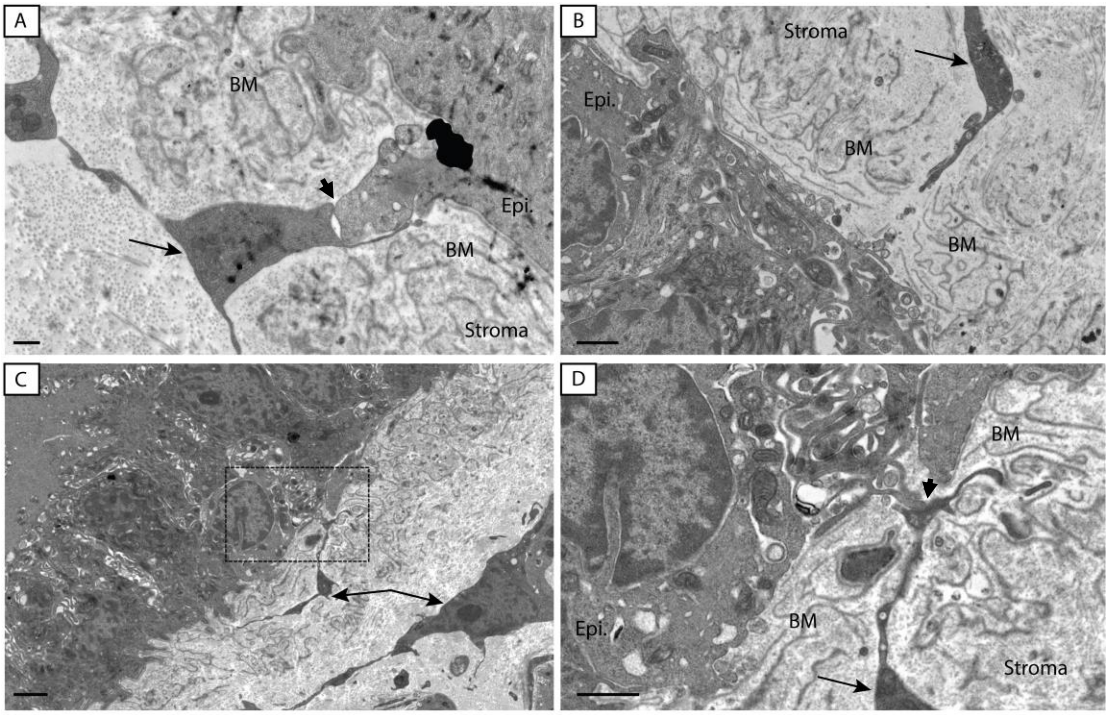

Figure 5.7 Transmission electron micrographs highlighting stromal-epithelial cell contacts and basement membrane interruptions within the limbal crypts.

The small black arrows point to direct contacts between stromal cell extensions and limbal basal epithelial cells that are facilitated by focal basement membrane interruptions. Box in C corresponds to area shown D. Large black arrows: Stromal cells or stromal cell extensions. Epi: epithelium, BM: Basement membrane, scale bars: 500nm A, 1μm B and D, 2μm C.

5.3.5 Distribution of limbal stromal cells expressing mesenchymal stem cell markers around the limbal circumference

In 2004, Polisetty et al. isolated a population of spindle cells from the limbal stroma that expressed mesenchymal stem cell markers such as CD90, CD105 and

CD34 when put in culture. To determine whether limbal mesenchymal cells were involved in the direct contact with LESCs, the expression of two mesenchymal stem cell (MSC) markers CD90 and CD105 was investigated in the central cornea the non-crypt and the crypt-rich limbus. Immunostaining for CD90 and CD105 was, as expected, negative for both MSC markers in the central cornea (Figure 5.8 A and 5B). However, a sub-population of limbal stromal cells in the limbus expressed both CD90 and CD105 mesenchymal markers. Interestingly, the distribution of these limbal mesenchymal cells was not uniform. In the non-crypt limbus a small population of stromal cells expressed CD105 and weakly expressed CD90 (Figure 5.8 C and D). On the other hand, in crypt rich regions, there was a sub-population of limbal stromal cells beneath the LCs that were highly positive for either CD90 or CD105 MSC markers (Figure 5.8 E and F).

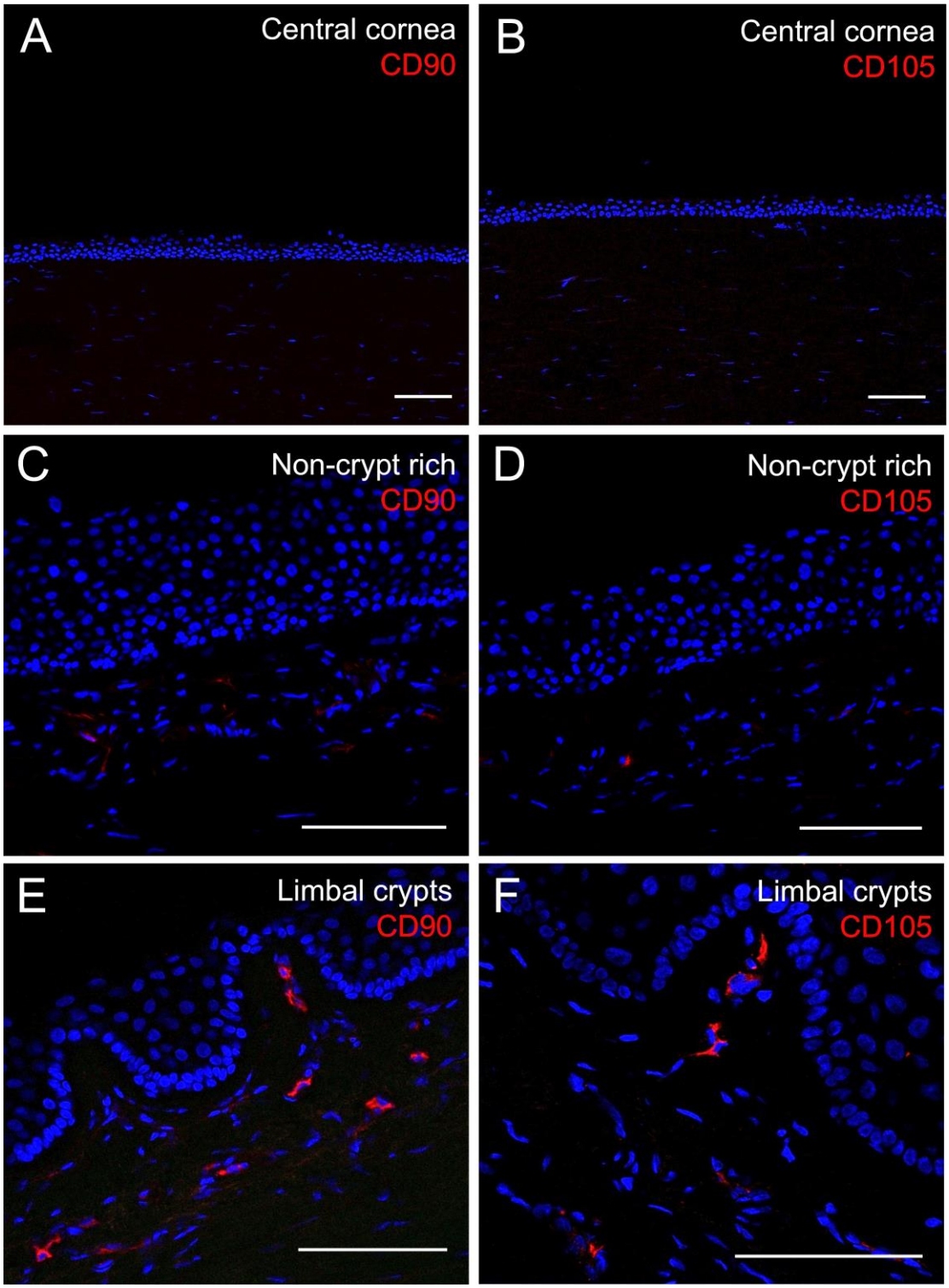
A
Central cornea
CD90
B
Central cornea
CD105
C
Non-crypt rich
CD90
D
Non-crypt rich
CD105
E
Limbal crypts
CD90
F
Limbal crypts
CD105

Figure 5.8 Results of immunohistochemistry staining for limbal mesenchymal cell markers CD90 and CD105 within the central cornea, the non-crypt rich limbus and the limbal crypts.

Immunofluorescence suggested that CD90 and CD105 expression is markedly increased by limbal stromal cells underlying the limbal crypts (E, F) compared to the non-crypt limbus (C, D). Central corneal sections were used as a negative control (A, B). Sections were counterstained with DAPI. Scale bars: 50 μm.

5.3.6 Assessment of N-cadherin expression in the limbal stem cell niche

N-cadherin is involved in direct interactions between stem and niche cells in numerous organs and organisms (Song & Xie, 2002). *In vitro,* N-cadherin mediated cell-to-cell interactions have been observed between limbal epithelial progenitors and 3T3 feeder cells (Higa et al., 2009). In order to check if N-cadherin was involved in epithelial/stromal cell-to-cell interaction revealed by SBFSEM, N-cadherin expression was assessed by immunohistochemistry in the central cornea (negative control), the non-crypt limbus and the limbal crypts. Generally, N-cadherin staining appeared weak within the central cornea and the non-crypt rich limbus as shown in figures 5.9 and 3.5 A and B (chapter 3, p100). Nevertheless, a positive staining was observed in small and compact basal epithelial cells (white arrows in figure 5.9 and figure 3.5C) that were located at the edge of the limbal crypt, where LESCs are believed to be located whereas no N-cadherin staining could be observed in stromal cells underlying the crypts and identified by their large and elongated nuclei.

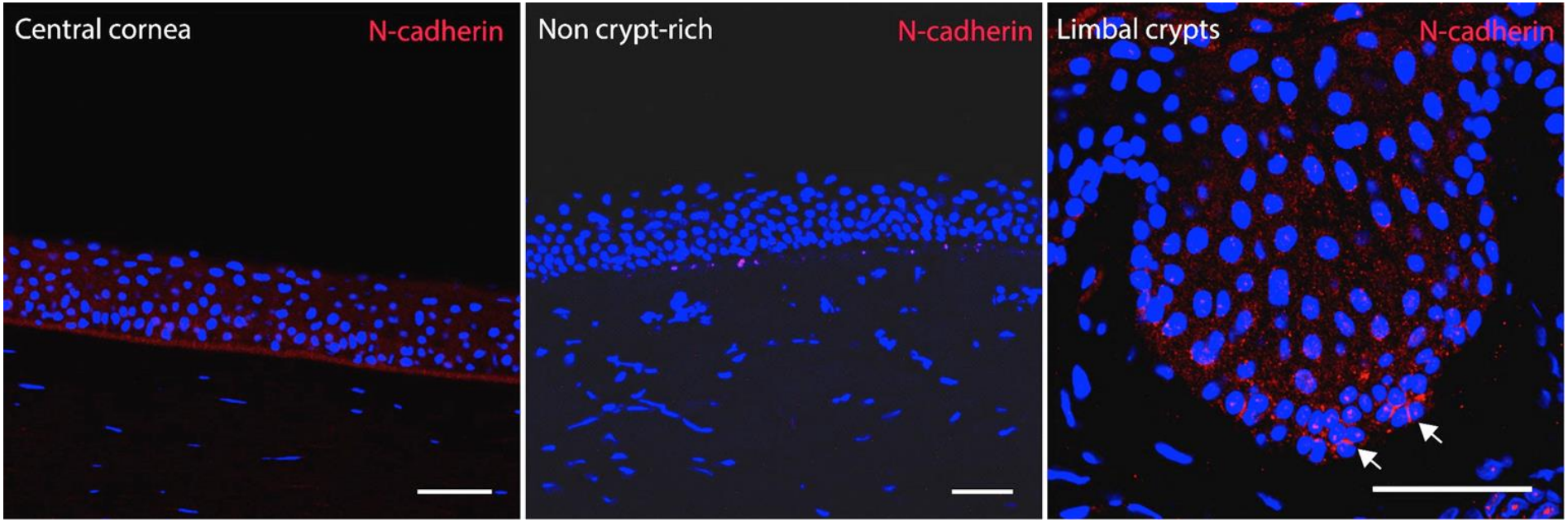

Figure 5.9 Results of immunohistochemistry staining for N-cadherin within the central corneal, the non-crypt rich limbus and the limbal crypts.

Immunofluorescence suggests that N-cadherin staining concentrates in clusters of small basal epithelial cells localized in the limbal crypt (White arrows). N-cadherin staining was negative for the central cornea and the non-crypt rich limbus. Scale bars: 50 μm.

5.3.7 Limbal melanocytes interact with LESC within the limbal crypts

Immunostaining for MelanA, specifically expressed by melanocytes, identified a population of these pigmented cells within the epithelial basal layer of the limbal crypts where LESCs are concentrated. As shown in figure 5.10A, limbal melanocytes were also observed, at a lower density, within the non-crypt limbus where they appeared dispersed between the epithelial layers. SBFSEM targeting the edge of the limbal crypt (figure 5.10C and 6D) revealed that pigmented dendritic cells with morphology consistent with limbal melanocytes were closely associated with the smallest basal limbal epithelial cells. After 3D reconstruction LESCs were found to directly connect with at least two non-epithelial cells (figure 5.10E). The apical aspect of the LESC connected with a dendritic limbal melanocyte (figure 5.10F) while the basal aspect connected with a limbal stromal cell (figure 5.10G).

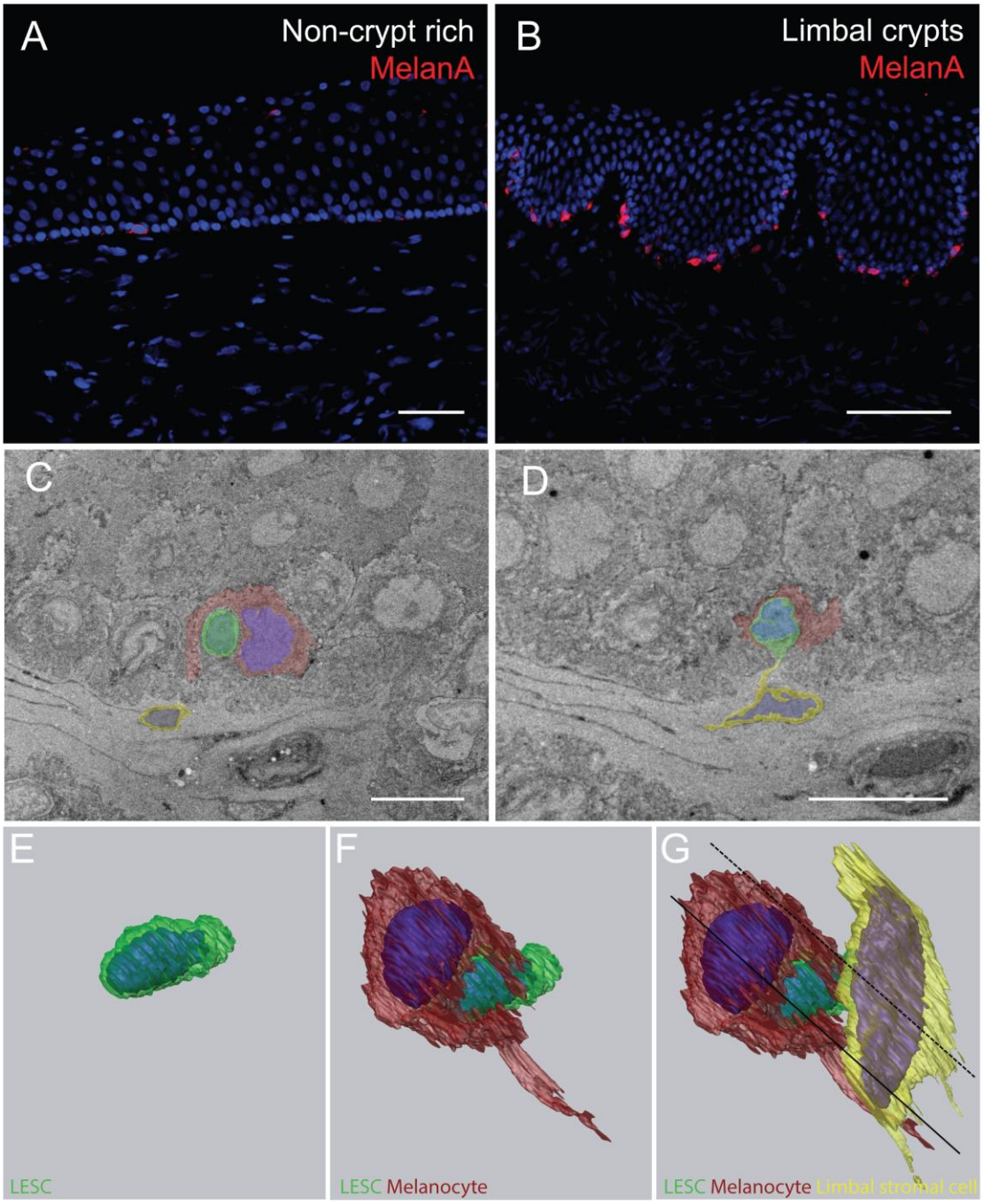

Figure 5.10 Melanocytes interact with LESCs in their niche. **Immunohistochemistry revealed a higher proportion of MelanA positive cells within the LCs than within the non-crypt limbal areas (A, B). Serial-block face scanning electron micrographs showing the lateral side of one limbal crypt (C, D). After manual segmentation and 3D reconstruction (E, F, G) LESC (smallest epithelial cell with a high nucleus/cytoplasm ratio) is represented in green, melanocyte (dendritic cell containing electron dense**

granules) in red, limbal stromal cell in yellow. Blue volumes correspond to nuclei. Continuous line in G corresponds to block face represented in C. Dashed line in G corresponds to block face represented in D. Scale bars: 50 μ m (A, B) and 7 μ m (C, D).

5.4 Discussion

Evidence for direct stromal-epithelial cell interactions in the native limbal stem cell niche is currently limited. In the present chapter investigations were focused on imaging LESCs in their native microenvironment by conventional TEM before further characterization of putative cell-to-cell interactions between epithelial progenitors and cells of the underlying stroma. Interestingly, small basal epithelial cells with high nucleus cytoplasm ratio were mainly observed within the limbal crypts, which, as previously demonstrated by single cell clonal analysis, constitute a reservoir for the limbal epithelial progenitors. Moreover, these small basal epithelial cells were closely associated with cells from the underlying stroma suggesting a direct route for crosstalk or cell-to-cell interaction. By high magnification SBFSEM it has been shown that LESCs were directly connected to “fibroblast-like cells” from the stroma via focal interruptions of the basement membrane.

Stem cell and somatic cell interactions have been observed in numerous species and organs and are still the subject of important investigations. In the drosophila ovary, direct contacts between germ stem cell (GSC) in the germarium and their non-stem cells neighbors (cap cells) are essential in the maintenance of the stem

cell character. When the female GSC divides, one daughter cell remains attached to the cap cell and maintains stem cell characteristics. The other daughter cell looses the interaction with the neighbor, differentiates and initiates oogenesis. The interaction between the stem cell and the cell from the niche is mediated by DE-Cadherins and Armadillo (catenin in vertebrates) that form a particular junction called an adherens junction generating a cell polarity. Finally, cap cells are expressing genes as Dpp, Gbb, Hh, Yb and Piwi involved in the maintenance and the control of the stem cell fate (Kirilly & Xie, 2007; Song & Xie, 2002). Genetic studies have demonstrated that a mutation of E-cadherin is responsible of the failure of cap cells to recruit and maintain stem cells in their environment and confirms importance of such cell-to-cell interaction.

The concept of a stem cell niche is an evolutionary conserved phenomenon and it is thus not surprising to observe the same mechanisms or the same basic molecular features preserving the cell stemness in mammals. Hematopoietic stem cells (HSCs) reside mainly within bone marrow during adulthood. The bone marrow is a complex organ containing numerous hematopoietic and non-hematopoietic cell types and functions as a complex regulatory system where alteration of one cell type can lead to perturbations in the whole hematopoietic lineage (Morrison & Scadden, 2014). The interaction of HSCs with stromal cells has been the subject of numerous investigations in the last decade. Cells regulating the adult HSCs include mature and immature mesenchymal lineages (Naveiras et al., 2009; Calvi et al., 2003; Asada et al., 2013; Méndez-Ferrer et al., 2010), neurons (Katayama et al., 2006), Schwann cells (Yamazaki et al., 2011) or perivascular and endothelial cells (Ding et al., 2012). In 2011, Méndez-Ferrer et

al. provided the evidence that a population of mesenchymal cells of the bone marrow had multi-lineage differentiation capacity into chondrocytes, osteocytes and adipocytes and also had the ability to generate fibroblastic colonies under specific culture conditions. These cells appeared positive for the expression of nestin, CD90, CD105 and negative for CD45. Interestingly, the authors observed that nestin +ve MSCs were spatially associated with HSCs and that such association was essential for maintenance and homing of HSCs in their niche (Méndez-Ferrer et al., 2010; Méndez-Ferrer et al., 2015; Isern et al., 2013).

Despite important functional and architectural dissimilarities between the bone marrow and the ocular surface, mesenchymal stem cells have also been identified within the stroma of the human limbus. In fact, Polisetty et al. 2008, isolated a population of limbal stromal cells that had the same properties mesenchymal cells isolated from the bone marrow. In addition to morphological similarities, limbal MSCs had the ability to produce multiple cell lineages (adipogeneic, osteogeneic, chondrogeneic) to generate colonies *in vitro* and expressed mesenchymal stem cell markers such as CD90, CD105 and CD34 whereas they remained negative for the expression of CD45. The authors finally speculated that these mesenchymal cells from the human limbus could potentially act as niche cells and play a role in maintenance of the limbal epithelial progenitors. On the other hand, Du et al. 2005 reported the existence of a side population of corneal stromal cells that showed stable expression of ABCG2 and Pax6 and that were mainly located within the limbal stroma. Identification of these cells was achieved according to their ability to efflux the DNA-binding dye Hoechst, reducing their fluorescent intensity and thus allowing

isolation of this cell population by flow cytometry (Du et al., 2005) . In culture, these cells were clonogenic and could be expanded to 100 population doublings. These cells had the ability to differentiate into keratocytes involved in the maintenance of the central corneal transparency, but also into cells that expressed markers of chondrogenesis and neural cell differentiation in response to different environmental stimuli. For this reason, these multipotent cells presented characteristics of adult stem cells and were termed corneal stromal stem cells (CSSCs). Although keratocytes have lost expression of Pax6, CSSCs maintain expression of this eye specific protein, and this expression allows as identification of CSSCs in the limbal stroma (Pinnamaneni & Funderburgh, 2012).

Another group described a limbal stromal cell population, which they termed peripheral and limbal corneal stromal cells (PLCSCs). These cells have been characterized by the expression of CD34 and their ability to generate cells with mesenchymal stem cells properties at passage 3 when put in culture (Branch et al., 2012). It has been suggested that CSSCs and MSC-like niche cells described by Polisetty et al. (Polisetty et al., 2008) are identical. However, gene expression patterns and differentiation potential assays between CSSCs and mesenchymal niche cells would be necessary to find a consensus in the appellation of these limbal stromal cells. Limbal stromal stem cells are the subject of intense investigations and it has been suggested that these cells could be involved in maintenance of the central corneal transparency by differentiating into keratocytes, play a role as niche factors to maintain the limbal epithelial progenitors as it is the case in the hematopoietic stem cell niche or involved in

the scarring process upon injury (Du et al., 2005; Funderburgh et al., 2005; Mariappan et al., 2010; Nakatsu et al., 2014).

Finally, it has recently been observed that a sub-population of cells from the limbal stroma that were positive for the expression of SSEA4 had the ability to trans-differentiate into epithelial cells expressing markers of corneal epithelial terminal differentiation under specific culture conditions (Katikireddy et al., 2013). Names, markers and functions of several human stromal cells mentioned above are summarized in table 5.1.

Name	Corneal stromal stem cells (CSSC)	Peripheral and limbal corneal stromal cells (PLCSC)	Limbal mesenchymal cells	Limbal mesenchymal cells	Limbal mesenchymal cells	Limbal niche cells	Limbal niche cells	Limbal niche cells	Limbal stromal cells	Limbal fibroblasts
Authors	Du et al. 2005	Branch et al. 2012	Polisetty et al.2008	Nakatsu et al. 2014	Dziasko et al. 2014	Chen et al. 2011	Higa et al. 2013	Li et al. 2014	Li et al. 2014	Katikireddy et al. 2013
Markers	Pax6; ABCG2; Bmi1; CD90; CD73	$CD34^+$; CD105	CD90; CD105; vimentin; $CD29; CD34^-$	CD105; $CD34^+$; N-cad; vimentin	CD90; CD105	$CD34^+$; Nanog; SSEA4; Sox2; Nestin; N-cad	AQP1; N-cad	Stromal cells located beneath limbal basal epithelium	Stromal cells located deeper	SSEA4; Oct4; Sox2; Nanog
Colony forming potential	-	Yes	Yes	-	-	-	-	-	-	Yes
Multipotency	Yes	Yes	Yes	-	-	-	-	-	-	-
Function	Transparency	Transdifferentiation	-	Support	Support (direct contact)	Support (direct contact)	Support (direct contact)	Support +	Support -	Transdifferentiation

Table 5.1 Stem cells of the human limbal stroma

Limbal stromal cells have been described in several publications and have been named according to the markers expressed, the ability to form colonies or their ability to differentiate into multiple lineages *in vitro* (Branch et al., 2012; S.-Y. Chen, Hayashida, Chen, Xie, & Tseng, 2011a; Du et al., 2005; 2005; Dziasko et al., 2014; Higa et al., 2012; Katikireddy et al., 2013; Y. Li et al., 2014; Nakatsu et al., 2014; Polisetty et al., 2008)**. Stromal cells have been proposed to be involved in maintenance of the corneal transparency, play a role as niche cells in the maintenance of the epithelial progenitors or as a replacement source of epithelial cells.**

Chen et al. 2011, have previously hypothesized the existence of direct stromal-epithelial interaction. In fact, the authors observed that digestion of limbal biopsies with collagenase that cleaves off the interstitial collagen but maintains the basement membrane not only isolated the epithelial progenitors but also their closely associated stromal cells. Those observations suggested that both cell types had the potential to directly interact *in vivo* but the authors did not provide any evidence of such interaction in the native niche. In culture, collagenase isolated LECs that maintained close association with their stromal cells were able to generate holoclone like colonies containing small and circular epithelial cells that were highly positive for the expression of stem cell markers such as p63α. They further characterized the stromal cell population isolated with LECs after collagenase treatment and observed that these cells were positive for the expression of mesenchymal stem cell markers such as CD34, Nestin, Nanog, Sox2 and Oct4. In the absence of feeders, maintenance of close association between stromal mesenchymal and LECs led to clonal growth in serum-free low calcium culture medium whereas disruption of such association by trypsin/EDTA resulted in the absence of clonal expansion, confirming the importance of this direct mesenchymal/epithelial interaction *in vitro*.

In the present chapter, it has been shown that small basal epithelial cells of the limbal crypts directly interact with elongated cells from the underlying stroma. Such direct mesenchymal/epithelial cell interaction has been highlighted in detail for the first time and could play an important role in the maintenance of the epithelial stem cell character in the native niche. As previously mentioned, HSC in the bone marrow have the ability to directly interact with the

surrounding MSCs and such direct cell-to-cell interaction is essential for maintenance of the hematopoietic stem cell phenotype. It has been shown that such an interaction was mediated by Cxcl12 signaling expressed by different cells in the murine bone marrow including MSCs. Cxcl12 signaling through its receptor Cxcr4 contributes to the maintenance of HSCs in a low proliferative state (Nie et al., 2008; Sharma et al., 2011; Sugiyama et al., 2006; Tseng et al., 2011). Moreover, it has been shown that in the human ocular surface, epithelial stem cell and mesenchymal cell reunion *in vitro* is mediated by SDF-1 (Cxcl12 in mice) that is uniquely expressed by limbal epithelial progenitors cells, and that its receptor Cxcr4 is strongly expressed by limbal mesenchymal niche cells. This relationship is similar to that previously described in the HSC niche. Epithelial progenitor and mesenchymal niche cell reunion generated sphere growth in three-dimensional Matrigel whereas disruption of such interaction by blocking Cxcr4 yielded reduced spheres with epithelial cells exhibiting a differentiated phenotype.

In the present chapter, after demonstrating the existence of direct stromal-epithelial contacts within the limbal crypts it has been observed that limbal stromal cells expressing mesenchymal markers such as CD90 and CD105 were more likely present within this limbal area. Direct interaction between limbal mesenchymal cells and LESCs could however not be confirmed at this stage in the native niche and would require further investigations.

Despite the detailed resolution in x, y and z planes obtained by SBFSEM, identification of the structures of interest is based on topographical analysis of serial micrographs. This is inconclusive because the limbal stroma beneath the

limbal epithelium likely contains a mixed population of stromal cells (table 5.1) that all present a similar morphological aspect. Further investigation involving correlative light and electron microscopy (CLEM) imaging techniques combining several mesenchymal markers would be required to determine the exact identity of the stromal cells physically interacting with the limbal epithelial progenitors in the native limbal stem cell niche.

Hayashi et al. 2007, observed that N-cadherin was expressed in a subpopulation of human basal limbal epithelial cells that were also positive for the expression of multiple LESCs markers such as ΔNp63, CK15, Bmi-1, ABCG2 and negative for CK3 and CK12 (Hayashi et al., 2007). Furthermore, Higa et al. 2009, showed that *in vitro*, N-cadherin +ve cells were clustered at the circumference of the epithelial colony and formed direct contacts with 3T3 feeder cells. They observed that epithelial peripheral cells that were directly interacting with the feeders remained undifferentiated whereas central epithelial cells that lost N-cadherin mediated interaction with the feeders expressed markers of terminal differentiation instead. Furthermore, when 3T3 feeder cells were transfected with N-cadherin siRNA, the size of colonies and secondary colony forming efficiency was significantly reduced suggesting that N-cadherin is vital in maintaining immature cells *in vitro*. In the present chapter, because N-cadherin mediated cell interaction involved physical cell-to-cell contact, it has been hypothesized that N-cadherin could be involved in the epithelial stromal interaction observed by SBFSEM. In the present chapter, N-cadherin staining of human tissue sections was very weak in both central corneal and limbal epithelial cells of non-crypt limbus. Nevertheless, basal and compact epithelial

cells were positive for N-cadherin staining within the limbal crypt. However, stromal cells identified by their elongated nuclei appeared negative, suggesting that N-cadherin might not be involved in the stromal-epithelial interaction observed by electron microscopy. Recently, Higa et al. 2014, showed that Aquaporin1 (AQP1) was expressed by stromal cells underlying N-cadherin +ve epithelial clusters. The authors suggested that AQP1 +ve stromal cells formed an intricate network with N-cadherin +ve basal epithelial progenitors but did not show any evidence of such N-cadherin mediated homotypic cell-to-cell adhesion. These AQP1 +ve cells were however located immediately beneath the basement membrane, in a similar position to where physical stromal-epithelial interactions have been observed. In the present study, IHC showed that CD90 and CD105 +ve mesenchymal cells seem to lie deeper in the limbal stroma.

In a new development, telocytes have been described as a new type of interstitial cells by electron microscopy. Telocytes present a small cell body and are characterized by very long and thin cell extensions called telopodes and organize as a network of connected cells (L. M. Popescu & Faussone-Pellegrini, 2010). It has been proposed that telocytes could be involved in the regenerative process because of their interaction and proximity with stem cells in a variety of organs including the heart, the lungs, the skeletal muscle and the skin (Ceafalan et al., 2012; Galiger et al., 2014; Gherghiceanu & Popescu, 2012; Suciu et al., 2012; Zheng et al., 2013). By transmission electron microscopy, Gherghiceanu and Popescu, observed that telocytes form a network in the human heart and have the ability to generate 'point contacts' with cardiomyocytes progenitors similarly to what has been observed here by SBFSEM in the limbal crypt. They further

suggested telocytes as active 'nursing' players in epicardial stem cell niches (Gherghiceanu & Popescu, 2012). Later, Luesma et al. 2013, observed interstitial cells with a morphology consistent with telocytes localized within the murine limbal stroma. Interestingly, limbal telocytes showed a similar morphology to stromal cells localized immediately beneath the human limbal crypt and with Aquaporine1 +ve stromal cells described by Higa et al. 2012 (Higa et al., 2012; Luesma et al. 2013). Nevertheless, identification of telocytes mostly relies on the analysis of morphological aspects of interstitial cells by electron microscopy. For this reason, investigation of specific telocyte markers would be necessary to discriminate the latter as a proper side population of limbal stromal cells to avoid more confusion about the identity of cells populating this specific area.

Pigmentation of the limbal palisades has previously been reported by Davanger et al. where they appeared particularly striking in highly pigmented individuals (Davanger & Evensen, 1971). The authors suggested that the pigmented lines could indicate the direction of migration of the limbal epithelial progenitors. As described in chapter 3, radial pigmented lines are arranged in pairs due to melanin granules concentrated in the basal cell layer that is vertical in relation to the surface along both sides of the crypt (figure 3.3 in chapter 3). In 2005, Higa et al. observed a proximity between Mart-1 +ve cells that specifically identify melanocytes and CK19 +ve cells that identify the limbal epithelial progenitors. The authors proposed that melanocytes could act as a 'sun screen' for the underlying structure including the limbal epithelial progenitors. In the present chapter, it has been shown that limbal melanocytes that were +ve for the expression of MelanA, highly concentrate within the limbal crypts that also

constitute a reservoir for the limbal epithelial progenitors. Furthermore, SBFSEM revealed that dendritic cells containing electron dense granules were closely associated with the smallest basal epithelial cell presumed to be the limbal epithelial progenitor. After manual segmentation and 3D reconstruction of the structures of interest, the first 3D model at a cellular scale of the limbal stem cell niche, in which the smallest basal epithelial cell is apically closely associated with pigmented limbal melanocytes and basally with limbal stromal cells, has been proposed. At this stage, functional involvement of melanocytes as a part of the LESC niche could not be confirmed. This was investigated in the next chapter.

Chapter 6: Isolation and culture of human melanocytes for the expansion of limbal epithelial progenitor cells

6.1 Introduction

Davanger and Evensen (1971), reported pigmentation of the POV (Davanger & Evensen, 1971). This pigmentation has been attributed to melanocytes located on the basal side of the epithelium and transfer of melanin granules into the surrounding limbal epithelial cells. Later, Higa et al. observed that melanin-containing epithelial cells were observed aligning the basal layers of the limbus in pigmented donors. They reported that pigment was specifically observed in most CK19 +ve limbal basal cells but not in central corneal basal cells and proposed that melanin granules released by melanocytes could act as a "sunscreen" protecting the limbal epithelial progenitors in the niche (Higa et al., 2005).

In the previous chapter, it has been shown that small basal epithelial cells were closely associated with melanocytes. The concentration of melanocytes in the LESC niche suggests that limbal melanocytes could potentially be an active component of the niche and influence LESCs behavior in a direction promoting quiescence and maintenance of the stemness.

If limbal melanocytes are niche cells involved in the maintenance of the limbal epithelial progenitors, then melanocytes might have the ability to support the expansion of limbal epithelial cells (LECs) and maintain stem cell characteristics *in vitro*. In the present chapter, the aim was to demonstrate a functional role for human limbal melanocytes (hLM) in the support of LECs maintaining stem cell characteristics by removing both cell types from their native niche and co-culturing them together *in vitro*. The first step was to develop a reproducible

protocol for the isolation and purification of a pure population of hLM from cadaveric corneas that could then used be as a feeder layer for the culture of LECs. Clonal growth, epithelial layer morphology and expression of stem cell markers were further assessed in 2D co-cultures and tissue equivalents (TEs) prepared using RAFTs (Real Architecture For 3D Tissue).

6.2 Methods

6.2.1 Isolation and culture of a human limbal stromal /melanocytes mixed population

Limbal biopsies of 3x10mm covering the limbus front to back were cut from human cadaveric corneas and transferred into a solution containing 1.2U/mL dispase II (Roche diagnostics GmbH, Mannheim, Germany) in corneal epithelial cell culture medium (CECM) and incubated overnight at 4°C. Crypt rich limbal biopsies were then gently scrapped with the points of thin forceps and cells were transferred into a T25 culture flask in 254 medium supplemented with HGMS-2 (Life technologies, Paisley, UK). Culture medium was changed every other day. After 10-12 days, melanocytes and stromal cells were mechanically separated from epithelial cells by using a solution of 0.025% trypsin-0.01% EDTA (Life technologies, Paisley, UK) and seeded into a new T25 flask in 254 medium. Mitotically active limbal stromal/melanocyte mixed populations of cells were seeded at a density of 20,000 cells/cm^2 and used as a feeder layer for expansion of LECs seeded at a density of 200 cells/cm^2.

6.2.2 Isolation of hLM from stromal/melanocyte mixed cell populations

After reaching 60-80% confluence, hLM/stromal cell cultures were treated with Geneticin (Life Technologies, Paisley, UK) (0.2 mg/mL) in 254 medium for 48 hours. After 48 hours, cultures were rinsed with PBS and maintained in 254 medium. At low concentration, geneticin has very limited toxicity towards melanocytes but is lethal for most fibroblasts or stromal cells (Halaban & Alfano, 1984). Therefore, an enriched population of mitotically active melanocytes was finally expanded in 254 medium and used as a feeder layer at the concentration of 20,000 cells/cm^2.

6.2.3 Flow cytometric analysis

Geneticin treated or untreated hLM were detached using 0.05% trypsin-0.02% EDTA before being fixed in 4% PFA for 10 minutes. Cells were washed with PBS, permeabilized with 0.5% triton-X and blocked with 10% goat serum in PBS for 30 minutes. Cells were then incubated with anti-MelanA or anti-MiTF primary antibodies for melanocyte specific staining, diluted 1:100 (Abcam ab51061 and Abcam12039, Cambridge, UK) for 1 hour at 37°C. Cells were then incubated with the secondary antibody Alexa-594 conjugated goat anti-rabbit or Alexa-488 conjugated goat anti-mouse, diluted 1:500 (A-11032 and A-11012, Life Technologies, Ltd Paisley, UK) for 30 minutes at 37°C before being washed and analyzed with a FACScalibur flow cytometer (Becton Dickinson).

6.2.4 Immunohistochemistry and immunocytochemistry

Immunohistochemistry and immunocytochemistry were performed as described in chapter 2 (general material and methods). As for limbal biopsies, RAFT tissue equivalents were embedded in OCT compound and 7μm thick frozen tangential sections were cut and mounted on superfrost plus microscope slides. SlideFlask chambers (Labtek Thermo Scientific Nunc) were used for immunocytochemical analysis. hLM-LECs 2D co-cultures were expanded in SlideFlasks for 12 days prior to fixation in 4% PFA.

6.2.5 Preparation of RAFT-Tissue equivalents (TEs)

RAFT-TEs were prepared as described in chapter 2 (section 2.4). Once hydrogels were formed, $4x10^4$ hLM were seeded on top of 'hLM' collagen constructs 24h before also seeding $1x10^5$ LECs on the same surface of each TE. Cultures were maintained, submerged in 0.5% FBS-CECM for 7 days. TEs were then transferred on top of cell culture inserts (Millipore, West Lothian, UK) in 6-well plates. CECM (850μl) containing 0.5% FBS was added underneath the culture insert every other day to maintain the TE at the air-liquid interface. RAFT-TEs were airlifted for a further 7 days in a humidified 5% CO_2 in air incubator.

6.2.6 Histological staining of RAFT constructs

Frozen sections (7μm) of hLM+ or hLM- RAFT-TE were fixed for 10 minutes in 4% PFA before being stained with hematoxylin and eosin and mounted in DPX. The sections were imaged using a Nikon Eclipse TS100 inverted microscope.

6.2.6 Statistical analysis

Student's *t* test was performed to analyze CFE and NC ratio. Bar graphs represent mean ± standard error of the mean. A p value of $p < 0.05$ was considered as statistically significant. For each culture conditions, 200 cells were randomly selected for NC ratio measurement (n=3).

6.3 Results

6.3.1 Localization of human limbal melanocytes within the limbus

Microphthalmia-associated transcription factor (MiTF) is an important regulator of mammalian pigmentation that controls melanogenesis but also cell differentiation, dendricity, proliferation and apoptosis of melanocytes and their progenitors (Cheli, Ohanna, Ballotti, & Bertolotto, 2010; Kondo & Hearing, 2011). Here, MiTF has been used in conjunction with MelanA as an antigen for specific melanocyte targeting.

Immunohistochemistry showed that limbal crypts contain a population of melanocytes associated with LCs that were positive for both MelanA and MiTF dispersed amongst the basal epithelial layer of the limbal epithelium (figure 6.1A). Interestingly, melanocytes (white arrows in 6.1B and red signal in 6.1C) co-localize with clusters of tightly packed epithelial cells at the edge of the limbal crypts.

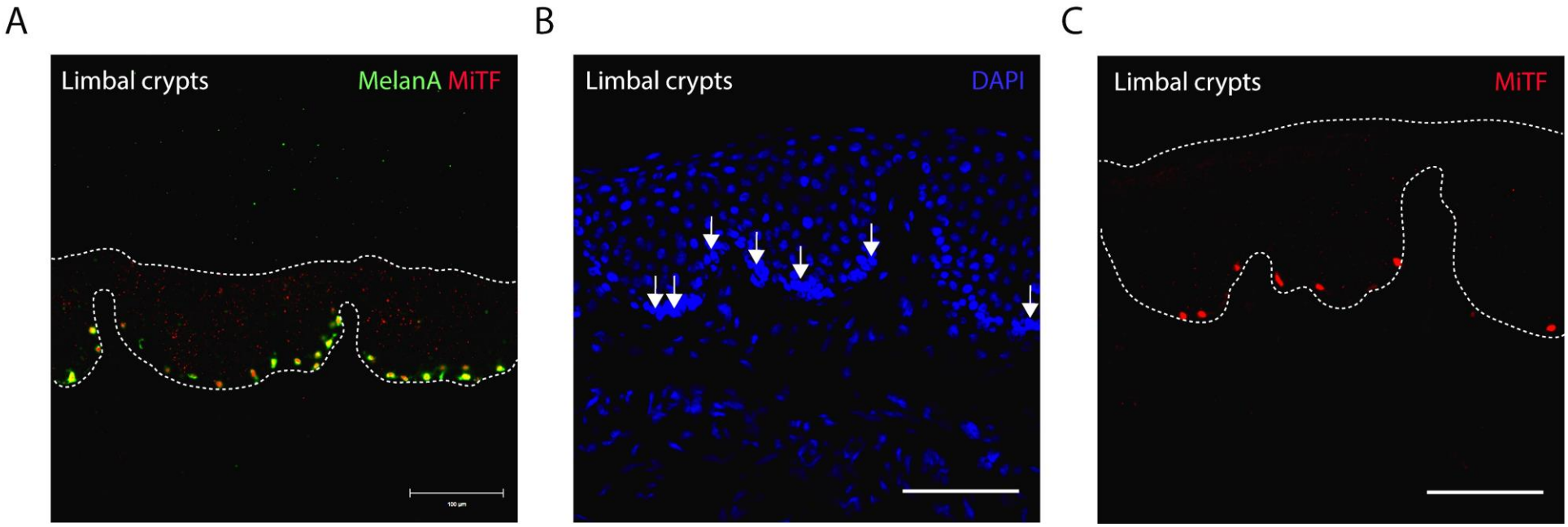

Figure 6.1 Localisation of human limbal melanocytes in the limbal crypts.

A: Double Immunostaining showing specificity of MiTF antibody for melanocytes. Immunohistochemistry shows clusters of small and compact epithelial cells on the basal side of the epithelium (B). MiTF +ve cells (white arrows) co-localize with clusters of compact basal epithelial cells observed in (B). Epi: epithelium Scale bars: 100μm. Dashed lines in A and C represent limits of the limbal epithelium.

6.3.2 Isolation and culture of a mixed population of limbal stromal cells and melanocytes and co-culture with limbal epithelial cells (LECs)

In pigmented donors limbal crypts are easily observed under a dissecting microscope (white arrows figure 6.2A). After dispase digestion, the isolation and expansion of cells from crypt-rich limbal biopsies generated 3 different cell populations (figure 6.2B): Epithelial cells growing in colonies (labeled Epi.), elongated stromal fibroblast like cells on the edge of colony (labeled St.) and small dendritic cells with extended processes with a morphology consistent with melanocytes (white arrows). A low concentration of trypsin was used to mechanically separate limbal stromal cells and melanocytes from epithelial cells. After centrifugation, a brown pellet suggested the presence of pigmented melanocytes in the sample (figure 6.2C).

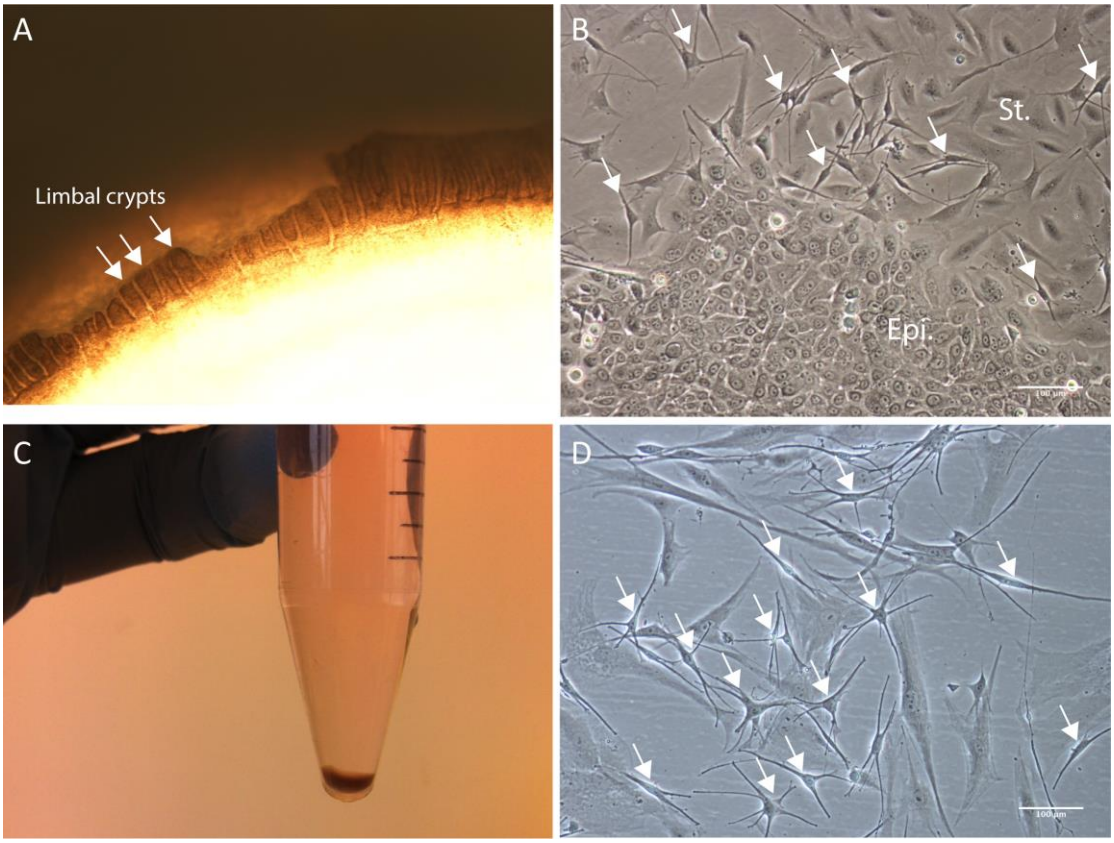

Figure 6.2 Isolation of hLM and stromal cells from human limbal biopsies

A: Macroscopic observation of limbal crypts (white arrows) under a dissecting microscope from a heavily pigmented donor.

B: Primary culture of a mixed population of limbal epithelial, stromal and melanocyte cells after dispase digestion of crypt-rich limbal biopsies.

C: Brown pellet suggesting the presence of pigmented melanocytes after separation of stromal cells and melanocytes from LECs in primary culture.

D: Mixed population of limbal stromal cells and melanocytes (at P1) in culture after separation from LECs.

White arrows in B and D point to cells with morphology consistent with melanocytes. Scale bars: 100 μm. Epi.: epithelial cells; St.: stromal cells.

In culture, melanocytes were identified by their dendritic appearance (white arrows in 6.2D and 6.3A) and by the expression of MelanA (6.3B). This mixed population of limbal melanocytes and limbal stromal cells was further used as a feeder layer for expansion limbal epithelial cells (figure 6.3A). LECs seeded on top of mitotically active melanocytes-stromal cells had the ability to generate large colonies that contained small and tightly packed epithelial cells (figure 6.3C and D). Interestingly, melanocyte like cells and their extensions were observed within the colony, inserted between epithelial cells (white arrowheads in 6.3D).

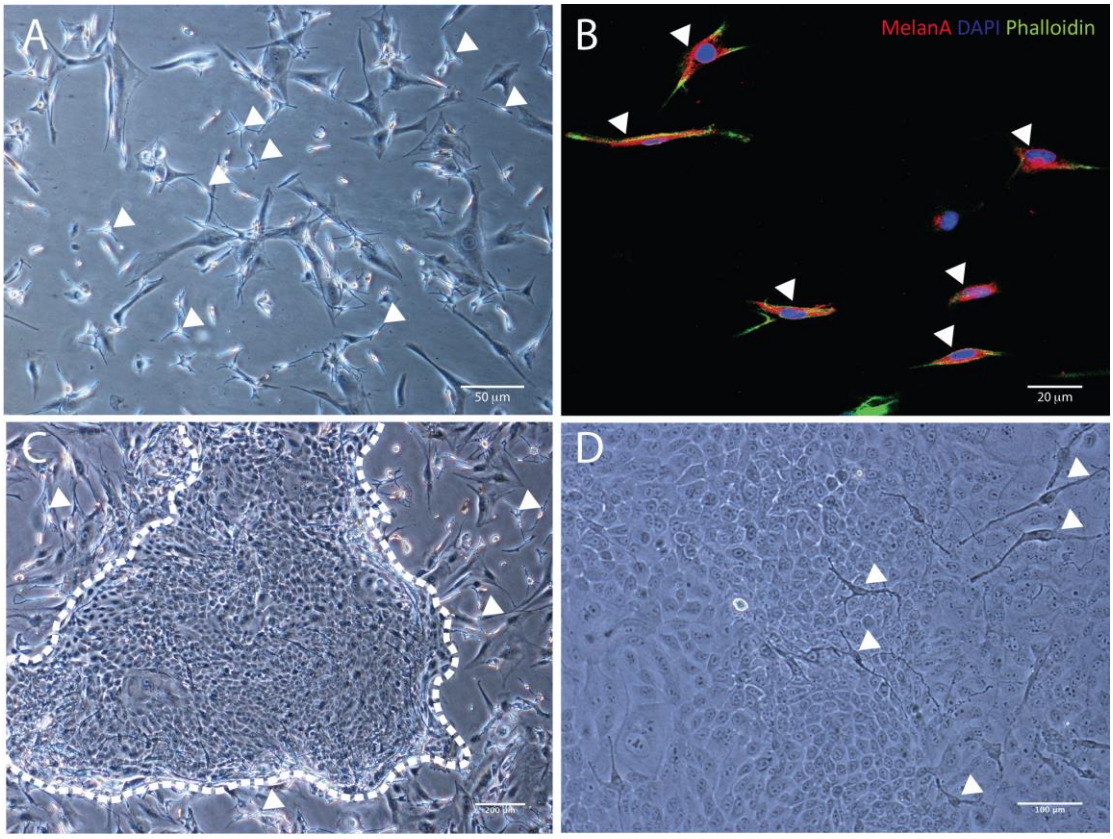

Figure 6.3 Culture of LECs on mixed population of limbal stromal/melanocytes feeder cells

A: Mixed population of limbal stromal/melanocyte feeder cells prior to LECs seeding.

B: Immunocytochemistry confirming the presence of melanocytes among the feeders shown in A (white arrow).
C and D: Large colony containing LECs with undifferentiated morphological aspect cultured on limbal stromal/hLM cells.
White arrows in A, C and D indicate putative melanocytes. Dashed line in C shows borders of the colony. Scale bars: 50μm A, 20μm B, 200μm C and 100μm D.

6.3.3 Isolation of a pure population of hLM from stromal/melanocyte mixed cells

Figure 6.4 represents stromal cell contamination (Top left panel) in melanocyte cultures 48 hours after geneticin treatment. Post geneticin treatment, most of cells in the culture were apoptotic and detached from the culture plate. At day 5, the remaining melanocytes showed proliferation and reached confluence by day 21 (figure 6.4). Flow cytometry analysis showed that a small proportion of cells was positive for MelanA (3.31%) before geneticin treatment. After treatment, the population of MelanA +ve cells increased and reached 95.02% whereas 91.4% of cells were positive for both melanocyte markers (figure 6.5A). Immunocytochemistry confirmed that the isolated cell population was positive for the expression of both melanocyte markers MelanA and MiTF (figure 6.5B). This highly enriched melanocyte preparation could be easily seeded at specific cell densities and was further used as a feeder layer for expansion of LECs.

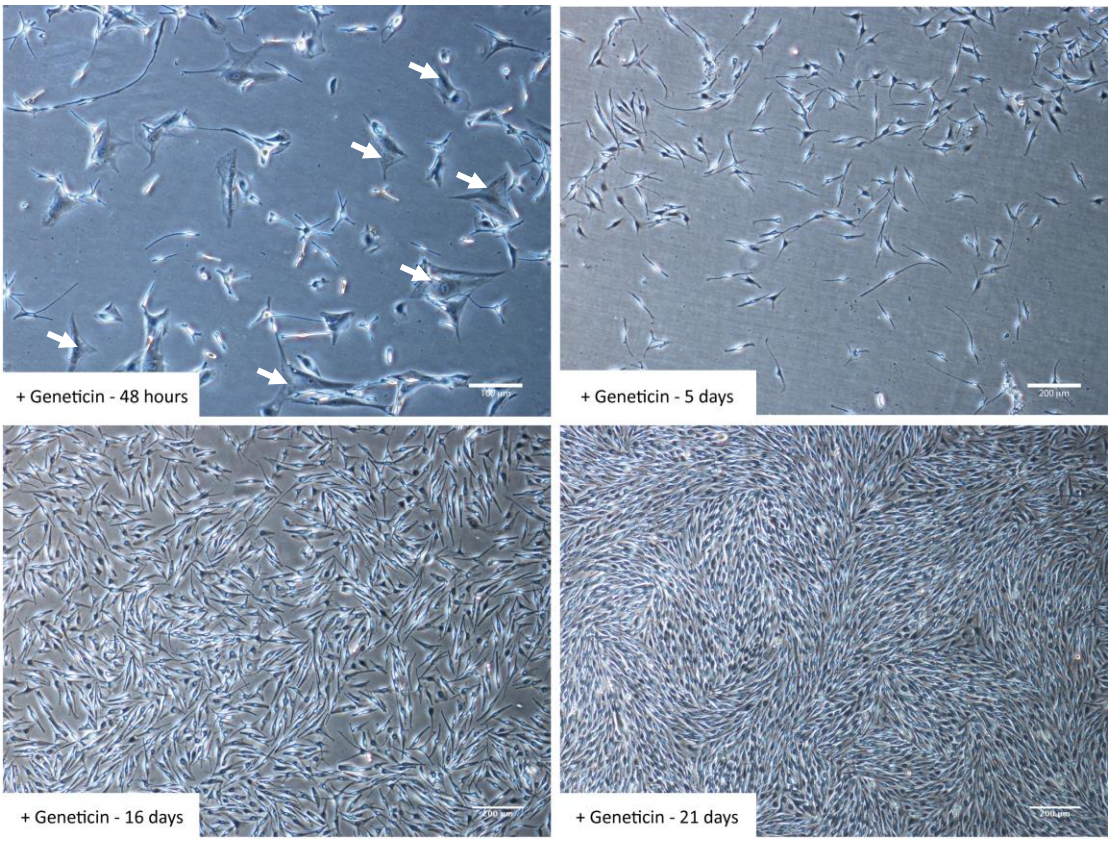

Figure 6.4 Removal of stromal contamination from hLM cultures by geneticin treatment.

Stromal cells are completely removed from the culture 5 days post geneticin treatment. A confluent layer of melanocyte was generated 21 days after geneticin treatment. Scale bars: 100μm A, 200μm B-D.

A

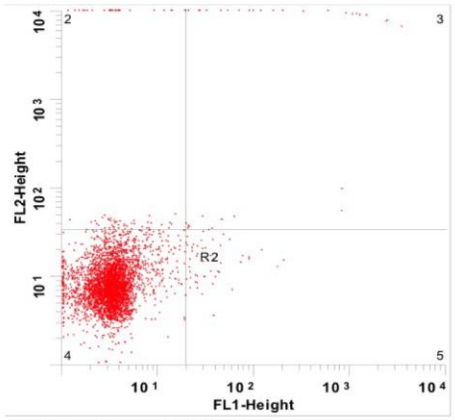

Ms-Alexa488 ctr

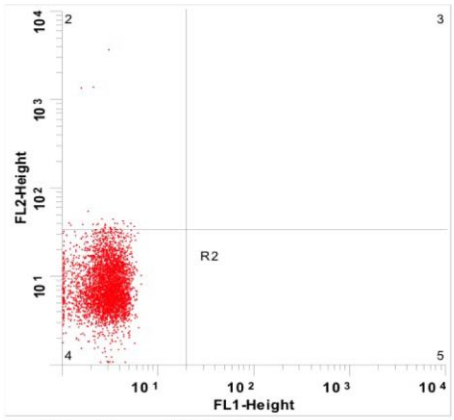

Rb-Alexa594 ctr

MelanA

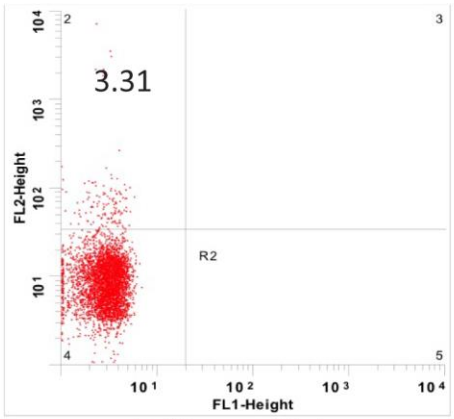

hLM - geneticin

MelanA

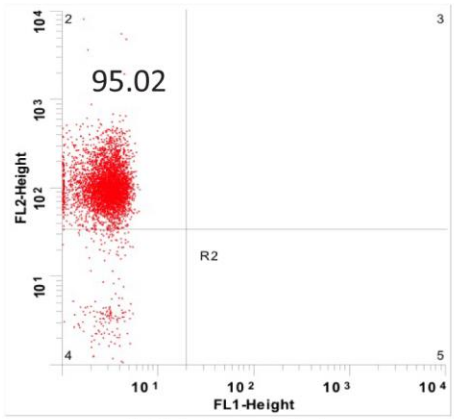

hLM + geneticin

MelanA

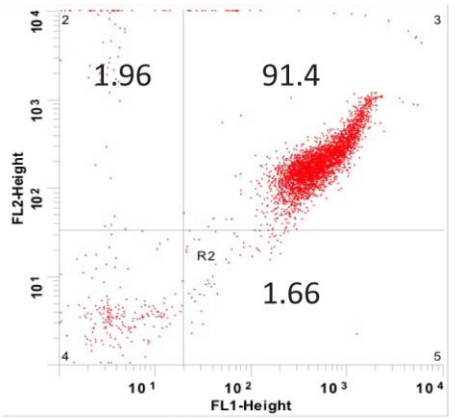

hLM + geneticin

MiTF

B

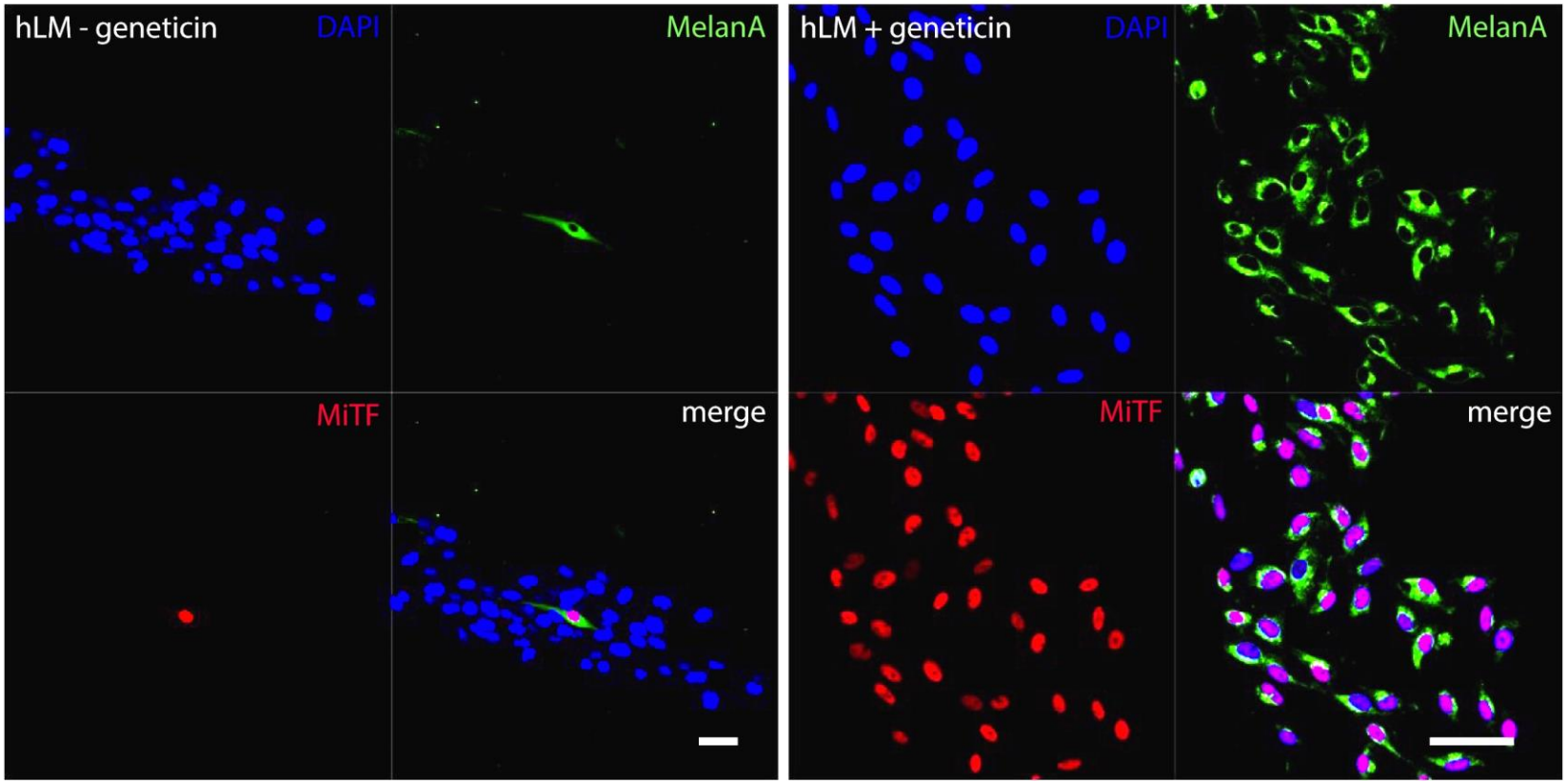

Figure 6.5 Assessment of purity of melanocyte sample after geneticin treatment.

Flow cytometric analysis for MelanA (bottom left and middle panels) and MelanA + MiTF double staining (bottom right panel) melanocyte markers in cells expanded before (bottom left panel) and after (middle and right panels) geneticin treatment. Top panels: negative control for non-specific binding of secondary Ab. Immuncytochemistry showing the expression of melanocyte +ve markers in cells expanded before and after geneticin treatment. Scale bars: 50μm.

6.3.4 Expansion of LECs in 2D co-cultures

LECs seeded on top of mitotically activated hLM had the ability to generate large holoclone-like colonies with smooth borders (figure 6.6A bottom left and 6.6B). LECs populating these colonies were compact and had morphological stem characteristics such as a small size and high circularity (figure 6.6A). Interestingly, hLM feeder cells were not only concentrated at the edge of the colony but were also inserted between LECs following a strict parallel alignment (white arrows figure 6.6A bottom right). No morphological differences could be observed when LECs isolated from the same donor were grown on either 3T3 or hLM feeder cells. Nucleus to cytoplasm ratio of LECs grown on hLM (0.631 ± 0.061) was similar to LECs grown on 3T3 fibroblasts (0.629 ± 0.099) ($p > 0.05$) (figure 6.6D). Furthermore, no growth of LECs could be observed in the absence of feeder cells in the same culture conditions (figure 6.6C). Nevertheless, LECs pre-expanded on 3T3s presented a greater secondary colony forming efficiency ($3.6\% \pm 0.52\%$) than the same LECs pre-expanded on hLM ($2.15\% \pm 0.57\%$) ($p < 0.05$) (figure 6.6D).

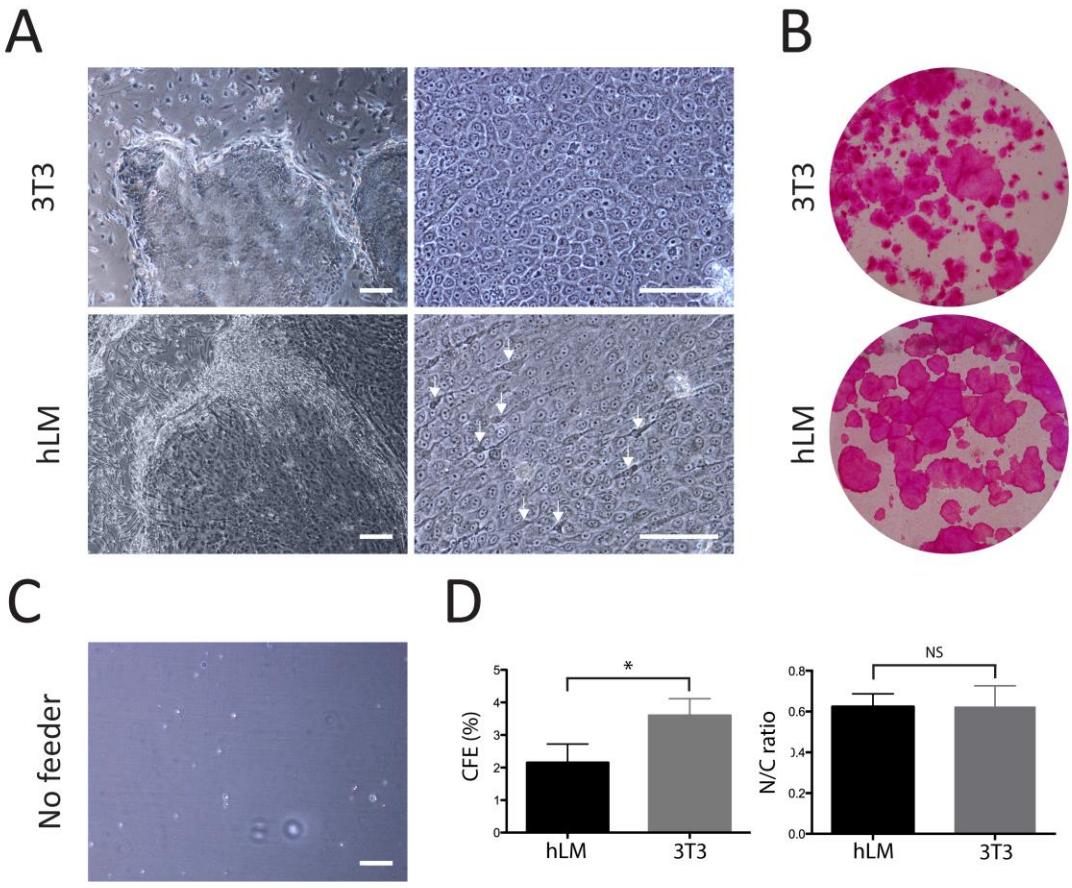

Figure 6.6 Characteristics of LECs expanded on 3T3 fibroblasts or mitotically active limbal melanocytes.

(A) LECs expanded either on hLM or 3T3s generate colonies, present a small size, a high circularity and a high nucleus/cytoplasm ratio. (B) LECs grown in petri dishes on either 3T3s or hLM feeder cells and stained with 1% rhodamine. LECs grown on 3T3s or HLM are able to generate large holoclone like colonies with smooth borders. (C) No proliferation of LECs in the absence of feeder cells. (D) Colony forming efficiency and nucleus/cytoplasm ratio of LECs pre-expanded one either 3T3s or hLM. (*: $p<0.05$; NS: $p>0.05$). Scale bars: 100μm (A) left panels and (C); 50μm (A) right panels.

6.3.5 Expression of LESCs markers in hLM-LECs co-cultures

Expression of stem/progenitor markers in hLM-LECs co-cultures was further investigated by immunocytochemistry. Phalloidin staining (figure 6.7A) shows the general appearance of epithelial colonies and LECs grown on hLM feeder cells. The small size of LECs within the colony confirms that LECs remain undifferentiated when cultured in the presence of hLM (figure 6.7A). MelanA staining demonstrates that melanocytes insert between LECs in the colony following the parallel alignment previously observed (figure 6.7A and B). LECs grown on hLM feeder cells were negative for the expression of the terminal cell differentiation marker CK3 (figure 6.8A) whereas clusters of LECs were +ve for CK15 (figure 6.8B). Finally, most of the LECs grown on hLM were Bmi1 (figure 6.9A) and p63α +ve (figure 6.10A and B). Staining for MiTF also showed the presence of melanocytes at the edge of the colony but also inserted between p63α +ve cells (figure 6.10A and B). Figure 6.9B shows expression of Bmi1 within the limbal crypts. Double immunolabelling revealed that Bmi1 was also expressed by MelanA +ve cells in the native niche explaining a positive signal for Bmi1 observed for melanocyte in the co-cultures.

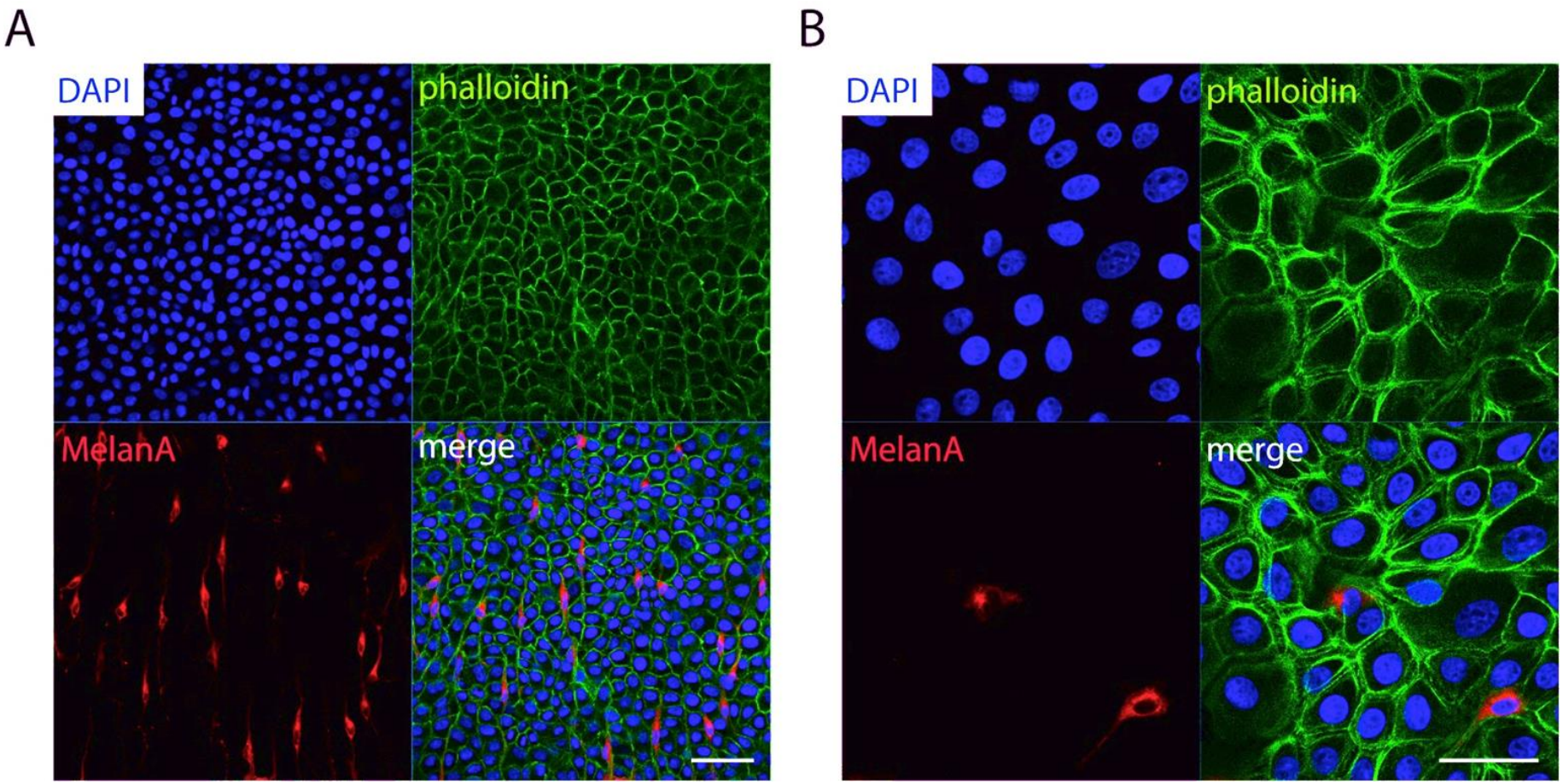

Figure 6.7 Expression of –ve and +ve stem cell markers by LECs expanded on hLM.

Phalloidin staining shows the morphology of LECs expanded on hLM. MelanA staining reveals melanocytes feeder cells insert between LECs in the colony. Scale bars: 50μm A, 20μm B.

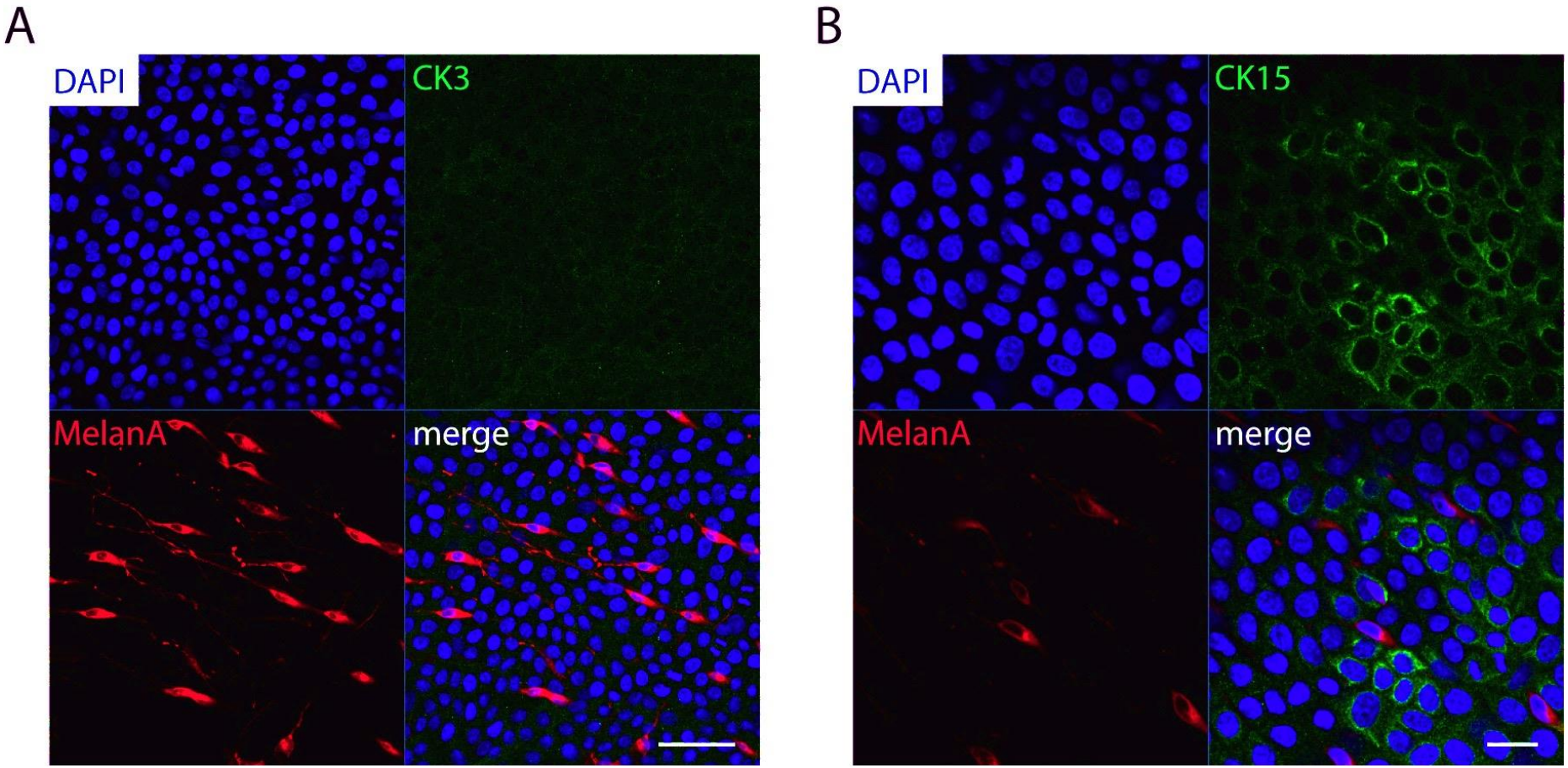

Figure 6.8 Expression of –ve and +ve stem cell markers by LECs expanded on hLM.

(A) and (B) respectively show that LECs expanded on hLM are CK3 –ve and CK15 +ve. Scale bars: 50μm.

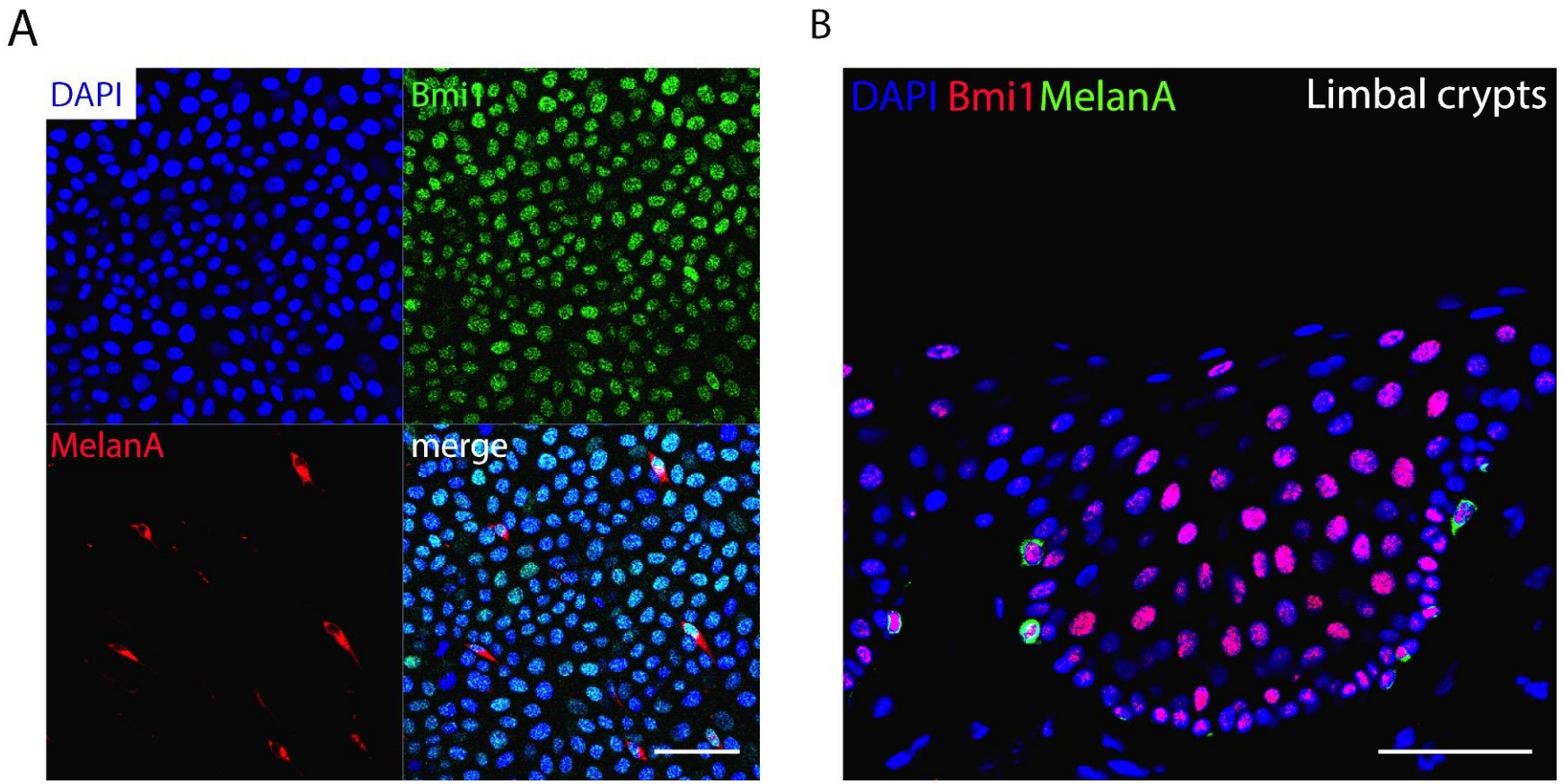

Figure 6.9 Expression of –ve and +ve stem cell markers by LECs expanded on hLM.

A: LECs expanded on hLM were mostly positive for the expression of Bmi1 as were hLM (MelanA +ve cells) inserted within the colony. B: Same observations were made in the limbal crypt where MelanA +ve cells also expressed Bmi1. Scale bars: 50μm.

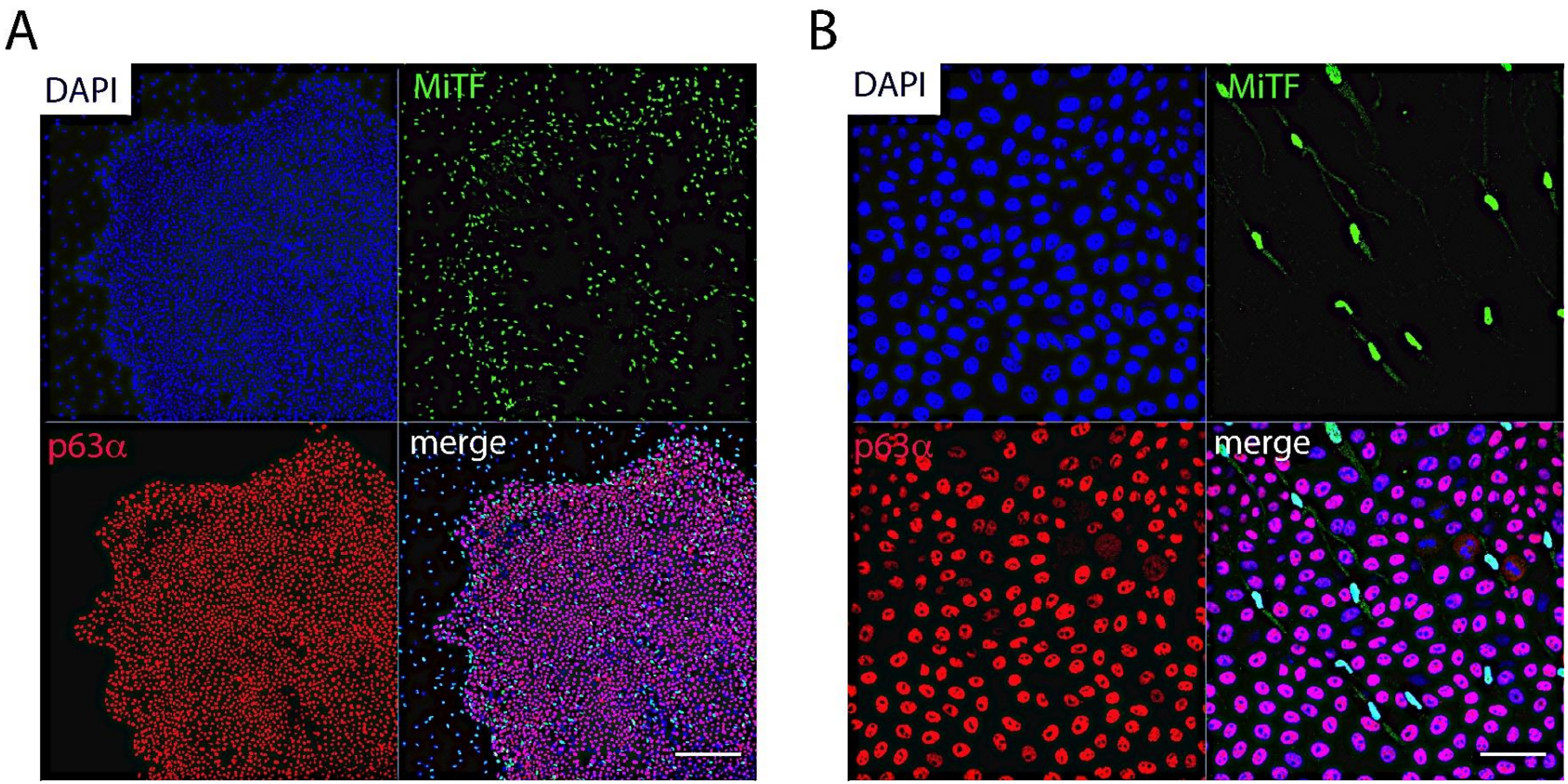

Figure 6.10 Expression of –ve and +ve stem cell markers by LECs expanded on hLM.

Immunocytochemistry shows that most of LECs expanded on hLM maintained expression of p63α stem cell marker (A). Higher magnification imaging in B confirmed insertion of MiTF +ve melanocytes between the limbal epithelial progenitors in the colony. Scale bars: 100μm A, 50μm B.

6.3.6 Ultrastructure of LECs sheets on RAFT constructs

After one week in submerged culture, and a further week of airlifting following seeding of hLM and LECs on RAFT-TE, multi-layering and stratification of the epithelial sheet was observed. hLM supported the formation of 5 to 7 layers of stratified LEC cells, while only two or three layers of epithelial cells were observed in the absence of feeders (figure 6.11A). Transmission electron microscopy showed the morphology of epithelial cells in different layers of the hLM+ RAFT collagen construct. Cells of the basal layer of the epithelial sheet were columnar and had a poorly differentiated morphology. Epithelial cells in the superficial layers appeared flattened, squamous-like and terminally differentiated (Figure 6.11B). Immunohistochemistry confirmed the presence of melanocytes in the RAFT-TE. Moreover, nuclei of basal epithelial cells in hLM+ RAFT construct were positive for p63α suggesting that cells populating this layer remained in a poorly differentiated state.

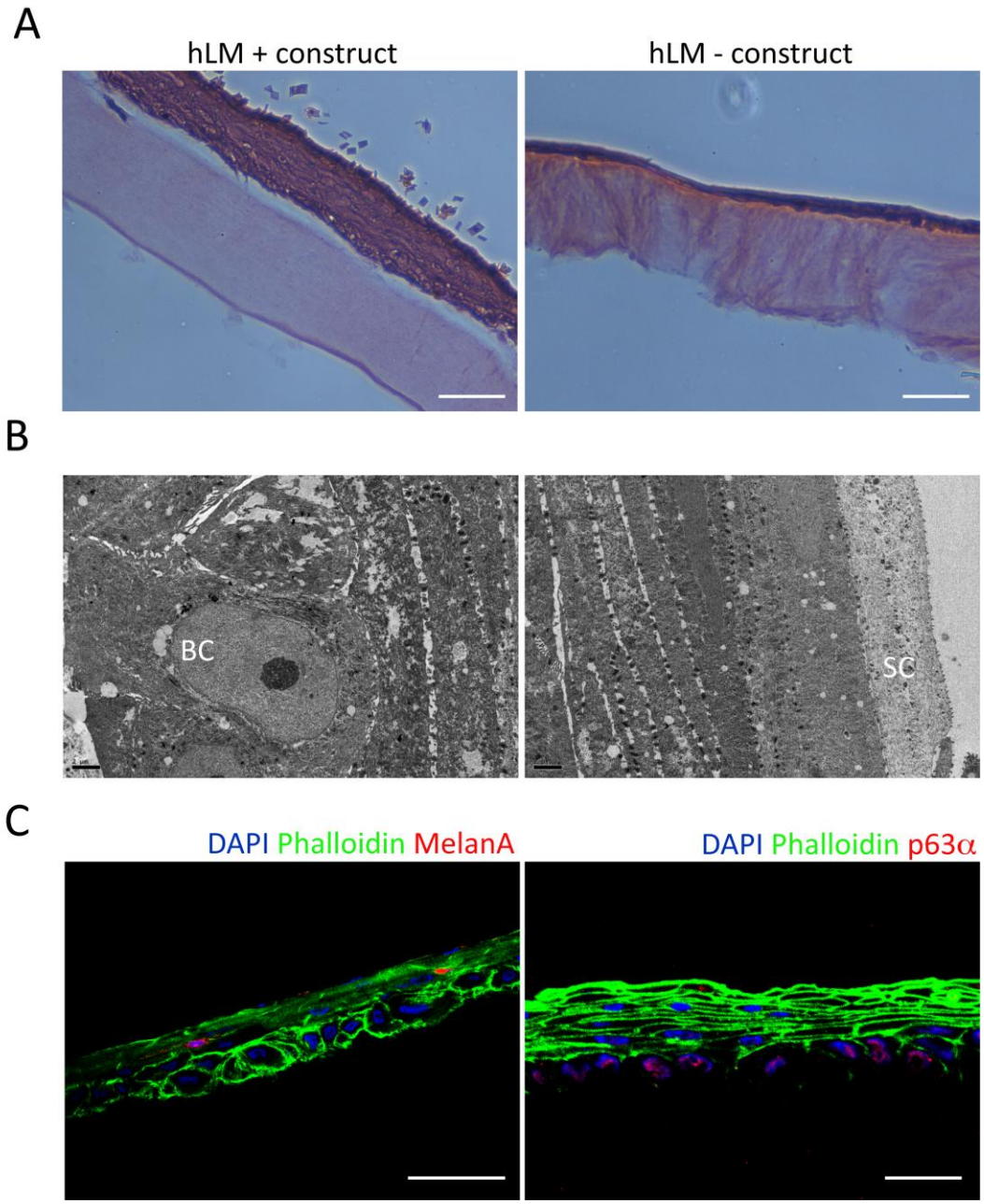

Figure 6.11 Epithelial layer morphology of LECs expanded on hLM RAFT collagen constructs.

(A) Hematoxylin and eosin staining of sections of LECs grown on RAFT in the presence (+) or absence (-) of hLM. (B) Transmission electron micrographs showing multilayering of LECs grown on hLM+ RAFT constructs. BC: Basal cell; SC: squamous cell. (C) Immunohistochemistry on frozen sections

staining for MelanA and p63α expression in hLM+ RAFT collagen constructs. Scale bars: 100μm (A); 2μm (B); 50μm (C).

6.4 Discussion

Mouse embryonic fibroblasts (3T3-J2) feeder cells are considered to be the gold standard for culturing keratinocytes for cell therapy and regenerative medicine (Barrandon et al., 2012). However, it has been shown that human fibroblasts and human fibroblast conditioned media can partially substitute 3T3s feeder cells for the expansion of limbal progenitors *in vitro* (Barrandon et al., 2012; Rheinwald & Green, 1975; Schrader et al., 2010). Studies support the notion that other 'support' cells can also facilitate the maintenance and function of epithelial stem cells *in vitro* and possibly *in vivo*. Therefore, to assess the role of limbal melanocytes in maintaining limbal epithelial progenitors *in vitro*, simplified models of the limbal stem cell niche were developed in which limbal melanocytes were used as feeder cells for the expansion of LECs.

Recently, Li et al. were able to isolate limbal stromal cells located immediately beneath the limbal basal epithelium in close vicinity to LESCs/progenitor cells. The authors termed these cells "limbal niche cells" and observed that this population was able to support clonal growth of LECs in culture more efficiently than cells lying deeper in the stroma that they termed "limbal stroma cells". LECs in co-cultures with "niche cells" were able to maintain expression of epithelial stem cell markers and had secondary clonogenic potential suggesting that cells

immediately beneath the limbal epithelium act as an important part of the limbal stem cell microenvironment (Li et al., 2014). Furthermore, Nakatsu et al. 2014, isolated limbal stromal cells that were expressing mesenchymal markers such as CD34, CD105 and vimentin. These cells had the ability to support expansion of LECs that maintained stem cell properties *in vitro,* suggesting again a role of these cells as an important element of the LESC microenvironment (Nakatsu et al., 2014). Our group has recently shown that limbal epithelial cells populating the basal layer of the LCs were highly positive for the expression of stem cell markers, had the highest proliferative potential and had the highest capacity to generate holoclones by single cell clonal analysis (Dziasko et al., 2014; Shortt et al., 2007). Furthermore, it was observed in the previous chapter that the LCs, which act as a niche for LESCs/progenitor cells, also contain a relatively high population of melanocytes. In the present study, it was observed that limbal melanocytes co-localized with clusters of compact epithelial cells at the edge of the crypt, an area that we believe corresponds to the limbal stem cell niche. Higa et al, previously observed that limbal melanocytes were closely associated with CK15 +ve and CK19 +ve basal epithelial cells. Hayashi et al. subsequently proposed that limbal melanocytes and LESCs were directly interacting through N-cadherin homotypic cell adhesion and suggested that melanocytes could act as niche cells maintaining LESCs/ progenitors in their microenvironment. N-cadherin mediated hLM-LECs cell interactions *in vitro* and its putative involvement in maintenance of "stemness" of LECs will be investigated in the future.

In the present chapter, human limbal melanocytes were initially isolated and expanded from limbal biopsies. Using a mixed population of limbal stromal/melanocyte feeders, LECs were successfully expanded in low serum (0.5%FBS) CECM. However, at this stage, involvement of melanocytes in this process could not be confirmed as several previously mentioned studies had already demonstrated the ability of limbal stromal cells to support LECs *in vitro* (Y. Li et al., 2014; Nakatsu et al., 2014; Schrader et al., 2010). In order to assess the specific functional role of hLM in the co-cultures, contaminating limbal stromal cells were effectively eliminated by geneticin at a dose that was not harmful to melanocytes (Halaban & Alfano, 1984; Horikawa et al., 1996). After confirming by immunocytochemistry and flow cytometry that the resulting cell population was highly enriched with limbal melanocytes, the latter was used as a feeder layer for the expansion of LECs. Human limbal melanocytes were successfully maintained in 0.5%FBS-CECM but not in 10% FBS-CECM (data not shown). Interestingly, LECs in culture with hLM feeder cells were able to generate large holoclone like colonies with smooth borders that contained epithelial cells with a morphology consistent with stem cells. Moreover, hLM feeder cells were not only concentrated at the edge of the colony, but were also inserted between poorly differentiated epithelial cells, as previously described in the native niche (Higa et al. 2005). On the other hand, in the same culture conditions, LECs could not be expanded in the absence of any feeder cells, confirming the functional role of hLM in initiating LEC proliferation *in vitro*. Although the morphology of epithelial cells isolated from the same donor and grown on either hLM or 3T3s was similar, secondary colony forming efficiency

appeared higher when LECs were initially pre-expanded on 3T3s. Similar observations have been made when LECs were grown on limbal niche cells (Li et al., 2014). Interestingly, immunocytochemistry revealed that limbal epithelial grown cells on hLM were +ve for the expression of stem cell markers such as CK15, p63α and Bmi1 whereas they remained negative for CK3 that is a marker of terminal cell differentiation. Furthermore, hLM were successfully cultured on RAFT-TEs that mimic aspects of the natural stem cell microenvironment. hLM were able to induce, after airlifting, multi-layering of LECs seeded on top of the RAFT-TE. Transmission electron microscopy revealed that basal epithelial cells in hLM+ constructs were morphologically round and circular whereas squamous-like differentiated cells were observed on the superficial surface of the RAFT. Finally, immunohistochemistry confirmed the presence of MelanA +ve cells in the TE and that basal epithelial cells were still in a poorly differentiated state.

In the present chapter we have presented the first evidence that hLM may act as more that a 'sun screen', protecting limbal epithelial progenitors from oxidative DNA base damage by synthesizing melanin, but that they also supported expansion of LECs *in vitro*. In this co-culture system, melanocytes support limbal epithelial cells in a direction that promotes cell proliferation and that prevents terminal cell differentiation. In 2007, Hayashi et al. suggested that limbal epithelial progenitors could be maintained by limbal melanocytes and that such an interaction was mediated by homophilic N-cadherin contacts in the niche. The authors also reported that the use of melanocytes as feeder cells could not

induce limbal epithelial cell proliferation but are maintaining epithelial cells in a quiescent state *in vitro*. Authors eventually conclude that *in vivo*, melanocyte-epithelial stem cell interactions may rather play a role in maintaining stem cell quiescence than inducing cell proliferation. This is in direct contradiction with the observations presented here. However the authors did not provide any data and information about their melanocyte-epithelial co-culture system that might explain these differences from our results.

In conclusion, a protocol was developed to successfully isolate human limbal melanocytes (hLM) from cadaveric corneas. A relatively pure population of hLM was isolated and used as a feeder layer for the successful expansion of limbal epithelial cells that maintained stem cell properties. Our data suggest that hLM could potentially act as 'niche cells' maintaining the limbal progenitors in their native microenvironment.

Chapter 7: General discussion and future work

7.1 General discussion

Transparency of the central corneal epithelium is essential for vision. As in other epithelial tissues, maintenance of the central corneal epithelium relies on a population of epithelial stem cells. It is generally accepted that epithelial stem cells of the human ocular surface are unipotent and located in the limbus, a highly vascularized and innervated ring of tissue at the interface between the transparent central cornea and the opaque conjunctiva (Chen et al., 2004; Cotsarelis et al., 1989; Lawrenson & Ruskell, 1991; 1991; Schermer et al., 1986). Understanding stem cells and the interactions in their native niche is essential to recreate a suitable microenvironment for their expansion *in vitro* and thus a potential cellular therapy. Despite great advances in the understanding of corneal stem cell biology over the last decades, the exact location of the human limbal epithelial progenitors remains incompletely understood (Dua, 2005; Majo et al., 2008; Shortt et al., 2007). In fact, recent findings have challenged the concept of a uniform distribution of the limbal epithelial progenitors around the limbal circumference and proposed that LESCs could be located in specific structures named limbal crypts (LCs), limbal epithelial crypts and focal stromal projections (Dua, 2005; Shortt et al., 2007).

The first aim of this thesis was to assess the distribution of LESCs within the previously identified LCs compared with non-crypt limbal biopsies. LCs located between the POV correspond to downward projections of the limbal epithelium into the limbal stroma. These structures concentrated within the POV are easily identified macroscopically under a dissecting microscope and observed on

histological sections. In the present study, immunohistochemistry showed that the LCs contained a high population of basal epithelial cells positive for the expression of the most recently reported LESCs markers such as Frizzled 7, ABCB5 and N-cadherin complementing previous findings showing a high positivity for the expression of p63α and ABCG2 in epithelial cells populating these structures (Higa et al., 2009; Ksander et al., 2014; Mei et al., 2014; Shortt et al., 2007). However, this immunohistochemical approach was limited by the fact that no single marker specific to stem cells has as yet been identified. Initially developed by Barrandon and Green in 1987, single cell clonal analysis remains today a reliable *in vitro* method to discriminate epithelial stem cells from early and late progenitors (Larsson et al., 2014). Single epithelial cells in culture can be classified into three clonal types dependent upon the frequency with which they give rise to terminally differentiated progeny. Thus, holoclones have been assigned to stem cells whereas meroclones and paraclones have been assigned to early and late progenitors respectively. In the present study, the proliferative potential of limbal epithelial cells isolated from the LCs and non-crypt biopsies was investigated. Interestingly, cells isolated from both limbal areas had the potential to grow clonally and to generate secondary colonies in CFE assays. Such observations are in contradiction with previous findings showing that no expansion of LECs could be observed when the latter were isolated from non-crypt limbal biopsies (Shortt et al., 2007). This difference could be explained by the fact that human corneas used in the present study were relatively fresh and cells were generally isolated and put in culture between 48h and 72h post-enucleation. In fact, Liu et al. 2014 showed that despite preservation of the

stratification of the limbal epithelium, the secondary colony forming potential of limbal epithelial cells in culture decreased significantly 4 days post-enucleation. Further investigations involving single cell clonal analysis revealed the difference in the proliferative potential of LECs isolated from either crypt rich or non-crypt limbal areas. In fact, both limbal areas contain cells with the ability to generate holoclones demonstrating the presence of stem cells around the whole human limbal circumference. However, the number of holoclones generated when cells were isolated from the LCs (18%) was significantly higher than from the non-crypt (2%) confirming for the first time, with functional data, that these structures constitute a niche for epithelial progenitors of the human ocular surface. These observations support the importance of targeted niche biopsies for the successful development of stem cell therapies because specific harvesting of the cells with the highest proliferative potential *in vitro* that could impact clinical outcomes after transplantation.

In order to image LESCs and their interactions with the surrounding niche cells, LCs were further targeted for high-resolution imaging using state-of-the-art EM. Conventional transmission electron microscopy confirmed the presence of cells with a morphology consistent with stem cells as reported by Schlötzer-Schrehardt et al. 2005 (Schlötzer-Schrehardt & Kruse, 2005) and Townsend et al. 1991 (Townsend, 1991). These cells appeared small, compact and circular and, interestingly, they were closely associated with extensions coming from the underlying stromal cells, suggesting a route for direct cell-to-cell interaction. Despite the good lateral resolution reached by TEM, the resolution in the z plane

was limited to the thickness of the section, about 70nm. For this reason putative epithelial-stromal contacts are difficult to observe with conventional EM techniques. Major advances in volume electron microscopy over the last decade have allowed 3-dimensional imaging of biological specimens with unprecedented details. By associating high-resolution surface imaging of resin embedded specimens to automated serial sectioning, serial block-face SEM allows serial imaging and 3D reconstruction of cellular and sub-cellular volumes in large pieces of tissues. In the present study, a protocol for SBF imaging has been optimized to image the human limbus at the epithelial stromal interface. Meticulous serial sectioning, manual segmentation and 3D reconstruction led to the first representation of direct epithelial-stromal cell interaction in the native human LESC niche. Manual segmentations and reconstructions of nuclei confirmed that this type of contact occurred between two distinct cells. Further conventional TEM analysis at higher magnification showed that this direct epithelial-stromal contact was facilitated by focal interruptions of the local basement membrane (Dziasko et al. 2014). In their study, Chen et al. 2011 observed that collagenase digestion of limbal biopsies maintained a direct association between stromal and epithelial cells that were highly positive for the expression LESC markers and that these had the greatest proliferative potential in culture. Morphologically, limbal stromal cells appeared large and elongated with multiple extensions, similarly to limbal mesenchymal cells or keratocyte progenitor cells described by Polisetty et al. 2008, and Funderbugh et al. 2005, respectively (Funderburgh, et al., 2005; Polisetty et al., 2008). The hypothesis of a direct cell-to-cell interaction between LESC and limbal mesenchymal cells has

further been assessed. Despite a greater population of stromal cells +ve for the expression of MSC markers CD90 and CD105, the latter seemed to be located deeper in the limbal stroma. Other markers expressed by stromal cells directly interacting with the epithelial progenitors *in vitro* will be investigated in the native niche in the future (Chen et al., 2011). Moreover, bridging the gap between 3-dimensional structural imaging and functional interpretation by correlative light and electron microscopy will be the next challenge to identify the exact stromal cell population involved in this direct interaction.

Further observations revealed that LCs, which contain a concentration LESCs, are also richly populated by limbal melanocytes. In 2005, Higa et al. observed that CK19 +ve limbal basal epithelial cells were interacting with melanocytes and that such interaction could play a protective role against ultraviolet radiation through the release of melanin granules (Higa et al., 2005). In the present study, SBF imaging revealed the close interaction between a LESC and a melanocyte in the limbal stem cell niche. These observations were then confirmed by IHC that showed melanocytes associated with clusters of small compact epithelial cells at the edge of LCs. Following these observations, a role for melanocytes as niche cells was hypothesized. After being isolated and purified from human cadaveric corneas, mitotically active human limbal melanocytes were used, for the first time, as a feeder layer for the expansion on LECs. Interestingly, hLM had the ability to support clonal growth of LECs that could not be expanded in the absence of feeders. Moreover, LECs grown on hLM maintained expression of LESCs markers and had the ability to generate colonies in secondary CFE assays.

Therefore, limbal melanocytes have the ability to support LECs with stem cell characteristics *in vitro* suggesting a role for these cells an important element of the LESC niche. In 2007, Hayashi et al. observed that a subpopulation of LECs and limbal melanocytes were +ve for the expression of N-cadherin (Hayashi et al., 2007). Furthermore, Higa et al. 2007, observed that LECs grown on 3T3s had the ability to directly interact with the feeders and that disruption of N-cadherin mediated cell interactions promoted terminal cell differentiation of the epithelial progenitors. Taken together, these data support the existence of a N-cadherin homotypic cell-to-cell interaction between melanocytes and LESCs. The mechanism of the effect of the disruption of N-cadherin mediated cell-to-cell interaction between hLM and LECs in the co-culture model will be the subject of future investigations.

7.2 Future work

- **Further characterization of the stromal cell population(s) located beneath the limbal crypts;**

Develop a pilot protocol for correlative light and volume electron microscopy in order to identify the population of stromal cells directly interacting with basal epithelial cells. The method would rely on post embedding (in a hydrophilic resin) combined immunofluorescence and immunogold labeling (quantum dots conjugated antibodies would be an other option)

- **Assess efficiency of limbal stromal cells for the expansion of LECs/progenitors in culture and compare to melanocytes.**

- **Investigate the association of melanocytes and limbal stromal cells for the expansion of LECs *in vitro*.**

- **Investigate N-cadherin expression in melanocytes and LESCs in the native niche by IHC and by ICC in co-cultures: Consequences of the disruption (N-cadherin knock down) of N-cadherin mediated cell-to-cell interaction in co-cultures.**

- **Reconstitute an artificial functional limbal stem cell niche by incorporating stromal cells (in) and melanocytes (on top) into RAFT collagen tissue equivalents**

Supplemental data

Supplemental Video1_Marc Dziasko.mpg
Supplemental Video2_Marc Dziasko.mov

Videos can be found on SD card attached on the inside-back cover of this thesis.

References

Ahmad, S. (2012). Concise review: limbal stem cell deficiency, dysfunction, and distress. *Stem cells translational medicine*, *1*(2), 110–115. doi:10.5966/sctm.2011-0037

Amitai-Lange, A., Altshuler, A., Bubley, J., Dbayat, N., Tiosano, B., & Shalom-Feuerstein, R. (2014). Lineage tracing of stem and progenitor cells of the murine corneal epithelium. *STEM CELLS*. doi:10.1002/stem.1840

Aoi, T., Yae, K., Nakagawa, M., Ichisaka, T., Okita, K., Takahashi, K., Chiba, T., et al. (2008). Generation of pluripotent stem cells from adult mouse liver and stomach cells. *Science*, *321*(5889), 699–702. doi:10.1126/science.1154884

Armer, H. E. J., Mariggi, G., Png, K. M. Y., Genoud, C., Monteith, A. G., Bushby, A. J., Gerhardt, H., et al. (2009). Imaging transient blood vessel fusion events in zebrafish by correlative volume electron microscopy. *PloS one*, *4*(11), e7716. doi:10.1371/journal.pone.0007716

Arpitha, P., Prajna, N. V., Srinivasan, M., & Muthukkaruppan, V. (2005). High expression of p63 combined with a large N/C ratio defines a subset of human limbal epithelial cells: implications on epithelial stem cells. *Investigative Ophthalmology & Visual Science*, *46*(10), 3631–3636. doi:10.1167/iovs.05-0343

Artavanis-Tsakonas, S., Rand, M. D., & Lake, R. J. (1999). Notch signaling: cell fate control and signal integration in development. *Science*, *284*(5415), 770–776.

Asada, N., Katayama, Y., Sato, M., Minagawa, K., Wakahashi, K., Kawano, H., Kawano, Y., et al. (2013). Matrix-embedded osteocytes regulate mobilization of hematopoietic stem/progenitor cells. *Cell stem cell*, *12*(6), 737–747. doi:10.1016/j.stem.2013.05.001

Barbaro, V., Testa, A., Di Iorio, E., Mavilio, F., Pellegrini, G., & De Luca, M. (2007). C/EBPdelta regulates cell cycle and self-renewal of human limbal stem cells. *The Journal of cell biology*, *177*(6), 1037–1049. doi:10.1083/jcb.200703003

Barrandon, Y., & Green, H. (1987). Three clonal types of keratinocyte with different capacities for multiplication. *Proceedings of the National Academy of Sciences of the United States of America*, *84*(8), 2302–2306.

Barrandon, Y., Grasset, N., Zaffalon, A., Gorostidi, F., Claudinot, S., Droz-Georget, S. L., Nanba, D., et al. (2012). Capturing epidermal stemness for regenerative medicine. *Seminars in cell & developmental biology*, *23*(8), 937–944. doi:10.1016/j.semcdb.2012.09.011

Belmadani, A., Tran, P. B., Ren, D., Assimacopoulos, S., Grove, E. A., & Miller, R. J. (2005). The chemokine stromal cell-derived factor-1 regulates the migration of sensory neuron progenitors. *The Journal of neuroscience : the official journal of the Society for Neuroscience*, *25*(16), 3995–4003. doi:10.1523/JNEUROSCI.4631-04.2005

Beltrami, A. P., Barlucchi, L., Torella, D., Baker, M., Limana, F., Chimenti, S., Kasahara, H., et al. (2003). Adult cardiac stem cells are multipotent and support myocardial regeneration. *Cell*, *114*(6), 763–776.

Birk, D. E., Fitch, J. M., Babiarz, J. P., Doane, K. J., & Linsenmayer, T. F. (1990). Collagen fibrillogenesis in vitro: interaction of types I and V collagen regulates fibril diameter. *Journal of Cell Science*, *95 (Pt 4)*, 649–657.

Booth, C., & Potten, C. S. (2000). Gut instincts: thoughts on intestinal epithelial stem cells. *The Journal of clinical investigation*, *105*(11), 1493–1499. doi:10.1172/JCI10229

Branch, M. J., Hashmani, K., Dhillon, P., Jones, D. R. E., Dua, H. S., & Hopkinson, A. (2012). Mesenchymal stem cells in the human corneal limbal stroma. *Investigative Ophthalmology & Visual Science*, *53*(9), 5109–5116. doi:10.1167/iovs.11-8673

Briggman, K. L., Helmstaedter, M., & Denk, W. (2011). Wiring specificity in the direction-selectivity circuit of the retina. *Nature*, *471*(7337), 183–188. doi:10.1038/nature09818

Budak, M. T. (2005). Ocular surface epithelia contain ABCG2-dependent side population cells exhibiting features associated with stem cells. *Journal of Cell Science*, *118*(8), 1715–1724. doi:10.1242/jcs.02279

Calvi, L. M., Adams, G. B., Weibrecht, K. W., Weber, J. M., Olson, D. P., Knight, M. C., Martin, R. P., et al. (2003). Osteoblastic cells regulate the haematopoietic stem cell niche. *Nature*, *425*(6960), 841–846. doi:10.1038/nature02040

Cancelas, J. A., Koevoet, W. L., de Koning, A. E., Mayen, A. E., Rombouts, E. J., & Ploemacher, R. E. (2000). Connexin-43 gap junctions are involved in multiconnexin-expressing stromal support of hemopoietic progenitors and stem cells. *Blood*, *96*(2), 498–505.

Ceafalan, L., Gherghiceanu, M., Popescu, L. M., & Simionescu, O. (2012). Telocytes in human skin--are they involved in skin regeneration? *Journal of cellular and molecular medicine*, *16*(7), 1405–1420. doi:10.1111/j.1582-4934.2012.01580.x

Cheli, Y., Ohanna, M., Ballotti, R., & Bertolotto, C. (2010). Fifteen-year quest for microphthalmia-associated transcription factor target genes. *Pigment cell &*

melanoma research, *23*(1), 27–40. doi:10.1111/j.1755-148X.2009.00653.x

Chen, J. J., & Tseng, S. C. (1991). Abnormal corneal epithelial wound healing in partial-thickness removal of limbal epithelium. *Investigative Ophthalmology & Visual Science*, *32*(8), 2219–2233.

Chen, S.-Y., Hayashida, Y., Chen, M.-Y., Xie, H. T., & Tseng, S. C. G. (2011a). A New Isolation Method of Human Limbal Progenitor Cells by Maintaining Close Association with Their Niche Cells. *Tissue Engineering Part C: Methods*, *17*(5), 537–548. doi:10.1089/ten.tec.2010.0609

Chen, W. Y., Mui, M. M., Kao, W. W., Liu, C. Y., & Tseng, S. C. (1994). Conjunctival epithelial cells do not transdifferentiate in organotypic cultures: expression of K12 keratin is restricted to corneal epithelium. *Current eye research*, *13*(10), 765–778.

Chen, Z., de Paiva, C. S., Luo, L., Kretzer, F. L., Pflugfelder, S. C., & Li, D.-Q. (2004). Characterization of putative stem cell phenotype in human limbal epithelia. *STEM CELLS*, *22*(3), 355–366. doi:10.1634/stemcells.22-3-355

Cheng, Y., Boll, W., Kirchhausen, T., Harrison, S. C., & Walz, T. (2007). Cryo-electron tomography of clathrin-coated vesicles: structural implications for coat assembly. *Journal of molecular biology*, *365*(3), 892–899. doi:10.1016/j.jmb.2006.10.036

Clinch, T. E., Goins, K. M., & Cobo, L. M. (1992). Treatment of contact lens-related ocular surface disorders with autologous conjunctival transplantation. *Ophthalmology*, *99*(4), 634–638.

Connon, C. J., Doutch, J., Chen, B., Hopkinson, A., Mehta, J. S., Nakamura, T., Kinoshita, S., et al. (2010). The variation in transparency of amniotic membrane used in ocular surface regeneration. *The British journal of ophthalmology*, *94*(8), 1057–1061. doi:10.1136/bjo.2008.153064

Cotsarelis, G., Cheng, S. Z., Dong, G., Sun, T. T., & Lavker, R. M. (1989). Existence of slow-cycling limbal epithelial basal cells that can be preferentially stimulated to proliferate: implications on epithelial stem cells. *Cell*, *57*(2), 201–209.

Cotsarelis, G., Sun, T. T., & Lavker, R. M. (1990). Label-retaining cells reside in the bulge area of pilosebaceous unit: implications for follicular stem cells, hair cycle, and skin carcinogenesis. *Cell*, *61*(7), 1329–1337.

Cyrklaff, M., Linaroudis, A., Boicu, M., Chlanda, P., Baumeister, W., Griffiths, G., & Krijnse Locker, J. (2007). Whole cell cryo-electron tomography reveals distinct disassembly intermediates of vaccinia virus. *PloS one*, *2*(5), e420. doi:10.1371/journal.pone.0000420

Davanger, M., & Evensen, A. (1971). Role of the pericorneal papillary structure in renewal of corneal epithelium. *Nature*, *229*(5286), 560–561.

Davies, S. B., Chui, J., Madigan, M. C., Provis, J. M., Wakefield, D., & Di Girolamo, N. (2009). Stem cell activity in the developing human cornea. *STEM CELLS*, *27*(11), 2781–2792. doi:10.1002/stem.209

De Winter, D. A. M., Schneijdenberg, C. T. W. M., Lebbink, M. N., Lich, B., Verkleij, A. J., Drury, M. R., & Humbel, B. M. (2009). Tomography of insulating biological and geological materials using focused ion beam (FIB) sectioning and low-kV BSE imaging. *Journal of microscopy*, *233*(3), 372–383. doi:10.1111/j.1365-2818.2009.03139.x

Denk, W., & Horstmann, H. (2004). Serial block-face scanning electron microscopy to reconstruct three-dimensional tissue nanostructure. *PLoS biology*, *2*(11), e329. doi:10.1371/journal.pbio.0020329

Di Girolamo, N., Bobba, S., Raviraj, V., Delic, N. C., Slapetova, I., Nicovich, P. R., Halliday, G. M., et al. (2014). Tracing the fate of limbal epithelial progenitor cells in the murine cornea. *Stem cells*. doi:10.1002/stem.1769

Ding, L., Saunders, T. L., Enikolopov, G., & Morrison, S. J. (2012). Endothelial and perivascular cells maintain haematopoietic stem cells. *Nature*, *481*(7382), 457–462. doi:10.1038/nature10783

Dominici, M., Le Blanc, K., Mueller, I., Slaper-Cortenbach, I., Marini, F., Krause, D., Deans, R., et al. (2006). Minimal criteria for defining multipotent mesenchymal stromal cells. The International Society for Cellular Therapy position statement. *Cytotherapy*, *8*(4), 315–317. doi:10.1080/14653240600855905

Doutch, J. J., Quantock, A. J., Joyce, N. C., & Meek, K. M. (2012). Ultraviolet light transmission through the human corneal stroma is reduced in the periphery. *Biophysical journal*, *102*(6), 1258–1264. doi:10.1016/j.bpj.2012.02.023

Dravida, S., Gaddipati, S., Griffith, M., Merrett, K., Lakshmi Madhira, S., Sangwan, V. S., & Vemuganti, G. K. (2008). A biomimetic scaffold for culturing limbal stem cells: a promising alternative for clinical transplantation. *Journal of Tissue Engineering and Regenerative Medicine*, *2*(5), 263–271. doi:10.1002/term.91

Du, Y., Funderburgh, M. L., Mann, M. M., SundarRaj, N., & Funderburgh, J. L. (2005). Multipotent stem cells in human corneal stroma. *STEM CELLS*, *23*(9), 1266–1275. doi:10.1634/stemcells.2004-0256

Dua, H. S. (2005). Limbal epithelial crypts: a novel anatomical structure and a putative limbal stem cell niche. *British Journal of Ophthalmology*, *89*(5), 529–532. doi:10.1136/bjo.2004.049742

Dua, H. S., Gomes, J. A. P., King, A. J., & Maharajan, V. S. (2004). The amniotic membrane in ophthalmology. *Survey of Ophthalmology*, *49*(1), 51–77.

Dua, H. S., Gomes, J. A., & Singh, A. (1994). Corneal epithelial wound healing. *British Journal of Ophthalmology*, *78*(5), 401–408.

Dziasko, M. A., Armer, H. E., Levis, H. J., Shortt, A. J., Tuft, S., & Daniels, J. T. (2014). Localisation of epithelial cells capable of holoclone formation in vitro and direct interaction with stromal cells in the native human limbal crypt. *PloS one*, *9*(4), e94283. doi:10.1371/journal.pone.0094283

Ebato, B., Friend, J., & Thoft, R. A. (1988). Comparison of limbal and peripheral human corneal epithelium in tissue culture. *Investigative Ophthalmology & Visual Science*, *29*(10), 1533–1537.

Espana, E. M., Kawakita, T., Romano, A., Di Pascuale, M., Smiddy, R., Liu, C.-Y., & Tseng, S. C. G. (2003). Stromal niche controls the plasticity of limbal and corneal epithelial differentiation in a rabbit model of recombined tissue. *Investigative Ophthalmology & Visual Science*, *44*(12), 5130–5135.

Evans, M. J., & Kaufman, M. H. (1981). Establishment in culture of pluripotential cells from mouse embryos. *Nature*, *292*(5819), 154–156.

Felts, R. L., Narayan, K., Estes, J. D., Shi, D., Trubey, C. M., Fu, J., Hartnell, L. M., et al. (2010). 3D visualization of HIV transfer at the virological synapse between dendritic cells and T cells. *Proceedings of the National Academy of Sciences of the United States of America*, *107*(30), 13336–13341. doi:10.1073/pnas.1003040107

Figueira, E. C., Di Girolamo, N., Coroneo, M. T., & Wakefield, D. (2007). The phenotype of limbal epithelial stem cells. *Investigative Ophthalmology & Visual Science*, *48*(1), 144–156. doi:10.1167/iovs.06-0346

Friedenstein, A. J., Gorskaja, J. F., & Kulagina, N. N. (1976). Fibroblast precursors in normal and irradiated mouse hematopoietic organs. *Experimental hematology*, *4*(5), 267–274.

Funderburgh, M. L., Du, Y., Mann, M. M., SundarRaj, N., & Funderburgh, J. L. (2005). PAX6 expression identifies progenitor cells for corneal keratocytes. *FASEB journal : official publication of the Federation of American Societies for Experimental Biology*, *19*(10), 1371–1373. doi:10.1096/fj.04-2770fje

Gago, N., Pérez-López, V., Sanz-Jaka, J. P., Cormenzana, P., Eizaguirre, I., Bernad, A., & Izeta, A. (2009). Age-dependent depletion of human skin-derived progenitor cells. *STEM CELLS*, *27*(5), 1164–1172. doi:10.1002/stem.27

Galiger, C., Kostin, S., Golec, A., Ahlbrecht, K., Becker, S., Gherghiceanu, M.,

Popescu, L. M., et al. (2014). Phenotypical and ultrastructural features of Oct4-positive cells in the adult mouse lung. *Journal of cellular and molecular medicine*, *18*(7), 1321–1333. doi:10.1111/jcmm.12295

Gherghiceanu, M., & Popescu, L. M. (2012). Cardiac telocytes - their junctions and functional implications. *Cell and Tissue Research*, *348*(2), 265–279. doi:10.1007/s00441-012-1333-8

Giangreco, A., Reynolds, S. D., & Stripp, B. R. (2002). Terminal bronchioles harbor a unique airway stem cell population that localizes to the bronchoalveolar duct junction. *The American journal of pathology*, *161*(1), 173–182. doi:10.1016/S0002-9440(10)64169-7

Gipson, I. K. (1989). The epithelial basement membrane zone of the limbus. *Eye (London, England)*, *3 (Pt 2)*, 132–140. doi:10.1038/eye.1989.21

Goldberg, M. F., & Bron, A. J. (1982). Limbal palisades of Vogt. *Transactions of the American Ophthalmological Society*, *80*, 155–171.

Goodell, M. A., Brose, K., Paradis, G., Conner, A. S., & Mulligan, R. C. (1996). Isolation and functional properties of murine hematopoietic stem cells that are replicating in vivo. *The Journal of experimental medicine*, *183*(4), 1797–1806.

Graves, B. (1934). CERTAIN CLINICAL FEATURES OF THE NORMAL LIMBUS. *British Journal of Ophthalmology*, *18*(6), 305–341.

Griffith, M., Osborne, R., Munger, R., Xiong, X., Doillon, C. J., Laycock, N. L., Hakim, M., et al. (1999). Functional human corneal equivalents constructed from cell lines. *Science*, *286*(5447), 2169–2172.

Grueterich, M., Espana, E. M., & Tseng, S. C. G. (2003). Ex vivo expansion of limbal epithelial stem cells: amniotic membrane serving as a stem cell niche. *Survey of Ophthalmology*, *48*(6), 631–646. doi:10.1016/j.survophthal.2003.08.003

Hadley, M. E., & Quevedo, W. C. (1966). Vertebrate epidermal melanin unit. *Nature*, *209*(5030), 1334–1335.

Halaban, R., & Alfano, F. D. (1984). Selective elimination of fibroblasts from cultures of normal human melanocytes. *In vitro*, *20*(5), 447–450.

Hambiliki, F., Ström, S., Zhang, P., & Stavreus-Evers, A. (2012). Co-localization of NANOG and OCT4 in human pre-implantation embryos and in human embryonic stem cells. *Journal of assisted reproduction and genetics*, *29*(10), 1021–1028. doi:10.1007/s10815-012-9824-9

Han, H.-M., Bouchet-Marquis, C., Huebinger, J., & Grabenbauer, M. (2013). Golgi apparatus analyzed by cryo-electron microscopy. *Histochemistry and cell biology*, *140*(4), 369–381. doi:10.1007/s00418-013-1136-3

Hanna, J., Wernig, M., Markoulaki, S., Sun, C.-W., Meissner, A., Cassady, J. P., Beard, C., et al. (2007). Treatment of sickle cell anemia mouse model with iPS cells generated from autologous skin. *Science*, *318*(5858), 1920–1923. doi:10.1126/science.1152092

Hass, R., Kasper, C., Böhm, S., & Jacobs, R. (2011). Different populations and sources of human mesenchymal stem cells (MSC): A comparison of adult and neonatal tissue-derived MSC. *Cell communication and signaling : CCS*, *9*, 12. doi:10.1186/1478-811X-9-12

Hassell, J. R., & Birk, D. E. (2010). The molecular basis of corneal transparency. *Experimental Eye Research*, *91*(3), 326–335. doi:10.1016/j.exer.2010.06.021

Hayashi, R., Yamato, M., Sugiyama, H., Sumide, T., Yang, J., Okano, T., Tano, Y., et al. (2007). N-Cadherin Is Expressed by Putative Stem/Progenitor Cells and Melanocytes in the Human Limbal Epithelial Stem Cell Niche. *Stem cells*, *25*(2), 289–296. doi:10.1634/stemcells.2006-0167

Henderson, G. P., Gan, L., & Jensen, G. J. (2007). 3-D ultrastructure of O. tauri: electron cryotomography of an entire eukaryotic cell. *PloS one*, *2*(8), e749. doi:10.1371/journal.pone.0000749

Hendry, C. E., & Little, M. H. (2012). Reprogramming the kidney: a novel approach for regeneration. *Kidney international*, *82*(2), 138–146. doi:10.1038/ki.2012.68

Heymann, J. A. W., Shi, D., Kim, S., Bliss, D., Milne, J. L. S., & Subramaniam, S. (2009). 3D imaging of mammalian cells with ion-abrasion scanning electron microscopy. *Journal of structural biology*, *166*(1), 1–7. doi:10.1016/j.jsb.2008.11.005

Higa, K., Kato, N., Yoshida, S., Ogawa, Y., Shimazaki, J., Tsubota, K., & Shimmura, S. (2012). Aquaporin 1-positive stromal niche-like cells directly interact with N-cadherin-positive clusters in the basal limbal epithelium. *Stem Cell Research*, *10*(2), 147–155. doi:10.1016/j.scr.2012.11.001

Higa, K., Shimmura, S., Miyashita, H., Kato, N., Ogawa, Y., Kawakita, T., Shimazaki, J., et al. (2009). N-cadherin in the maintenance of human corneal limbal epithelial progenitor cells in vitro. *Investigative Ophthalmology & Visual Science*, *50*(10), 4640–4645. doi:10.1167/iovs.09-3503

Higa, K., Shimmura, S., Miyashita, H., Shimazaki, J., & Tsubota, K. (2005). Melanocytes in the corneal limbus interact with K19-positive basal epithelial cells. *Experimental Eye Research*, *81*(2), 218–223. doi:10.1016/j.exer.2005.01.023

Horikawa, T., Norris, D. A., Zekman, T., & Morelli, J. G. (1996). Effective

elimination of fibroblasts in cultures of melanocytes by lowering calcium concentration in TPA depleted medium following geneticin treatment. *Pigment cell research / sponsored by the European Society for Pigment Cell Research and the International Pigment Cell Society*, *9*(2), 58–62.

Ilari, L., & Daya, S. M. (2002). Long-term outcomes of keratolimbal allograft for the treatment of severe ocular surface disorders. *Ophthalmology*, *109*(7), 1278–1284.

Isern, J., Martín-Antonio, B., Ghazanfari, R., Martín, A. M., López, J. A., del Toro, R., Sánchez-Aguilera, A., et al. (2013). Self-renewing human bone marrow mesenspheres promote hematopoietic stem cell expansion. *Cell reports*, *3*(5), 1714–1724. doi:10.1016/j.celrep.2013.03.041

Jester, J. V., Moller-Pedersen, T., Huang, J., Sax, C. M., Kays, W. T., Cavangh, H. D., Petroll, W. M., et al. (1999). The cellular basis of corneal transparency: evidence for 'corneal crystallins'. *Journal of Cell Science*, *112 (Pt 5)*, 613–622.

Jones, P. H., & Watt, F. M. (1993). Separation of human epidermal stem cells from transit amplifying cells on the basis of differences in integrin function and expression. *Cell*, *73*(4), 713–724.

Joyce, N. C. (2003). Proliferative capacity of the corneal endothelium. *Progress in retinal and eye research*, *22*(3), 359–389.

Katayama, Y., Battista, M., Kao, W.-M., Hidalgo, A., Peired, A. J., Thomas, S. A., & Frenette, P. S. (2006). Signals from the sympathetic nervous system regulate hematopoietic stem cell egress from bone marrow. *Cell*, *124*(2), 407–421. doi:10.1016/j.cell.2005.10.041

Katikireddy, K. R., Dana, R., & Jurkunas, U. V. (2013). Differentiation potential of limbal fibroblasts and bone marrow mesenchymal stem cells to corneal epithelial cells. *Stem cells*. doi:10.1002/stem.1541

Kirilly, D., & Xie, T. (2007). The Drosophila ovary: an active stem cell community. *Cell Research*, *17*(1), 15–25. doi:10.1038/sj.cr.7310123

Klenkler, B., & Sheardown, H. (2004). Growth factors in the anterior segment: role in tissue maintenance, wound healing and ocular pathology. *Experimental Eye Research*, *79*(5), 677–688. doi:10.1016/j.exer.2004.07.008

Knott, G., & Genoud, C. (2013). Is EM dead? *Journal of Cell Science*, *126*(Pt 20), 4545–4552. doi:10.1242/jcs.124123

Knott, G., Marchman, H., Wall, D., & Lich, B. (2008). Serial section scanning electron microscopy of adult brain tissue using focused ion beam milling. *The Journal of neuroscience : the official journal of the Society for Neuroscience*, *28*(12), 2959–2964. doi:10.1523/JNEUROSCI.3189-07.2008

Koizumi, N. J., Inatomi, T. J., Sotozono, C. J., Fullwood, N. J., Quantock, A. J., & Kinoshita, S. (2000). Growth factor mRNA and protein in preserved human amniotic membrane. *Current eye research*, *20*(3), 173–177.

Kondo, T., & Hearing, V. J. (2011). Update on the regulation of mammalian melanocyte function and skin pigmentation. *Expert review of dermatology*, *6*(1), 97–108. doi:10.1586/edm.10.70

Koning, R. I., Zovko, S., Bárcena, M., Oostergetel, G. T., Koerten, H. K., Galjart, N., Koster, A. J., et al. (2008). Cryo electron tomography of vitrified fibroblasts: microtubule plus ends in situ. *Journal of structural biology*, *161*(3), 459–468. doi:10.1016/j.jsb.2007.08.011

Kopriwa, B. M. (1984). Block-staining tissues with potassium ferrocyanide-reduced osmium tetroxide and lead aspartate for electron microscopic radioautography. *Journal of Histochemistry and Cytochemistry*, *32*(5), 552–554.

Ksander, B. R., Kolovou, P. E., Wilson, B. J., Saab, K. R., Guo, Q., Ma, J., McGuire, S. P., et al. (2014). ABCB5 is a limbal stem cell gene required for corneal development and repair. *Nature*, *511*(7509), 353–357. Nature Publishing Group. doi:10.1038/nature13426

Larsson, H. M., Gorostidi, F., Hubbell, J. A., Barrandon, Y., & Frey, P. (2014). Clonal, self-renewing and differentiating human and porcine urothelial cells, a novel stem cell population. *PloS one*, *9*(2), e90006. doi:10.1371/journal.pone.0090006

Lawrenson, J. G., & Ruskell, G. L. (1991). The structure of corpuscular nerve endings in the limbal conjunctiva of the human eye. *Journal of anatomy*, *177*, 75–84.

Lesueur, L., Arne, J. L., Mignon-Conte, M., & Malecaze, F. (1994). Structural and ultrastructural changes in the developmental process of premature infants“ and children”s corneas. *Cornea*, *13*(4), 331–338.

Levis, H. J., Massie, I., Dziasko, M. A., Kaasi, A., & Daniels, J. T. (2013). Rapid tissue engineering of biomimetic human corneal limbal crypts with 3D niche architecture. *Biomaterials*, *34*(35), 8860–8868. doi:10.1016/j.biomaterials.2013.08.002

Li, L., & Xie, T. (2005). Stem cell niche: structure and function. *Annual review of cell and developmental biology*, *21*, 605–631. doi:10.1146/annurev.cellbio.21.012704.131525

Li, Y., Inoue, T., Takamatsu, F., Kobayashi, T., Shiraishi, A., Maeda, N., Ohashi, Y., et al. (2014). Differences between niche cells and limbal stromal cells in

maintenance of corneal limbal stem cells. *Investigative Ophthalmology & Visual Science*, *55*(3), 1453–1462. doi:10.1167/iovs.13-13698

Liu, T., Wang, Y., Duan, H.-Y., Qu, M.-L., Yang, L.-L., Xu, Y.-Y., Zang, X.-J., et al. (2012). Effects of preservation time on proliferative potential of human limbal stem/progenitor cells. *International journal of ophthalmology*, *5*(5), 549–554. doi:10.3980/j.issn.2222-3959.2012.05.02

Ljubimov, A. V., Burgeson, R. E., Butkowski, R. J., Michael, A. F., Sun, T. T., & Kenney, M. C. (1995). Human corneal basement membrane heterogeneity: topographical differences in the expression of type IV collagen and laminin isoforms. *Laboratory investigation; a journal of technical methods and pathology*, *72*(4), 461–473.

Luesma, M. J., Gherghiceanu, M., & Popescu, L. M. (2013). Telocytes and stem cells in limbus and uvea of mouse eye. *Journal of cellular and molecular medicine*, *17*(8), 1016–1024. doi:10.1111/jcmm.12111

Maimon, T., Elad, N., Dahan, I., & Medalia, O. (2012). The human nuclear pore complex as revealed by cryo-electron tomography. *Structure (London, England : 1993)*, *20*(6), 998–1006. doi:10.1016/j.str.2012.03.025

Majo, F., Rochat, A., Nicolas, M., Jaoudé, G. A., & Barrandon, Y. (2008). Oligopotent stem cells are distributed throughout the mammalian ocular surface. *Nature*, *456*(7219), 250–254. doi:10.1038/nature07406

Mariappan, I., Maddileti, S., Savy, S., Tiwari, S., Gaddipati, S., Fatima, A., Sangwan, V. S., et al. (2010). In vitro culture and expansion of human limbal epithelial cells. *Nature Protocols*, *5*(8), 1470–1479. doi:10.1038/nprot.2010.115

Matic, M., Petrov, I. N., Chen, S., Wang, C., Dimitrijevich, S. D., & Wolosin, J. M. (1997). Stem cells of the corneal epithelium lack connexins and metabolite transfer capacity. *Differentiation; research in biological diversity*, *61*(4), 251–260. doi:10.1046/j.1432-0436.1997.6140251.x

Mazzinghi, B., Ronconi, E., Lazzeri, E., Sagrinati, C., Ballerini, L., Angelotti, M. L., Parente, E., et al. (2008). Essential but differential role for CXCR4 and CXCR7 in the therapeutic homing of human renal progenitor cells. *The Journal of experimental medicine*, *205*(2), 479–490. doi:10.1084/jem.20071903

Mei, H., Nakatsu, M. N., Baclagon, E. R., & Deng, S. X. (2014). Frizzled 7 maintains the undifferentiated state of human limbal stem/progenitor cells. *Stem cells*, *32*(4), 938–945. doi:10.1002/stem.1582

Méndez-Ferrer, S., Michurina, T. V., Ferraro, F., Mazloom, A. R., Ben D MacArthur, Lira, S. A., Scadden, D. T., et al. (2010). Mesenchymal and haematopoietic stem cells form a unique bone marrow niche. *Nature*, *466*(7308), 829–834.

Nature Publishing Group. doi:10.1038/nature09262

Méndez-Ferrer, S., Scadden, D. T., & Sánchez-Aguilera, A. (2015). Bone marrow stem cells: current and emerging concepts. *Annals of the New York Academy of Sciences*, *1335*(1), 32–44. doi:10.1111/nyas.12641

Mills, A. A., Zheng, B., Wang, X. J., Vogel, H., Roop, D. R., & Bradley, A. (1999). p63 is a p53 homologue required for limb and epidermal morphogenesis. *Nature*, *398*(6729), 708–713. doi:10.1038/19531

Molvaer, R. K., Andreasen, A., Heegaard, S., Thomsen, J. S., Hjortdal, J., Urbak, S. F., & Nielsen, K. (2013). Interactive 3D computer model of the human corneolimbal region: crypts, projections and stem cells. *Acta ophthalmologica*, *91*(5), 457–462. doi:10.1111/j.1755-3768.2012.02446.x

Morrison, S. J., & Scadden, D. T. (2014). The bone marrow niche for haematopoietic stem cells. *Nature*, *505*(7483), 327–334. doi:10.1038/nature12984

Mort, R. L., Ramaesh, T., Kleinjan, D. A., Morley, S. D., & West, J. D. (2009). Mosaic analysis of stem cell function and wound healing in the mouse corneal epithelium. *BMC developmental biology*, *9*, 4. doi:10.1186/1471-213X-9-4

Murphy, G. E., Lowekamp, B. C., Zerfas, P. M., Chandler, R. J., Narasimha, R., Venditti, C. P., & Subramaniam, S. (2010). Ion-abrasion scanning electron microscopy reveals distorted liver mitochondrial morphology in murine methylmalonic acidemia. *Journal of structural biology*, *171*(2), 125–132. doi:10.1016/j.jsb.2010.04.005

Müller, L. J., Pels, E., & Vrensen, G. F. (2001). The specific architecture of the anterior stroma accounts for maintenance of corneal curvature. *British Journal of Ophthalmology*, *85*(4), 437–443.

Nakamura-Ishizu, A., Okuno, Y., Omatsu, Y., Okabe, K., Morimoto, J., Uede, T., Nagasawa, T., et al. (2012). Extracellular matrix protein tenascin-C is required in the bone marrow microenvironment primed for hematopoietic regeneration. *Blood*, *119*(23), 5429–5437. doi:10.1182/blood-2011-11-393645

Nakatsu, M. N., Ding, Z., Ng, M. Y., Truong, T. T., Yu, F., & Deng, S. X. (2011). Wnt/ -Catenin Signaling Regulates Proliferation of Human Cornea Epithelial Stem/Progenitor Cells. *Investigative Ophthalmology & Visual Science*, *52*(7), 4734–4741. doi:10.1167/iovs.10-6486

Nakatsu, M. N., González, S., Mei, H., & Deng, S. X. (2014). Human Limbal Mesenchymal Cells Support the Growth of Human Corneal Epithelial Stem/Progenitor Cells. *Investigative Ophthalmology & Visual Science*. doi:10.1167/iovs.14-14999

Naveiras, O., Nardi, V., Wenzel, P. L., Hauschka, P. V., Fahey, F., & Daley, G. Q. (2009). Bone-marrow adipocytes as negative regulators of the haematopoietic microenvironment. *Nature*, *460*(7252), 259–263. Nature Publishing Group. doi:10.1038/nature08099

Nie, Y., Han, Y.-C., & Zou, Y.-R. (2008). CXCR4 is required for the quiescence of primitive hematopoietic cells. *The Journal of experimental medicine*, *205*(4), 777–783. doi:10.1084/jem.20072513

Nishida, K., Kinoshita, S., Ohashi, Y., Kuwayama, Y., & Yamamoto, S. (1995). Ocular surface abnormalities in aniridia. *American journal of ophthalmology*, *120*(3), 368–375.

Notara, M., Shortt, A. J., Galatowicz, G., Calder, V., & Daniels, J. T. (2010). IL6 and the human limbal stem cell niche: A mediator of epithelial–stromal interaction. *Stem Cell Research*, *5*(3), 188–200. Elsevier B.V. doi:10.1016/j.scr.2010.07.002

Notara, M., Shortt, A. J., O'Callaghan, A. R., & Daniels, J. T. (2012). The impact of age on the physical and cellular properties of the human limbal stem cell niche. *Age (Dordrecht, Netherlands)*. doi:10.1007/s11357-011-9359-5

Okita, K., Ichisaka, T., & Yamanaka, S. (2007). Generation of germline-competent induced pluripotent stem cells. *Nature*, *448*(7151), 313–317. doi:10.1038/nature05934

Ordonez, P., & Di Girolamo, N. (2012). Limbal Epithelial Stem Cells: Role of the Niche Microenvironment. *Stem cells*, *30*(2), 100–107. doi:10.1002/stem.794

Ordonez, P., Chow, S., Wakefield, D., & Di Girolamo, N. (2013). Human limbal epithelial progenitor cells express αvβ5-integrin and the interferon-inducible chemokine CXCL10/IP-10. *Stem Cell Research*, *11*(2), 888–901. doi:10.1016/j.scr.2013.05.013

Otsuru, S., Tamai, K., Yamazaki, T., Yoshikawa, H., & Kaneda, Y. (2008). Circulating bone marrow-derived osteoblast progenitor cells are recruited to the bone-forming site by the CXCR4/stromal cell-derived factor-1 pathway. *STEM CELLS*, *26*(1), 223–234. doi:10.1634/stemcells.2007-0515

Pajoohesh-Ganji, A., & Stepp, M. A. (2005). In search of markers for the stem cells of the corneal epithelium. *Biology of the cell / under the auspices of the European Cell Biology Organization*, *97*(4), 265–276. doi:10.1042/BC20040114

Pearton, D. J., Yang, Y., & Dhouailly, D. (2005). Transdifferentiation of corneal epithelium into epidermis occurs by means of a multistep process triggered by dermal developmental signals. *Proceedings of the National Academy of*

Sciences of the United States of America, *102*(10), 3714–3719. doi:10.1073/pnas.0500344102

Peddie, C. J., & Collinson, L. M. (2014). Exploring the third dimension: volume electron microscopy comes of age. *Micron (Oxford, England : 1993)*, *61*, 9–19. doi:10.1016/j.micron.2014.01.009

Pellegrini, G., Dellambra, E., Golisano, O., Martinelli, E., Fantozzi, I., Bondanza, S., Ponzin, D., et al. (2001). p63 identifies keratinocyte stem cells. *Proceedings of the National Academy of Sciences of the United States of America*, *98*(6), 3156–3161. doi:10.1073/pnas.061032098

Pellegrini, G., Golisano, O., Paterna, P., Lambiase, A., Bonini, S., Rama, P., & De Luca, M. (1999). Location and clonal analysis of stem cells and their differentiated progeny in the human ocular surface. *The Journal of cell biology*, *145*(4), 769–782.

Pellegrini, G., Traverso, C. E., Franzi, A. T., Zingirian, M., Cancedda, R., & De Luca, M. (1997). Long-term restoration of damaged corneal surfaces with autologous cultivated corneal epithelium. *Lancet*, *349*(9057), 990–993. doi:10.1016/S0140-6736(96)11188-0

Pinali, C., Bennett, H., Davenport, J. B., Trafford, A. W., & Kitmitto, A. (2013). Three-dimensional reconstruction of cardiac sarcoplasmic reticulum reveals a continuous network linking transverse-tubules: this organization is perturbed in heart failure. *Circulation research*, *113*(11), 1219–1230. doi:10.1161/CIRCRESAHA.113.301348

Pinnamaneni, N., & Funderburgh, J. L. (2012). Concise review: Stem cells in the corneal stroma. *Stem cells*, *30*(6), 1059–1063. doi:10.1002/stem.1100

Pinto, D., Gregorieff, A., Begthel, H., & Clevers, H. (2003). Canonical Wnt signals are essential for homeostasis of the intestinal epithelium. *Genes & development*, *17*(14), 1709–1713. doi:10.1101/gad.267103

Polisetty, N., Fatima, A., Madhira, S. L., Sangwan, V. S., & Vemuganti, G. K. (2008). Mesenchymal cells from limbal stroma of human eye. *Molecular vision*, *14*, 431–442.

Popescu, L. M., & Faussone-Pellegrini, M.-S. (2010). TELOCYTES - a case of serendipity: the winding way from Interstitial Cells of Cajal (ICC), via Interstitial Cajal-Like Cells (ICLC) to TELOCYTES. *Journal of cellular and molecular medicine*, *14*(4), 729–740. doi:10.1111/j.1582-4934.2010.01059.x

Rama, P., Bonini, S., Lambiase, A., Golisano, O., Paterna, P., De Luca, M., & Pellegrini, G. (2001). Autologous fibrin-cultured limbal stem cells permanently restore the corneal surface of patients with total limbal stem cell deficiency. *Transplantation*, *72*(9), 1478–1485.

Rama, P., Matuska, S., Paganoni, G., Spinelli, A., De Luca, M., & Pellegrini, G. (2010). Limbal stem-cell therapy and long-term corneal regeneration. *The New England journal of medicine*, *363*(2), 147–155. doi:10.1056/NEJMoa0905955

Rheinwald, J. G., & Green, H. (1975). Serial cultivation of strains of human epidermal keratinocytes: the formation of keratinizing colonies from single cells. *Cell*, *6*(3), 331–343.

Rochat, A., Kobayashi, K., & Barrandon, Y. (1994). Location of stem cells of human hair follicles by clonal analysis. *Cell*, *76*(6), 1063–1073.

Saha, K., Keung, A. J., Irwin, E. F., Li, Y., Little, L., Schaffer, D. V., & Healy, K. E. (2008). Substrate modulus directs neural stem cell behavior. *Biophysical journal*, *95*(9), 4426–4438. doi:10.1529/biophysj.108.132217

Scadden, D. T. (2006). The stem-cell niche as an entity of action. *Nature*, *441*(7097), 1075–1079. doi:10.1038/nature04957

Scadden, D. T. (2014). Nice neighborhood: emerging concepts of the stem cell niche. *Cell*, *157*(1), 41–50. doi:10.1016/j.cell.2014.02.013

Schermer, A., Galvin, S., & Sun, T. T. (1986). Differentiation-related expression of a major 64K corneal keratin in vivo and in culture suggests limbal location of corneal epithelial stem cells. *The Journal of cell biology*, *103*(1), 49–62.

Schlötzer-Schrehardt, U., & Kruse, F. E. (2005). Identification and characterization of limbal stem cells. *Experimental Eye Research*, *81*(3), 247–264. doi:10.1016/j.exer.2005.02.016

Schlötzer-Schrehardt, U., Dietrich, T., Saito, K., Sorokin, L., Sasaki, T., Paulsson, M., & Kruse, F. E. (2007). Characterization of extracellular matrix components in the limbal epithelial stem cell compartment. *Experimental Eye Research*, *85*(6), 845–860. doi:10.1016/j.exer.2007.08.020

Schneider, P., Meier, M., Wepf, R., & Müller, R. (2011). Serial FIB/SEM imaging for quantitative 3D assessment of the osteocyte lacuno-canalicular network. *Bone*, *49*(2), 304–311. doi:10.1016/j.bone.2011.04.005

Schnepf, E., Hausmann, K., & Herth, W. (1982). The osmium tetroxide-potassium ferrocyanide (OsFeCN) staining technique for electron microscopy: a critical evaluation using ciliates, algae, mosses, and higher plants. *Histochemistry*, *76*(2), 261–271.

Schofield, R. (1978). The relationship between the spleen colony-forming cell and the haemopoietic stem cell. *Blood cells*, *4*(1-2), 7–25.

Schrader, S., Notara, M., Tuft, S. J., Beaconsfield, M., Geerling, G., & Daniels, J. T. (2010). Simulation of an in vitroniche environment that preserves conjunctival progenitor cells. *Regenerative Medicine*, *5*(6), 877–889. doi:10.2217/rme.10.73

Scoville, D. H., Sato, T., He, X. C., & Li, L. (2008). Current view: intestinal stem cells and signaling. *Gastroenterology*, *134*(3), 849–864. doi:10.1053/j.gastro.2008.01.079

Secker, G. A., & Daniels, J. T. (2008). Corneal Epithelial Stem Cells: Deficiency and Regulation. *Stem Cell Reviews and Reports*, *4*(3), 159–168. doi:10.1007/s12015-008-9029-x

Shanmuganathan, V. A., Foster, T., Kulkarni, B. B., Hopkinson, A., Gray, T., Powe, D. G., Lowe, J., et al. (2007). Morphological characteristics of the limbal epithelial crypt. *British Journal of Ophthalmology*, *91*(4), 514–519. doi:10.1136/bjo.2006.102640

Sharma, A., & Coles, W. H. (1989). Kinetics of corneal epithelial maintenance and graft loss. A population balance model. *Investigative Ophthalmology & Visual Science*, *30*(9), 1962–1971.

Sharma, M., Afrin, F., Satija, N., Tripathi, R. P., & Gangenahalli, G. U. (2011). Stromal-derived factor-1/CXCR4 signaling: indispensable role in homing and engraftment of hematopoietic stem cells in bone marrow. *Stem cells and development*, *20*(6), 933–946. doi:10.1089/scd.2010.0263

Shimmura, S., Miyashita, H., Higa, K., Yoshida, S., Shimazaki, J., & Tsubota, K. (2006). Proteomic analysis of soluble factors secreted by limbal fibroblasts. *Molecular vision*, *12*, 478–484.

Shimmura, S., Suematsu, M., Shimoyama, M., Tsubota, K., Oguchi, Y., & Ishimura, Y. (1996). Subthreshold UV radiation-induced peroxide formation in cultured corneal epithelial cells: the protective effects of lactoferrin. *Experimental Eye Research*, *63*(5), 519–526.

Shimmura, S., & Tsubota, K. (1997). Ultraviolet B-induced mitochondrial dysfunction is associated with decreased cell detachment of corneal epithelial cells in vitro. *Investigative Ophthalmology & Visual Science*, *38*(3), 620–626.

Shortt, A. J., Secker, G. A., Munro, P. M., Khaw, P. T., Tuft, S. J., & Daniels, J. T. (2007). Characterization of the limbal epithelial stem cell niche: novel imaging techniques permit in vivo observation and targeted biopsy of limbal epithelial stem cells. *STEM CELLS*, *25*(6), 1402–1409. doi:10.1634/stemcells.2006-0580

Song, X., & Xie, T. (2002). DE-cadherin-mediated cell adhesion is essential for

maintaining somatic stem cells in the Drosophila ovary. *Proceedings of the National Academy of Sciences of the United States of America*, *99*(23), 14813–14818. doi:10.1073/pnas.232389399

Starborg, T., Kalson, N. S., Lu, Y., Mironov, A., Cootes, T. F., Holmes, D. F., & Kadler, K. E. (2013). Using transmission electron microscopy and 3View to determine collagen fibril size and three-dimensional organization. *Nature Protocols*, *8*(7), 1433–1448. doi:10.1038/nprot.2013.086

Steinmann, U., Borkowski, J., Wolburg, H., Schröppel, B., Findeisen, P., Weiss, C., Ishikawa, H., et al. (2013). Transmigration of polymorphnuclear neutrophils and monocytes through the human blood-cerebrospinal fluid barrier after bacterial infection in vitro. *Journal of neuroinflammation*, *10*, 31. doi:10.1186/1742-2094-10-31

Suciu, L. C., Popescu, B. O., Kostin, S., & Popescu, L. M. (2012). Platelet-derived growth factor receptor-β-positive telocytes in skeletal muscle interstitium. *Journal of cellular and molecular medicine*, *16*(4), 701–707. doi:10.1111/j.1582-4934.2011.01505.x

Sugiyama, T., Kohara, H., Noda, M., & Nagasawa, T. (2006). Maintenance of the hematopoietic stem cell pool by CXCL12-CXCR4 chemokine signaling in bone marrow stromal cell niches. *Immunity*, *25*(6), 977–988. doi:10.1016/j.immuni.2006.10.016

Takahashi, K., & Yamanaka, S. (2006). Induction of pluripotent stem cells from mouse embryonic and adult fibroblast cultures by defined factors. *Cell*, *126*(4), 663–676. doi:10.1016/j.cell.2006.07.024

Takahashi, K., Tanabe, K., Ohnuki, M., Narita, M., Ichisaka, T., Tomoda, K., & Yamanaka, S. (2007). Induction of pluripotent stem cells from adult human fibroblasts by defined factors. *Cell*, *131*(5), 861–872. doi:10.1016/j.cell.2007.11.019

Talbot, M., Carrier, P., Giasson, C. J., Deschambeault, A., Guérin, S. L., Auger, F. A., Bazin, R., et al. (2006). Autologous transplantation of rabbit limbal epithelia cultured on fibrin gels for ocular surface reconstruction. *Molecular vision*, *12*, 65–75.

Tapia, J. C., Kasthuri, N., Hayworth, K. J., Schalek, R., Lichtman, J. W., Smith, S. J., & Buchanan, J. (2012). High-contrast en bloc staining of neuronal tissue for field emission scanning electron microscopy. *Nature Protocols*, *7*(2), 193–206. doi:10.1038/nprot.2011.439

Thoft, R. A., & Friend, J. (1977). Biochemical transformation of regenerating ocular surface epithelium. *Investigative Ophthalmology & Visual Science*, *16*(1), 14–20.

Thoft, R. A., & Friend, J. (1983). The X, Y, Z hypothesis of corneal epithelial maintenance. *Investigative Ophthalmology & Visual Science*, *24*(10), 1442–1443.

Thomas, P. B., Liu, Y.-H., Zhuang, F. F., Selvam, S., Song, S. W., Smith, R. E., Trousdale, M. D., et al. (2007). Identification of Notch-1 expression in the limbal basal epithelium. *Molecular vision*, *13*, 337–344.

Thomson, J. A., Itskovitz-Eldor, J., Shapiro, S. S., Waknitz, M. A., Swiergiel, J. J., Marshall, V. S., & Jones, J. M. (1998). Embryonic stem cell lines derived from human blastocysts. *Science*, *282*(5391), 1145–1147.

Townsend, W. M. (1991). The limbal palisades of Vogt. *Transactions of the American Ophthalmological Society*, *89*, 721–756.

Tsai, R. J., Li, L. M., & Chen, J. K. (2000). Reconstruction of damaged corneas by transplantation of autologous limbal epithelial cells. *The New England journal of medicine*, *343*(2), 86–93. doi:10.1056/NEJM200007133430202

Tseng, S. C. (1989). Concept and application of limbal stem cells. *Eye (London, England)*, *3 (Pt 2)*, 141–157. doi:10.1038/eye.1989.22

Tzeng, Y.-S., Li, H., Kang, Y.-L., Chen, W.-C., Cheng, W.-C., & Lai, D.-M. (2011). Loss of Cxcl12/Sdf-1 in adult mice decreases the quiescent state of hematopoietic stem/progenitor cells and alters the pattern of hematopoietic regeneration after myelosuppression. *Blood*, *117*(2), 429–439. doi:10.1182/blood-2010-01-266833

Varnum-Finney, B., Xu, L., Brashem-Stein, C., Nourigat, C., Flowers, D., Bakkour, S., Pear, W. S., et al. (2000). Pluripotent, cytokine-dependent, hematopoietic stem cells are immortalized by constitutive Notch1 signaling. *Nature Medicine*, *6*(11), 1278–1281. doi:10.1038/81390

Villinger, C., Gregorius, H., Kranz, C., Höhn, K., Münzberg, C., Wichert, von, G., Mizaikoff, B., et al. (2012). FIB/SEM tomography with TEM-like resolution for 3D imaging of high-pressure frozen cells. *Histochemistry and cell biology*, *138*(4), 549–556. doi:10.1007/s00418-012-1020-6

Vujković, V., Mikac, G., & Kozomara, R. (2002). Distribution and density of conjunctival goblet cells. *Medicinski pregled*, *55*(5-6), 195–200.

Wagner, W., Horn, P., Bork, S., & Ho, A. D. (2008). Aging of hematopoietic stem cells is regulated by the stem cell niche. *Experimental gerontology*, *43*(11), 974–980. doi:10.1016/j.exger.2008.04.007

Wagoner, M. D. (1997). Chemical injuries of the eye: current concepts in pathophysiology and therapy. *Survey of Ophthalmology*, *41*(4), 275–313.

Wang, F., Thirumangalathu, S., & Loeken, M. R. (2006). Establishment of new mouse embryonic stem cell lines is improved by physiological glucose and oxygen. *Cloning and stem cells*, *8*(2), 108–116. doi:10.1089/clo.2006.8.108

Watt, F. M. (1989). Terminal differentiation of epidermal keratinocytes. *Current opinion in cell biology*, *1*(6), 1107–1115.

Wei, D., Jacobs, S., Modla, S., Zhang, S., Young, C. L., Cirino, R., Caplan, J., et al. (2012). High-resolution three-dimensional reconstruction of a whole yeast cell using focused-ion beam scanning electron microscopy. *BioTechniques*, *53*(1), 41–48. doi:10.2144/000113850

White, D. L., Mazurkiewicz, J. E., & Barrnett, R. J. (1979). A chemical mechanism for tissue staining by osmium tetroxide-ferrocyanide mixtures. *Journal of Histochemistry and Cytochemistry*, *27*(7), 1084–1091.

Wierzbicki, R., Køobler, C., Jensen, M. R. B., Lopacińska, J., Schmidt, M. S.,
Skolimowski, M., Abeille, F., et al. (2013). Mapping the complex morphology of cell interactions with nanowire substrates using FIB-SEM. *PloS one*, *8*(1), e53307. doi:10.1371/journal.pone.0053307

Williams, R. L., Hilton, D. J., Pease, S., Willson, T. A., Stewart, C. L., Gearing, D. P., Wagner, E. F., et al. (1988). Myeloid leukaemia inhibitory factor maintains the developmental potential of embryonic stem cells. *Nature*, *336*(6200), 684–687. doi:10.1038/336684a0

Willingham, M. C., & Rutherford, A. V. (1984). The use of osmium-thiocarbohydrazide-osmium (OTO) and ferrocyanide-reduced osmium methods to enhance membrane contrast and preservation in cultured cells. *Journal of Histochemistry and Cytochemistry*, *32*(4), 455–460.

Xie, H. T., Chen, S.-Y., Li, G.-G., & Tseng, S. C. G. (2011). Limbal epithelial stem/progenitor cells attract stromal niche cells by SDF-1/CXCR4 signaling to prevent differentiation. *STEM CELLS*, *29*(11), 1874–1885. doi:10.1002/stem.743

Yamaguchi, Y., Brenner, M., & Hearing, V. J. (2007). The Regulation of Skin Pigmentation. *Journal of Biological Chemistry*, *282*(38), 27557–27561. doi:10.1074/jbc.R700026200

Yamazaki, S., Ema, H., Karlsson, G., Yamaguchi, T., Miyoshi, H., Shioda, S., Taketo, M. M., et al. (2011). Nonmyelinating Schwann cells maintain hematopoietic stem cell hibernation in the bone marrow niche. *Cell*, *147*(5), 1146–1158. doi:10.1016/j.cell.2011.09.053

Yee, R. W., Matsuda, M., Schultz, R. O., & Edelhauser, H. F. (1985). Changes in the normal corneal endothelial cellular pattern as a function of age. *Current eye research*, *4*(6), 671–678.

Yeung, T. M., Chia, L. A., Kosinski, C. M., & Kuo, C. J. (2011). Regulation of self-renewal and differentiation by the intestinal stem cell niche. *Cellular and Molecular Life Sciences*, *68*(15), 2513–2523. doi:10.1007/s00018-011-0687-5

Yoshida, S., Shimmura, S., Kawakita, T., Miyashita, H., Den, S., Shimazaki, J., & Tsubota, K. (2006). Cytokeratin 15 can be used to identify the limbal phenotype in normal and diseased ocular surfaces. *Investigative Ophthalmology & Visual Science*, *47*(11), 4780–4786. doi:10.1167/iovs.06-0574

Young, R. D., Knupp, C., Pinali, C., Png, K. M. Y., Ralphs, J. R., Bushby, A. J., Starborg, T., et al. (2014). Three-dimensional aspects of matrix assembly by cells in the developing cornea. *Proceedings of the National Academy of Sciences of the United States of America*, *111*(2), 687–692.

Zheng, T., & Xu, J. (2008). Age-related changes of human limbus on in vivo confocal microscopy. *Cornea*, *27*(7), 782–786. doi:10.1097 /ICO.0b013 e31816f5ec3

Zheng, W., Wang, S., Ma, D., Tang, L., Duan, Y., & Jin, Y. (2009). Loss of proliferation and differentiation capacity of aged human periodontal ligament stem cells and rejuvenation by exposure to the young extrinsic environment. *Tissue Engineering Part A*, *15*(9), 2363–2371. doi:10.1089/ten.tea.2008.0562

Zheng, Y., Zhang, M., Qian, M., Wang, L., Cismasiu, V. B., Bai, C., Popescu, L. M., et al. (2013). Genetic comparison of mouse lung telocytes with mesenchymal stem cells and fibroblasts. *Journal of cellular and molecular medicine*, *17*(4), 567–577. doi:10.1111/jcmm.12052

Zhou, S., Schuetz, J. D., Bunting, K. D., Colapietro, A. M., Sampath, J., Morris, J. J., Lagutina, I., et al. (2001). The ABC transporter Bcrp1/ABCG2 is expressed in a wide variety of stem cells and is a molecular determinant of the side-population phenotype. *Nature Medicine*, *7*(9), 1028–1034. doi:10.1038/nm0901-1028

Zuk, P. A., Zhu, M., Ashjian, P., De Ugarte, D. A., Huang, J. I., Mizuno, H., Alfonso, Z. C., et al. (2002). Human adipose tissue is a source of multipotent stem cells. *Molecular biology of the cell*, *13*(12), 4279–4295. doi:10.1091/mbc.E02-02-0105

Publications

1. Dziasko, M. A., Armer, H. E., Levis, H. J., Shortt, A. J., Tuft, S., & Daniels, J. T. (2014). Localisation of epithelial cells capable of holoclone formation in vitro and direct interaction with stromal cells in the native human limbal crypt. *PloS one*, *9*(4), e94283. doi:10.1371/journal.pone.0094283

2. Massie, I., Dziasko, M., Dziasko, M., Levis, H. J., Morgan, L., Neale, M., Sheth, R., et al. (2015). Advanced imaging and tissue engineering of the human limbal epithelial stem cell niche. *Methods in molecular biology (Clifton, N.J.)*, *1235*, 179–202. doi:10.1007/978-1-4939-1785-3_15

3. Dziasko, M. A., Tuft, S. J., & Daniels, J. T. (2015). Limbal melanocytes support limbal epithelial stem cells in 2D and 3D microenvironments. *Experimental Eye Research*, *138*(C), 70–79. Elsevier Ltd. doi:10.1016/j.exer.2015.06.026